Optimization of Hybrid Hemodynamics from Mechanical Support Devices in Cardiogenic Shock

by

Efrat Marcus Goffer

B.S., Mechanical Engineering
Tel-Aviv University, 2013

Submitted to the Harvard-MIT Program in Health Sciences and Technology in Partial Fulfillment of the Requirements for the Degree of

Doctor of Philosophy in Medical Engineering and Medical Physics

at the

MASSACHUSETTS INSTITUTE OF TECHNOLOGY

February 2023

Signature of Author: _____
Harvard-MIT Program in Health Sciences and Technology
August 30, 2022

Certified by: _____
Elazer R. Edelman, M.D., PhD.
Edward J. Poitras Professor in Medical Engineering and Science
Director, Institute for Medical Engineering and Science
Thesis Supervisor

Accepted by: _____
Collin M. Stultz, M.D., Ph.D.
Director, Harvard-MIT Program in Health Sciences and Technology
Nina T. and Robert H. Rubin Professor, Electrical Engineering & Computer Science and Institute for Medical Engineering & Science

(This page was intentionally left blank)

Optimization of Hybrid Hemodynamics from Mechanical Support Devices in Cardiogenic Shock

by

Efrat Marcus Goffer

Submitted to the Harvard-MIT Program of Health Sciences and Technology
On February 1st, 2023, in partial fulfillment of the requirements for the degree
of Doctor of Philosophy in Medical Engineering and Medical Physics

Abstract

Cardiovascular mechanical circulatory support (MCS) offers the promise of maintenance of forward blood flow and distal tissue perfusion without taxing the failing heart. However, there are no firm determinants of device initiation and titration, and demonstration of definitive clinical benefit remains elusive. In part this is due to limited understanding of pathophysiologic interplay and impact of these devices and the patients they serve.

We hypothesized that MCS use cannot be optimized without appreciation of its coupling with aortic dynamics – extending the concept of ventriculo:vascular coupling in native circulation to machine-augmented support. In both controlled porcine studies and a mock cardiovascular flow-loop with material properties, pressures, and flows that match human conditions, we examined the relative impact of the following MCS devices, alone and in combination: arterial unloading in the form of aortic counterpulsation; ventricular unloading and decoupling in the form of transvalvular impeller pump; and cardiopulmonary bypass in the form of extracorporeal membrane oxygenation.

This coupling paradigm allowed us to generate heatmaps of multiple hemodynamic metrics that define the shock and MCS-supported states and a framework by which to appreciate MCS with adjunctive pharmacologic and mixed mechanical modalities. Indeed, optimum support was defined

by the balance of these metrics which can best be reduced to matching of ventricular load with vascular compliance for optimization of 'Hybrid Flows' – flow patterns that emerged as the cumulative sum of native heart and MCS contributions.

Translation of this work to the clinic could better inform MCS initiation, titration, and weaning and contribute to improving outcomes for cardiac failure and shock.

Thesis Supervisor:
Elazer R. Edelman, MD, PhD
Edward J. Poitras Professor in Medical Engineering and Science
Director, Institute for Medical Engineering and Science MIT

Thesis Chair:
Ellen Roche, PhD
W.M. Keck Career Development Professor of Biomedical Engineering; Associate Professor of Mechanical Engineering and of the Institute for Medical Engineering & Science, MIT

Thesis Readers:
Thomas Heldt, PhD
Associate Professor of Electrical and Biomedical Engineering, MIT

Steven P. Keller, MD, PhD
Assistant Professor of Medicine and Biomedical Engineering, Johns Hopkins Hospital

Acknowledgments

It is with a profound sense of gratitude that I acknowledge the invaluable opportunity to be a part of the HST MEMP program, and the support provided to me throughout this PhD. I extend my deepest thanks to the individuals who have played a significant role in its successful completion.

I would like to express my heartfelt gratitude to my advisor, Dr. Elazer Edelman. Dr. Edelman has always been a source of inspiration, not only as a brilliant scholar, but also as a warm person who treats his students like family. His expertise and knowledge in the field were invaluable, but it was his dedication and commitment to my success that truly set him apart. He provided unwavering support, both academically and personally, and always went above and beyond to ensure that I had the resources and guidance needed to achieve my goals. I am forever grateful for the time and effort he invested in mentoring me. I consider myself truly fortunate to have had such an exceptional advisor, who not only shaped my academic career but also my personal growth.

To my thesis committee - I cannot express enough gratitude to Dr. Steve Keller for his pivotal role in making this research a success. His clinical insight, determination, and devotion to the research process were absolutely essential and made an invaluable contribution to the thesis. I extend my heartfelt thanks to him for his dedication and support throughout the entire process. I am grateful to have had the opportunity to work with my thesis chair, Prof. Ellen Roche, who not only provided leadership and expertise in the field, but also served as a shining example and role model throughout my journey. My appreciation also goes to the thesis reader, Prof. Thomas Heldt, for his valuable feedback and insights. I am grateful for his time and dedication to helping me improve my work.

I would like to express my gratitude to my HST friends and community. More specifically, Drs. Das, Horvath, Varela, and Emerson. Their companionship and camaraderie made them a second family to me. Their presence throughout this journey has greatly enhanced my experience, and I am grateful for the positive impact they have had on my academic and personal growth. Thank you for being a constant source of inspiration and for making this process a memorable and enjoyable experience. I would like to especially thank Kim Lamberti, my dynamic duo. Your unwavering support, friendship, and endless hours of stimulating conversation about research, teaching and life have been a constant source of inspiration and motivation. Your contributions have been invaluable and have made this experience all the more meaningful. Your kindness and generosity have meant the world to me, and I cannot thank you enough for being a such an important part of my life.

To my dear mother, father and brother, my heartfelt appreciation and love go out to you for your constant love and support. You have always been there for me, and I am forever grateful for your encouragement (daily at times). Your belief in me and my abilities has been the driving force behind my success. I am here today, only because of you. To Rei, you have been my sounding board, and my constant source of inspiration. Your love and support have been the foundation that has made this work possible. I am blessed to have you by my side, and I could not have done this without you. Can't wait to see what our next mutual adventures hold.

Lastly, I would like to dedicate this work to my past and my future. To Quique, my beloved grandpa who was a brilliant pioneer, engineer, and one of the kindest and hardest working people I have ever known. His dedication, intelligence, and quietness have always inspired me and will continue to do so. His legacy lives on through this work. And to Nur, my future and greatest inspiration, who at three years old says she is a "heart scientist" - keep asking the brightest questions, researching, and never give up. This is for you Quique and for you Nur, my beloved grandpa and my daughter.

(This page was intentionally left blank)

Table of Contents

List of Tables

List of Figures

(This page was intentionally left blank)

Chapter 1: Introduction

1.1 Cardiogenic Shock

Cardiovascular disease (CVD) has been the leading cause of death in the United States for decades. Although the number of deaths attributed to CVD has declined over this period, CVD is still responsible for about 630,000 deaths a year in the US. Over half of these cases are attributed to coronary artery disease (CAD) whose consequences include loss of cardiac tissue and function from myocardial infarction (MI) that can lead to cardiogenic shock (CS), and the spiral of accelerated heart failure (1). CS is characterized by decreased cardiac output (CO) that leads to hypotension and a vicious cycle of successive decline in tissue perfusion and damage to end-organs, including the heart itself. One of the most common causes of CS is severe MI where more than 40% of the left ventricle (LV) has been infarcted. CS occurs in an estimated 10% of MI patients and mortality rates from CS approach 50% (2–4). Other causes of CS include myocarditis (inflammation of the myocardium, e.g., caused by COVID-19 infection), endocarditis, arrhythmias, tamponade, and valvular disease.

1.1.1 Standard of Care

During CS, patient stabilization can be achieved through prompt medical care which includes treatment to augment CO, tissue perfusion pressure and revascularization (5–7). Medical treatment includes balance management of volume state, vasomotor tone, and contractility (in the Frank-Starling paradigm preload, afterload, and inotropy modulation respectively), and is often under close monitoring in the intensive care unit. These interventions are intended to increase blood supply; however, they often add to myocardial strain and increase myocardial oxygen

consumption. Thus, clinical management becomes challenging, with the aim of balancing supply and demand. Revascularization attempts to reverse the occlusion of coronary arteries to restore perfusion. If achieved early enough, revascularization can save myocardial tissue and recover some heart function. Despite these interventions, patients who survive and are discharged from the hospital have poor prognosis: one-year mortality rate for these patients is 22%, and the rate of re-hospitalization is 59% (8). In part, these numbers reflect the cycle of heart failure. Where heart failure, physiologic compensatory mechanisms, and all the more so aggressive exogenous pharmacological approaches, strain the marginalized heart and induce greater damage and worsened failure.

Mechanical circulatory support (MCS) has become increasingly popular as it offers the potential of support without increased myocardial load, decoupling supply, and demand. Machines assume native cardiac function rather than pushing tissues to work harder and have the promise of restoring end-organ perfusion and hemodynamic stability while allowing the heart to rest and recover. Although there have been many technological advancements in the field of MCS, including an abundance of new devices with different mechanisms of action, data regarding safety, efficacy and pathophysiological indications for the introduction, titration of care and weaning off the different devices are still emerging (9,10).

1.2 Acute MCS Devices

In this paradigm MCS must be administered early in the course of treatment before permanent significant heart damage is evident. Such early initiation is correlated with improved outcomes (11).

The earliest forms of mechanical support included full cardiopulmonary bypass (CPB) on the most extreme end of the spectrum and intra-aortic balloon pump (IABP) on the other. CPB has changed cardiac surgery forever and can be used in extreme cases in some form of extracorporeal support but it is the search for minimal or least invasive interventions that has supported continued use of the IABP. The pump is the inflation of a 35-50 cc non-compliant balloon with an inert gas (usually nitrogen) in counter-timing to cardiac ejection. Balloon inflation is timed to occur while the aortic valve is closed and deflated in ventricular systole with aortic valve opening. Cyclical inflation-deflation is thought to aid in afterload reduction immediately prior to systole and coronary perfusion by enhanced retrograde flow in ventricular diastole. Even after years of use, IABP mechanism of assistance remain unclear and a large, randomized trial showed no significant reduction in mortality rates with the use of IABP in CS complicating MI (12). Thus while CS rates have been steadily increasing over the past two decades, and IABP's use has been declining as its effectiveness remains a topic of debate.

Newer MCS technologies have therefore appeared, in general moving from the aorta into the heart from the IABP position in the aorta, and their use is building but with some caveats. First, we have not fully advanced a complete understanding of how MCS supports the failing heart and when it is best used. It is not surprising then that we do not have unambiguous and definitive demonstration of benefit for MCS in heart failure. One hypothesis and indeed the central tenet of this work is that the movement away from IABP to intracardiac MCS creates the potential for imbalance in ventriculo-vascular coupling. Whereas the IABP builds on and amplifies native ventriculo:vascular coupling (VVC) emerging MCS serve to augment contractile and pumping function of the heart but in decoupling heart and vascular events and loads may in fact come at the expense of balanced VVC. **We therefore compared quantitatively clinically available acute MCSs for CS support through the perspective of VVC.** An extracardiac pulsatile device - the

IABP, and two constant flow generating devices - a percutaneous ventricular assist device (pVAD) and, veno-arterial extracorporeal membrane oxygenation (VA-ECMO) (16).

Review of MCS

Contemporary MCS vary in the extent of the support they can provide, invasiveness, and finally, the length of intended support (13–15). In this body of work we examined three different forms of support – the IABP that resides within the aorta, pVADs which are placed within the ventricle to move blood volume in tandem with the native heart, and modifications of cardiac and or cardiopulmonary bypass such as ECMO that bypass the heart and/or lungs in augmenting circulatory perfusion.

1.2.1 Intra-Aortic Balloon Pump

IABP counter pulsation is the most mature MCS technology and has been in use since 1968 (**Figure 1.1** A). Comprised of a catheter-mounted balloon that resides in the descending aorta and aims to provide hemodynamics stabilization. It counterpulsates with the cardiac cycle – it deflates during systole, reducing systolic blood pressure and thus afterload, leading to a reduction in myocardial work. It then inflates during diastole, augmenting diastolic blood pressure and increasing coronary perfusion. By the nature of this device placement, in the descending aorta (i.e. extracardiac), it acts as a vascular coupling modulator. Its usage enables alteration of a single vascular parameter – afterload, and might be beneficial in clinical cases where vascular state alteration will lead to optimization of cardiovascular coupling.

A multicenter, open-label study (SHOCK II) randomized 600 acute myocardial infarction patients to IABP vs. optimal medical therapy, showed no benefit for the IABP (no significant reduction of 30-day mortality). Since then, IABP has been downgraded in international guidelines,

and usage has been decreasing (12). However, it is still widely used, and its usage remains a source of debate. More recently IABP has been suggested to be used as a secondary MCS when using VA-ECMO, as means of unloading the LV. However, this approach as well has raised debate in the field and with lack of mechanistic studies remains an open question (17). Existing data mainly relay on retrospective analysis but are abundant in confounding factors, and hemodynamic data is rarely taken into account.

1.2.2 Percutaneous Ventricular Assist Device

pVAD (**Figure 1.1** B), specifically in our research we utilize Abiomed's Impella CP (Abiomed, Danvers, MA) (18), is designed to augment or completely replace heart function when its ability to pump blood and perfuse end-organs is compromised. It is a catheter-based (9 Fr) axial pump which is inserted percutaneously, and advanced through the aorta into the LV. Its inlet resides in the LV, making it an intracardiac device which allows for control of multiple cardiac parameters. It continuously pumps blood and propels it into the ascending aorta. The catheter is connected to a controller (AIC), which provides the clinician with the ability to control the device's P-level ranging from P1 – P9, Increase in P level results in increased pump RPM and thus forward flow. However, higher P levels are also associated with deleterious effects including LV suction events and hemolysis. The AIC also displays a placement signal which uses a pressure sensor mounted directly next to the pump outlet.

pVAD use in acute cardiogenic events has been steadily increasing in the past decade (19). In order to study ventricular:vascular coupling in the setting of circulatory support, we would ideally utilize a device that: a) is placed transvalvular, and operates in tandem with the ventricle propelling blood into the ascending aorta; b) has steady flow allowing to determine ventricular

state; c) enables interrogation of the system. Thus, Abiomed's Impella meets these criteria. It generates constant flow, in tandem with native CO, by drawing blood from the LV and propelling it into the ascending aorta. While generating forward flow and unloading the LV, flow rate is limited and in severe cases might not provide enough circulatory support.

1.2.3 Veno-Arterial Extracorporeal Membrane Oxygenation

ECMO (**Figure 1.1** C) is a percutaneous heart-lung machine for cardiac and/or respiratory support. When utilized for support of CS patients, the peripheral venoarterial ECMO configuration is most commonly used; Introduced through a venous drainage cannula (femoral vein, 21-25 Fr), draws deoxygenated blood, and propels it through a centrifugal pump and an oxygenator. Oxygenated blood then flows through the arterial return cannula (15-21 Fr), usually introduced into the femoral artery. It continuously propels the oxygenated blood in a retrograde fashion into the aorta (4,20,21). Support titration is done via pump RPM and is titrated manually by the physician, requiring constant monitoring and an extensive and highly-trained team of caretakes.

VA-ECMO can be deployed at the bedside in the ICU, and it provides high degree of circulatory support (typically 4-6 lpm in adults). However, the retrograde flow into the aorta increases afterload and further compromises the LV. It creates cardiac bypass and, with the increase in afterload, might impede aortic valve opening leading to LV stasis and lethal thrombus formation (22). Other complications include hemorrhage and bleeding, neurologic morbidity, circuit clotting and distal ischemia.
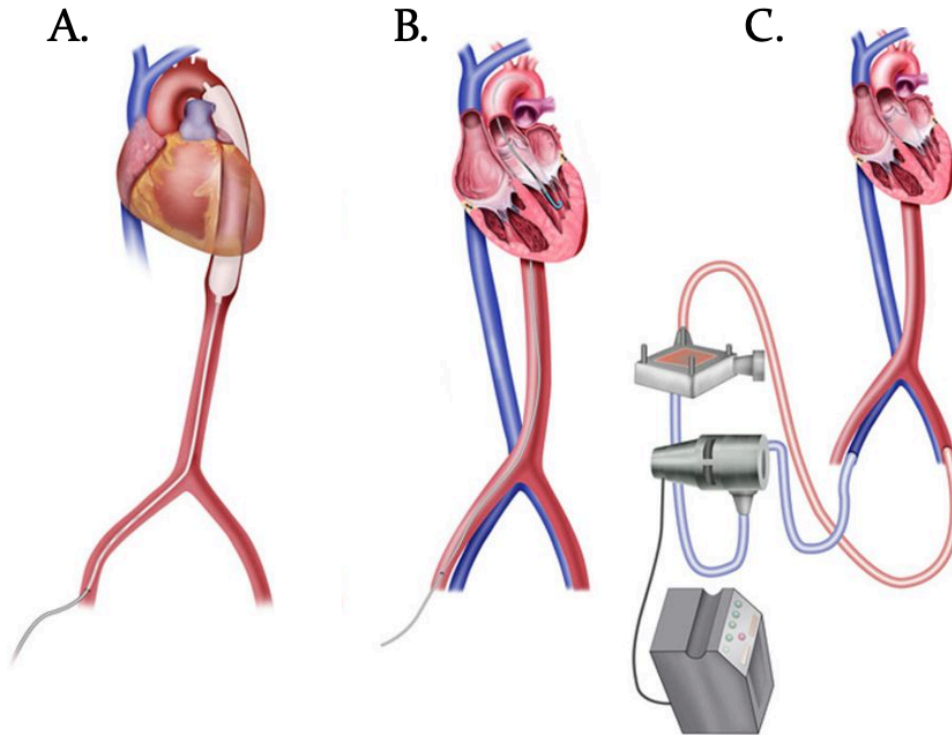
Figure 1.1 - Acute Mechanical Circulatory Devices Discussed in This Dissertation *Adapted from Mandawat et. al, 2017; A. Intra-aortic balloon pump - provides extracardiac counterpulsation, aims to reduce afterload, promote forward flow and diastolic coronary perfusion. B. Impella CP – percutaneous ventricular assisst device, vents the LV, provides continous parallel to native forward flow. C. VA-ECMO – provides high degree of support, retrograde continous flow into the descending aorta.*

1.2.4 Myocardial Recovery

The devices discussed above (**Figure 1.1**) are often used during CS as bridge to recovery. In essence, they support hemodynamic stability i.e. provide adequate systemic perfusion, while enabling treatment of the underlying CS cause (9,23,24). As such, while providing circulatory support the clinician will aim to reduce myocardial stress (myocardial oxygen consumption or metabolic demand) to help facilitate recovery.

Inotropes and vasopressors, the gold standard medical treatment before escalating to MCS, increase metabolic demand and might exacerbate supply and demand mismatch (25,26). Moreover, certain MCS modalities, while increasing supply also increase demand (e.g. afterload increase

during VA-ECMO support), impeding myocardial recovery. Taken together, there exists a balance of drug therapy and support modality that can enable optimal demand for a given patient state, favoring (or, not impeding) myocardial recovery. Towards this goal, LV thermodynamic parameters provide a useful framework to quantify shifts in myocardial strain and demand, by which to evaluate drug and device selection, and titration. Chapters 3-5 of this thesis discuss this framework and its results for the evaluation of MCS intervention, and cardiovascular response to implantation.

1.3 Hemodynamics

Understanding hemodynamics of native and shock cardiovascular systems allows us to appreciate the forces needed to maintain adequate blood circulation for organ perfusion. In health, hemodynamics is modulated to balance organ demand and myocardial work. In disease states, the balance is deeply altered, and these alterations play significant roles in disease processes (27,28). Invasive hemodynamic monitoring measure pressure, flow, and oxygenation in the cardiovascular system, in order to obtain measurements of vascular capacity, blood volume, ventricular pumping ability and tissue perfusion. These data can be measured using arterial and venous catheters, pulmonary artery catheter and, experimentally, LV pressure-volume (PV) conductance catheter. PV data are traditionally used to generate PV loops, which help us assess cardiac mechanics and key physiological hemodynamic parameters – the thermodynamic work of the circulatory system. For example: LV end diastolic pressure (LVEDP) and volume (surrogate for diastolic function, preload), end systolic pressure and volume (surrogate for contractile function, afterload), stroke volume and ejection fraction (important determinants of CO).

1.3.1 Hybrid Flow

Classically, we speak about CO (limited to ventricular performance), systemic vascular resistance (SVR) and LVEDP, but when examining complex flows, we need to expand SVR to involve impedances, examine flow as well as volume. MCS completely alter hemodynamics and create complex flows, or 'Hybrid Flows' - a superposition of native pulsatile CO and continuous MCS flow (**Figure 1.2**). Mixing zone (MZ) defines the specific site where these flows meet. In the ideal these flows work synchronously, in actuality they may oppose or negate each other. We wish to study these special hemodynamic patterns, in order to guide titration of care and achieve optimal end-organ perfusion and myocardial stress for a given state. A preliminary *in vivo* study (29), compared the effects of continuous vs. pulsatile ECMO on the LV. They showed a beneficial effect of pulsatile synchronized ECMO flow on native LV function. Specifically, they showed an increase in stroke volume, and, at some levels of support, reduction of LV end diastolic pressure (LVEDP).
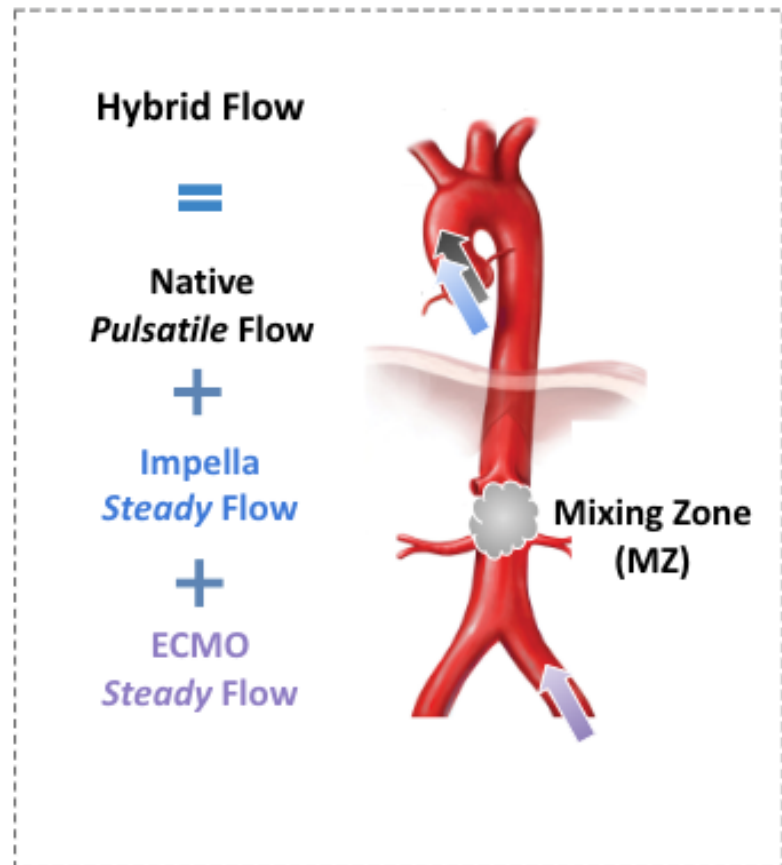
Figure 1.2 - Hybrid flow diagram
Hybrid flows are created by superposition of residual native pulsatile flow with one or more steady flow mechanical circulatory support device. Mixing zone is a phenomena created with retrograde perfusion – i.e. VA-ECMO. Describes the location at which forward and retrograde flow collide.

1.3.2 Pressure-Flow Analysis in the Frequency Domain

The characteristic impedance of the system can be found by transforming pressure and flow measurements into the frequency domain. This analysis enables the decomposition of any signal with periodicity into its steady components and harmonic components, and thus might be especially adequate for hemodynamic characterization of hybrid flows. The harmonic decomposition is done using Fourier transforms and yields 3 parameters for the inspected waves – modulus (amplitude), period (temporal frequency) and phase angle (position in time relative to the cardiac cycle). Summation of all components will generate the original waveform. Using this technique, cardiac and vascular state can be assessed by obtaining: Input impedance, a metric for LV load, Aortic characteristic impedance (Zc), Systemic vascular resistance (zero harmonic) and the pulsatility index of the system (2-3 harmonics) (30,31).

1.4 Ventricular-Vascular Coupling

Classic hemodynamics do not do justice with ventricular-vascular coupling (VVC), which sees the aorta as an important third chamber where its tone sets ventricular load and its elastance limits aortic filling. VVC analysis examines the efficiency of energy transmission from the LV to the aorta, or, how the relation between ventricular and arterial functional characteristics determines the amount of CO that the ventricle can generate (32,33). It is defined in the PV plane as Ea/Ees (arterial elastance and LV elastance at end systole respectively) and the ratio is equal ~1 in healthy subjects.

Pulse wave velocity (PWV) is a metric of vascular biomechanics health and hemodynamic state where the velocity of the blood through the arterial system is quantified through analysis of pulse wave mechanics. PWV is calculated by measuring pressure in two locations in the arterial system and dividing the distance between the measuring points by the difference in timing of the

initiation of systolic upstroke in the pressure waveform (34,35). The resulting aortic pressure waveform is the superposition of a forward pressure wave generated by the LV and a reflected wave, traveling back from the peripheral arterial system, reflected from sites of impedance mismatch (36). PWA can be used to determine VVC in health and its alteration in disease states. Metrics including LV stroke indices, arterial stiffness, ejection duration and augmentation index have been described for different pathologies (37,38) but the effects of MCS usage on these metrics can give a valuable insight into VVC in the setting of MCS.

VVC indices has been studied and described extensively in health, disease, and aging population. However, its use in the clinical setting is limited by inability to properly quantify it and a limited understanding of its implications. Moreover, the effects of shock (39), and subsequent implantation of MCS on these metrics have been rarely described. With deeper understanding we could provide a framework to determine cardiovascular state and describe changes in LV energetics and arterial elastance with initiation of support.

Specifically for our studies, we would like to utilize the VVC and cardiac energetics framework to MCS support. The interplay between the ventricle and the vasculature is usually described as a pump and a load, respectively. But with hemodynamic-altering MCS devices, this relationship does not go one way. Ventricular-vascular relation profoundly affect vascular dynamics, becoming more dominant in the setting of continuous flow MCS devices. In turn, vascular-ventricular relation affects ventricular dynamics and thus LV state and performance. The latter relationship, simply described as afterload, becomes complex in the setting of MCS support. As constant flow is propelled into the aorta regardless of the timing in the cardiac cycle, while some degree of native pulsatility is preserved. A mechanistic understanding of this complex interplay, and further identification of their effects on MCS signals could lead to an additional tool for evaluation and optimization of MCS:cardiovascular performance.

1.5 Overview of Chapters

In this dissertation, I studied acute MCS devices used for the treatment of CS. Specifically, I aimed to investigate the effects of the introduction of these devices on hemodynamics, and their interactions with the left ventricle and the vasculature. By virtue of their function, MCS devices profoundly alter hemodynamic patterns and thus ventricular-vascular coupling. Hence, we proposed an approach to evaluate cardiovascular state and response to MCS implantation through hybrid flows and cardiac thermodynamic work. This research's ultimate goal is to optimize the use of MCS devices, from initiation of treatment to device selection and titration for a given patient state. The following thesis outlines the experiments, results and conclusions examining the different aspects of device-cardiovascular interaction.

In chapter 2, I discuss the design, fabrication, and optimization of a benchtop flow loop for the study of hybrid flows. Further, different models and approached and their limitations are evaluated. In order to study the effects of MCS implantation on pathophysiological hemodynamics and to quantify the changes with each approach of circulatory support a unique setup was developed. I will also highlight a key finding with the use of the flow loop – with the use of retrograde circulatory perfusion (VA-ECMO), the mixing zone (the location in the aorta of the collision of forward cardiac output with the retrograde oxygenated flow) location and characteristics

Chapter 3 discusses quantification of changes in VVC ratio with different support methodologies in an acute CS porcine model. Specifically, I examine the driving factors of the change in the ratio and discuss potential clinical implications.

Chapters 4 and 5 are a natural continuum, exploring the use of VA-ECMO in an acute CS porcine model. Specifically, investigate ECMO flow titration effects on cardiac thermodynamic efficiency metrics, vascular response, and perfusion. While VA-ECMO provides high degree of

circulatory support, it increases afterload, impeding LV forward flow (potentially creating stasis and lethal thrombus formation), and further increases myocardial oxygen demand. Therefore, clinicians have increasingly been using a secondary device to vent the LV when using VA-ECMO in profound CS state with minimal residual cardiac pulsatility. However, mechanistic studies are lacking, and secondary device selection, initiation, and the complex titration relays mostly on anecdotal clinician's experience. In chapter 5 we compare two LV unloading modalities with the use of ECMO – extracardiac pulsatile device and an intracardiac continuous flow device (IABP vs. pVAD).

The results of these studies revealed the following key themes – initial cardiovascular state and degree of shock severity can predict benefit from VA-ECMO support. Subjects can be categorized into those who will benefit or not from support initiation, and, of those who benefit, the ones that are sensitive to flow titration. We discuss the key parameters to observe when determining the subject's response. Future studies and clinical data analysis are needed to validate these findings. Lastly, during LV unloading, based on our experimental findings, combined MCS with VA-ECMO and pVAD provide a means to sustain end-organ perfusion while simultaneously decreasing LV preload and promoting forward flow across the aortic valve.

Taken together, this work explores novel frameworks to mechanistically evaluate and quantify the effects of MCS on the diseased cardiovascular system, and suggests initial findings towards optimization of device selection, initiation, and titration during CS. Further studies and clinical data evaluation will be done for validation of the trends, metrics and key findings presented in this thesis.

(This page was intentionally left blank)

Chapter 2: Modeling Considerations of Ventricular-Vascular Coupling with Continuous-Flow Mechanical Support Devices - Methods and Limitations

Abstract

This chapter explores the considerations and limitations of benchtop modeling of the cardiovascular system with continuous flow mechanical support devices. The focus is on the factors that influence the accuracy and reliability of these models, including design, flow patterns, and hemodynamic parameters.

The experimental model was used to study the dynamics of the mixing zone area, and the findings reveal that the mixing zone location is determined by a complex interplay of forces greater than cardiac:support device fractional flow alone. We found that the mixing zone will always land in bifurcating areas, as it is determined by the influence of local vascular anatomy and resistances as well as fractional flow. I discuss current limitations and potential solutions to improve the validity of these laboratory models in simulating real-world scenarios. Ultimately, the goal is to provide a comprehensive understanding of the complexities and limitations of using continuous flow mechanical support devices in cardiovascular research and to guide future development in this field.

2.1 Introduction

Further understanding of pathophysiological phenomena require the study of physical processes that deviate from normal physiology. Depending on the question investigated, different

models can be used to explore the governing mechanisms, while considering the limitations of each approach, to find the design allowing for proper interrogation of the problem at hand.

Cardiology is flow (40). The study of cardiovascular pathophysiology cannot be carried out without proper understanding the dynamics of flow in the circulatory system. Fluid dynamics has been studied for centuries with use of bench-top physical models, and more recently, using computational fluid dynamics (CFD) models. CFD includes control of fluid, material properties, geometry and boundary conditions, enabling the replication of flow patterns difficult to mimic and interpret in any physical model (e.g. wall shear stress). The ability to reproduce specific pathologies *in-silico, in-vitro* and *in-vivo* allows for the validation of results with clinical outcomes. To name a few - hemodynamic patterns of post-artificial valve implantation, flow characteristics in coronaries post stenting, and pre-interventional abdominal aortic aneurysms have all been modeled to determine patient specific or optimal treatment (41–44).

When considering hybrid flows from mechanical circulatory support (MCS) devices, successfully interpreting fluid flow patterns is critical for understanding the dynamics of their effect on cardiovascular thermodynamic efficiency. In the past decade an abundance of CFD studies have been published (45–48), but benchtop models and *in-vivo* work lag. Due to inherent limitations in CFD models, and the need to validate these models with experimental work (49), we opted to design a physical left ventricular (LV)-vascular flow loop model for the study of the effects of MCS hybrid flows on cardiovascular dynamics.

In this chapter, the design and development of a bench-top model will be discussed. Lastly, the usage of different models employed for the study similar questions will be discussed, focusing on differences and limitations.

2.1.1 Computational Fluid Dynamics

In-silico models are widely used in the field of hemodynamics; CFD enables us to specify anatomy, fluid properties and boundary conditions, in order to compute flow patterns which arise in a particular setting. This method is highly reproducible and can be used to test a variety of scenarios systematically. Additionally, patient-specific anatomies can be used, permitting customized preparation and care for each case. Advances in imaging modalities enable validation of some of these models, specifically 4D flow MRI (49).

Computational studies have been published on the effect of ECMO on arterial hemodynamics, often times with patient-specific models. Their outcomes seem promising, showing the interactions between native and ECMO flows, but the results have not been validated yet (50). However, these studies mainly study the flow fields in the aorta, and only a small portion of these studies simulate effects of MCS on ventricular function (10), including ventricular pressure-volume relations. These studies enable the assessment of MCS hybrid flows and their effects on ventricular-vascular coupling (VVC). But their results remain limited due to lack of clinical validation.

Moreover, numerical methods have high sensitivity to the chosen input boundary conditions and geometry meshing (the method to discretize the flow domain) and thus need to be evaluated in conjunction with other models to assess the validity of their results. These models operate under extensive assumptions and are not fully validated. Validation of these studies require the design of an accurate *in-vitro* model, *in-vivo* protocol, or retrospective human data. One key limitation for modeling MCS hybrid flows is the rigid walls commonly used for the anatomy in the simulations (51). Aortic compliance is a key factor of VVC and determinant of thermodynamic efficiency, it affects pulse wave propagation and is profoundly altered in disease states (36). Fluid structure interactions (FSI) simulations account for material propertied of the aortic wall and consider the contribution of aortic compliance. However, these models are more recently

developed, not fully validated and computationally costly. Moreover, MCS flow alters cardiac afterload, preload and physiological vascular responses which will significantly change systemic hemodynamics and affect end-organ perfusion. The range of physiological interactions and the complex interplay between MCS and the heart are challenging to model. For these reasons, we prioritized *in-vitro* and *in-vivo* models for our studies.

2.1.2 Mock Circulatory Flow Loops

In-vitro flow loops are used to mimic physiological blood flow to assess a wide range of hemodynamic scenarios, pathologies and to test medical device function (52–54). They serve as an initial testbed to gain insight before testing in a complex animal model and enable us to control the variables of the system in a manner that cannot be achieved *in-vivo*. Specifically, these models are used to monitor hemodynamic parameters (pressure waveforms and flow rates) in phantom vessels, in a pulsatile flow regime in physiological dimensions (55). Flow visualization techniques (e.g. particle image velocimetry) enable the generation of flow field matrices, which can be interpreted and quantified with the use of computational techniques (56). Accurate *in-vitro* models can assist in validation of *in silico* results and provide boundary conditions as an input for the simulations. Most flow loops use engineering tools to reproduce pressure signals – rigid tubes, connectors, and chambers that simulate the different locations within the cardiovascular system. But while accurately mimicking pressure patterns, this approach yields gross inaccuracies in flow behavior. Due to the importance of flow representation when studying MCS hybrid flows and their effects on VVC, the need for a novel flow loop emerged. This chapter will discuss the development of a flow loop to address these limitations, by using a compliant continuous ventricle-aortic valve-aorta phantom, allowing for MCS implantation and more accurate flow patterns formation in regions of interest.

2.1.3 *In-Vivo* Studies

In-vivo studies enable insights into the hemostatic and physiologic regulation with the use of MCS devices in state of cardiogenic shock (CS). Using these models, we can explore the range of physiological interactions and the complex interplay between MCS and the cardiovascular system, in health and in disease. Key metrics can be continuously monitored in these models including ventricular state, vascular response, end-organ function assessment, native heart stress state, renal and liver function (using biomarkers - lactic acid, creatinine and liver enzymes), all of which cannot be studied in other models. CS animal models traditionally use coronary balloon occlusion or coronary ligation techniques, known to induce malignant arrhythmias leading to unacceptable levels of specimen mortality (57,58). The lack of stability in the *in-vivo* models led to slow advancement in the field, and improvements in techniques towards more stable protocols greatly benefited the field in the past decade. Our group has been working extensively and developing a stable acute porcine CS model. In this model, diffuse microvascular ischemia is induced in the LV, by instilling Hydropearl microbeads (45-105 um diameter; Terumo, Inc., Tokyo, Japan) boluses into the left anterior descending coronary artery. Bolus injections of spheres are followed by re-assessment of cardiovascular function, and shock state is determined to have been achieved when predetermined criteria (below) are met. The major challenge with these models is the wealth of data and the profound physiologic variability between the specimens. Due to the complexity and costly nature of these studies, they usually include a handful of specimens, which prove to be challenging when drawing conclusions and predictions.

2.2 Material and Methods

2.2.1 Mock Circulatory Loop – Design and Validation

A benchtop flow loop was designed (**Figure 2.2**, **Figure 2.5**) to enable hemodynamic measurements and study of hybrid flow patterns. The specifications for our flow loop design included: (1) Anatomically correct, i.e. physical ventricle and an aorta with branching vessels of interest (2) MCS implantation capability (3) Seamless model, without rigid connectors to minimize flow disturbance (4) Control of ventricular and vascular function - pressures, flow, resistance and compliance (5) Transparent to enable flow visualization.

A custom-made seamless, compliant ventricular-vascular model of an adult aorta was manufactured by United Biologics (Santa Ana, CA). The aorta is casted out of silicone with similar mechanical properties a typical healthy aorta ($E \approx 1\ MPa$, with modulus $0.5 - 6MPa$ (59,60)) (**Figure 2.4**, Table 2.1). The LV resides in a custom-built chamber, which is connected to a positive displacement pump (ViVitro Superpump Victoria, BC, Canada), and an LV compliance chamber (**Figure 2.3**). LV waveforms can be controlled by programing the displacement profile of the pump's piston, BPM and % systole out of the cycle. Pump stroke volume and rate can be adjusted in real time to maintain desired cardiac output (CO). Further LV contraction and relaxation control is achieved by titration of LV compliance – a chamber filled with part water part air, acting as a spring. By tuning the ratio of water/air and air pressure, a range of LV compliances can be mimicked.

Silicone Properties	
Durometer: Shore A	40
Elongation	400
Tear Resistance [N/mm] (ppi)	21 (120)
100% Modulus [N/mm²] (psi)	0.62 (90)
Tensile Strength [N/mm²] (psi)	5.5 (800)
Specific Gravity	1.07
Color Transparent with red tint	
Refractive index	1.41

Table 2.1 - United Biologic's aortic model - material properties

A tri-leaflet aortic valve deployed in a nitinol frame (Medtronic CoreValve, trans-catheter aortic valve), anchored in a 3d printed silicone sleeve for paravalvular leakage prevention sits at the LV outlet. A second compliance chamber (upper body compliance chamber) was added and connected in line to the brachiocephalic, left common carotid artery and left subclavian artery. The compliance chamber with adjustable tube clamps along the flow loop outlets, enable the regulation of systemic compliance and resistance, and boundary conditions can be adjusted to mimic a range of physiologic states. The design was finalized after numerous iterations, recreating proper LV and aortic pressure waveform. This configuration yielded good results within physiologic range of systemic vascular resistance (affects the closing pressure of the valve during LV diastolic phase).

Collecting tubes drain the outlets back into the fluid reservoir. The diameter and connection of the tubing affects systemic resistance and thus flow rate. Numerous iterations were done to achieve acceptable flow rates while preserving physiological pressure waveforms and absolute values. The flow of fluids through a pipe (vessel) can be described by Poiseuille's Law:

$$Q = \frac{\pi \Delta P r^4}{8\eta L}$$

And the resistance to flow:

$$R = \frac{8\eta L}{\pi r^4}$$

Where Q – flow rate; dP – pressure gradient; r – radius of the vessel; η = viscosity; R = resistance.

The radius of the pipe has the largest effect on volumetric flow rate for a given pressure gradient. Thus, collection tubes diameter was increased significantly throughout the loop development process.

The reservoir outlet is connected to an inline flow meter (ME 13 PXN, Transonic) used for monitoring bulk flow through the cardiac cycle, followed by a one-way valve preceding the LV which acts as a mitral valve. Glycerol solution 36% by volume in water at 37 °C served as surrogate fluid, which has been shown to mimic blood viscosity and density (55).

Pressure sensors (PRESS-S-000, PendoTech, Princeton, NJ) enable LV, Carotid, renal and femoral arteries pressure measurements (**Figure 2.1**), and an additional 5F pressure catheter (Ventri-Cath 510, Millar) connected to MPVS Ultra acquisition system (Millar) is used for pressure measurement in the ascending or descending aorta, depending on the experimental setup. Similarly, when needed, a Millar pressure-volume catheter was used to monitor LV volumes.

Pressure and flow are monitored in real-time and recorded continuously using ADInstruments data acquisition PowerLab (Colorado Springs, CO), Quad Bridge Amp and LabChart *(LabChart Pro v8.1.16, ADInstruments)* displays and registers the data.

Further extensive studies we done to better understand and thus control the dynamics effects of input parameter modulation. Modulation of parameters was done in a systematic manner, changing one parameter at a time. Sweeping through a range of magnitudes for each of the

following parameters - heart rate (pump BPM), pump stroke volume, LV compliance, systole duration, LV inotropy (speed of contraction) and arterial resistances. See results in section *2.3.1*.
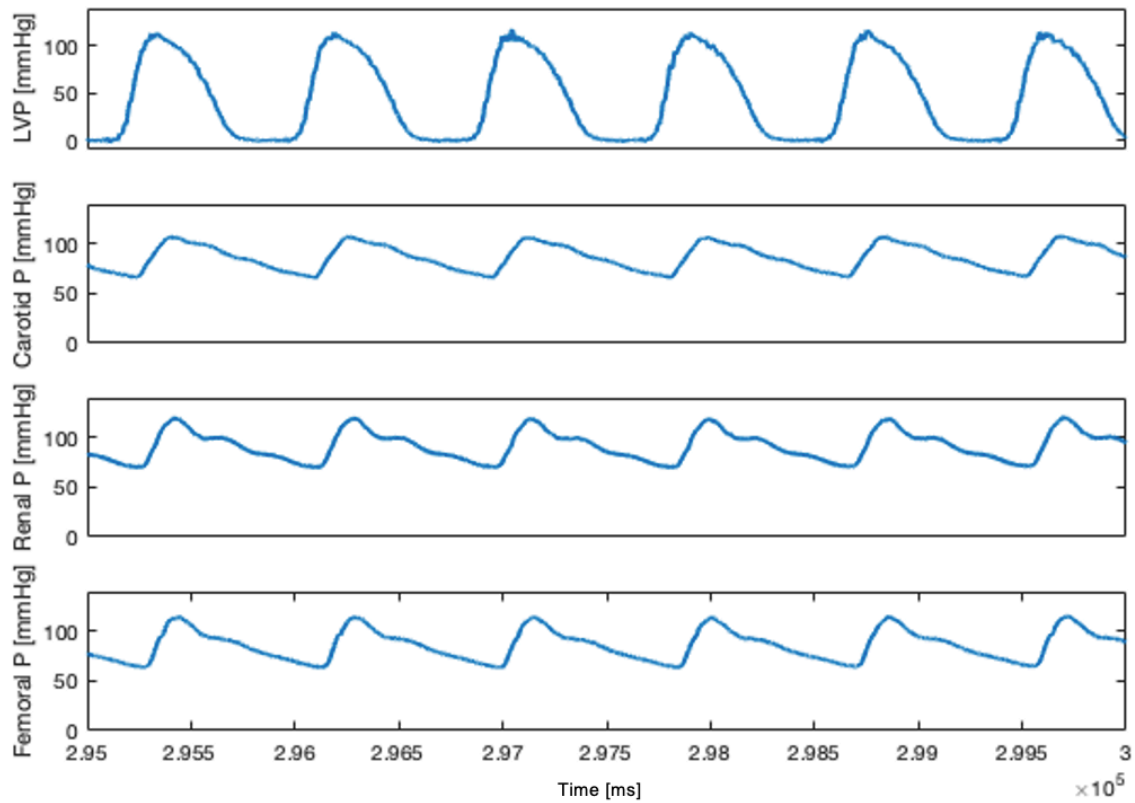
Figure 2.1 – Flow loop pressure waveforms during the iteration and optimization process. *Top to bottom panels – left ventricular pressure (LVP), carotid pressure, renal artery pressure and femoral artery pressure. Waveforms were recorded after the resolution of aortic valve closure issues and valvular leakage, but prior to the addition of a second, systemic compliance chamber.*
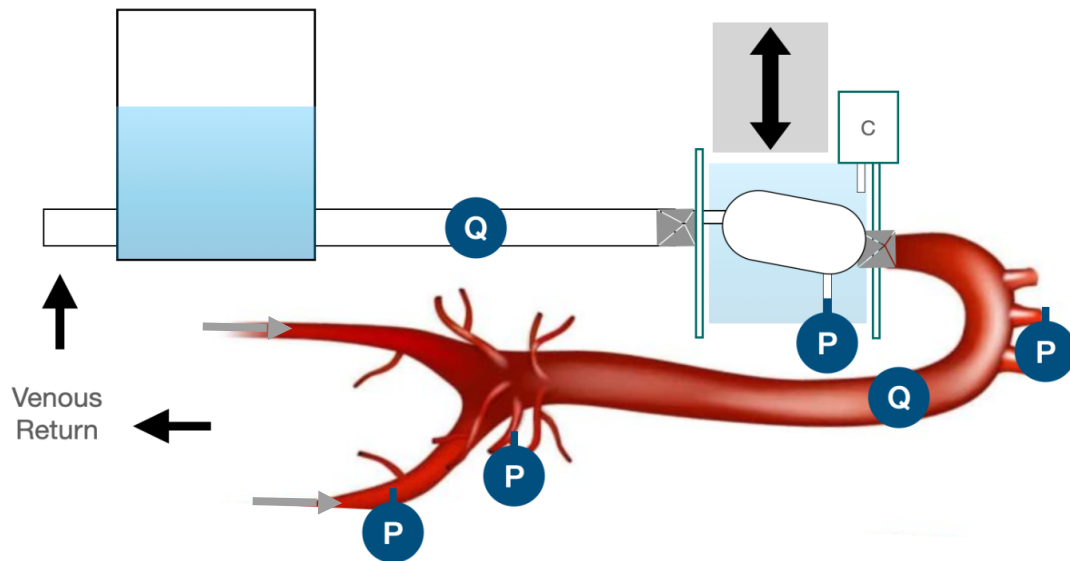
Figure 2.2 – Flow loop design schematic. *Top left to right – fluid reservoir, connected through a one way valve (grey square) to the left ventricle (LV). The LV resides in a water-filled chamber connected to a positive displacement pump (grey box, black arrow) and an LV compliance chamber (white box, denoted with C). LV connected to the aorta with a TAVR valve (grey square). Grey arrows denote MCS introduction access. Black arrows denote venous return – pipes connected to the aortic outlets and returning fluid to the reservoir. Blue circles represent pressure sensors (P) and flow meters (Q).*
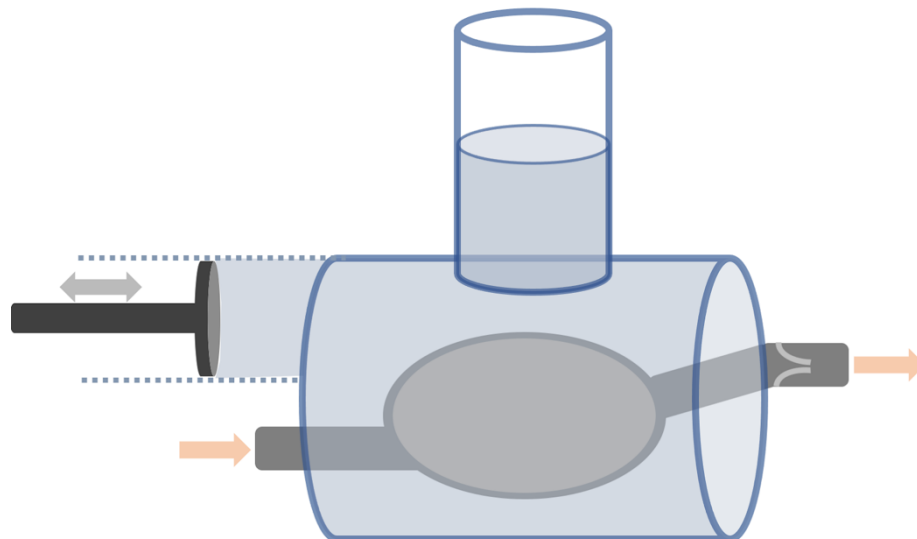
Figure 2.3 – Left ventricular (LV) chamber schematic. *The design allows for control of LV compliance and stroke volume.*
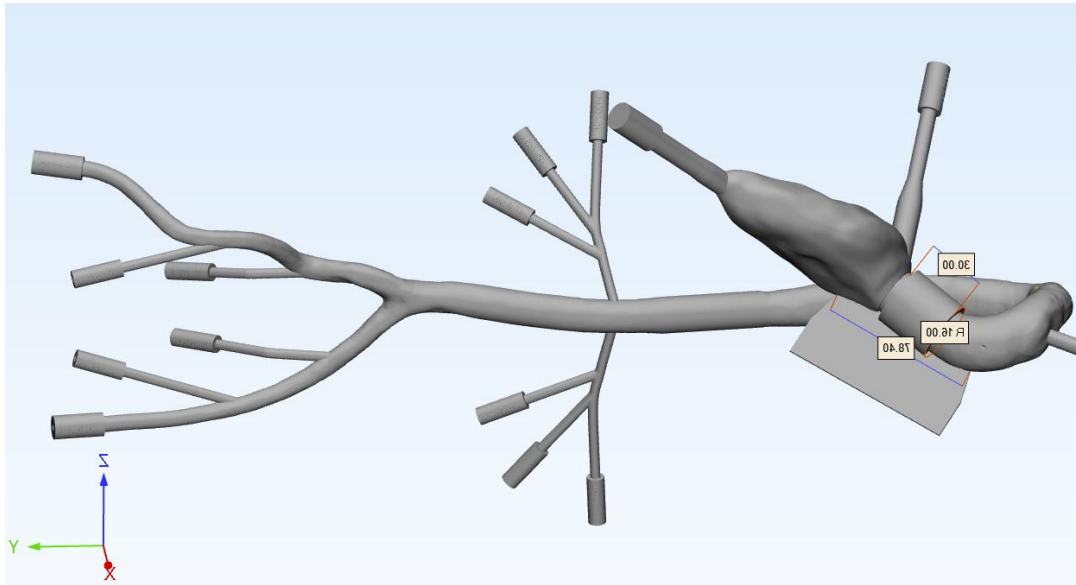
Figure 2.4 – CAD drawing of aortic model.
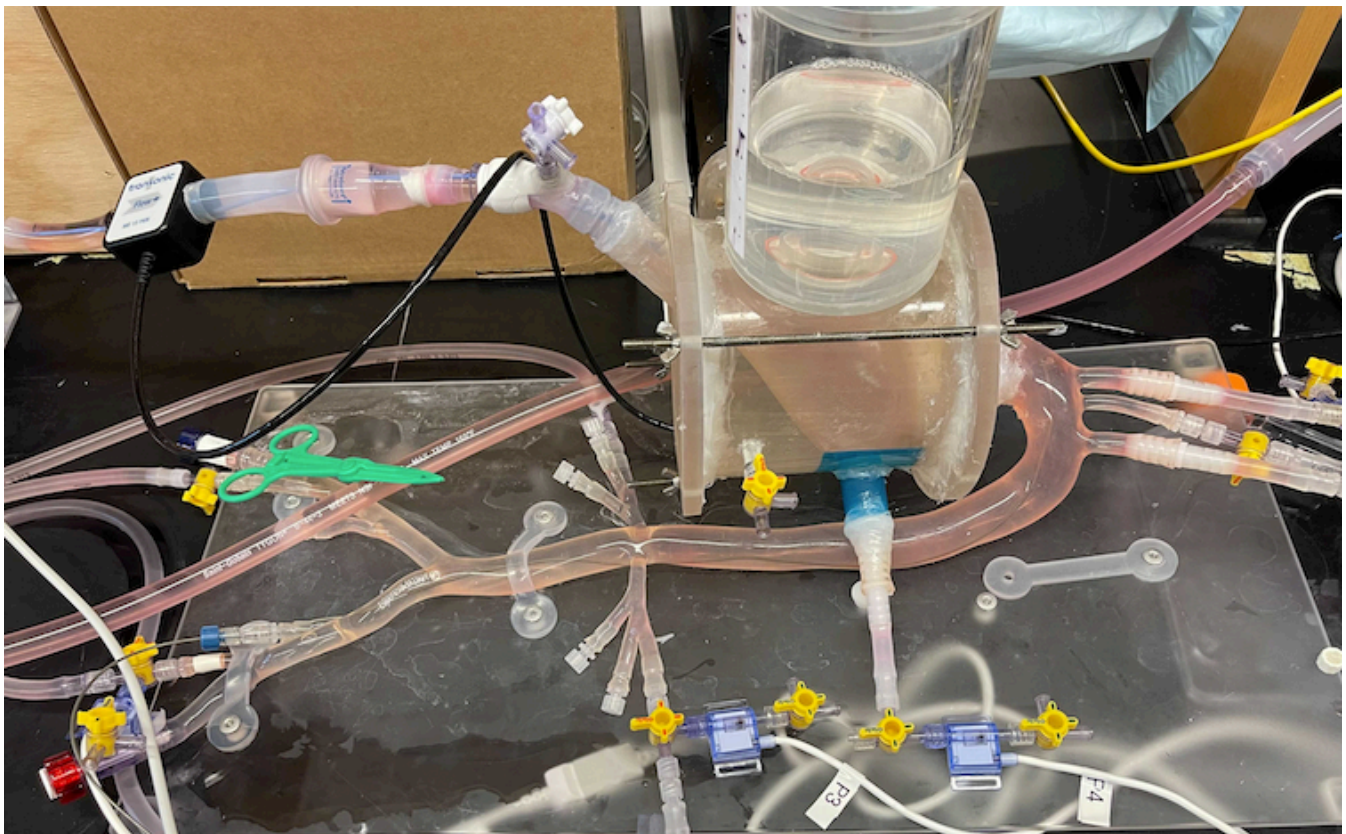
Figure 2.5 – Picture of the assembled flow loop in its final configuration.

2.2.2 Vessel Resistance Quantification

Outlet resistance is a major determinant of flow and pressures throughout the arterial tree. The summation of systemic resistance results in systemic vascular resistance (SVR) which drives cardiac afterload and affects ventricular-vascular coupling dynamics. Our mock circulatory loop has 7 major outlets corresponding to the native brachiocephalic, left common carotid, left subclavian artery, right and left renal, right and left iliac arteries. These specific vessels were included in the aortic model for the analysis of resulting flows to the cerebral and renal circulation with the introduction of MCS devices, and quantification of perfusion changes with different support regimes. The iliac arteries were included for the introduction of acute MCS devices.

For proper assessment of flow through the arterial tree, outlet resistances need to be tunable to values that are proportional to each other according to physiologic ratios (for the creation of proper flow fractions through each outlet). Moreover, for study reproducibility, a method to record vessel resistance was needed. A method to calculate single outlet resistance was developed, using Doppler flow and straight tip catheter pressure. An in-house made tissue mimicking material (61) which mimics ultrasound characteristics of human tissue was wrapped tightly around the vessel of interest, and a doppler probe (Butterfly iQ, Burlington, MA) was used to scan the fluid flow profile. For proper doppler signal acquisition, a blood mimicking fluid with particles was used (PBS, water, glycerin, polyamide particles (5 um), Synperonic F108 surfactant, dextran). A straight tip pressure catheter (Ventri-Cath 510, Millar) was advanced into the vessel of interest. Using the Butterfly's iQ B-mode setting, flow waveform was obtained. Post processing was done to extract the upper half of the binary image which represents forward flow through the vessel, and doppler signal outlines were plotted (**Figure 2.6**).

Lastly, the extracted flow waveform and the recorded pressure waveform were time synchronized and plotted (**Figure 2.7**) and, using ohm's law $dP = Q * R$, vessel resistance was

estimated. This process is then repeated for in outlets, for mapping of the relative resistances of each outlet.
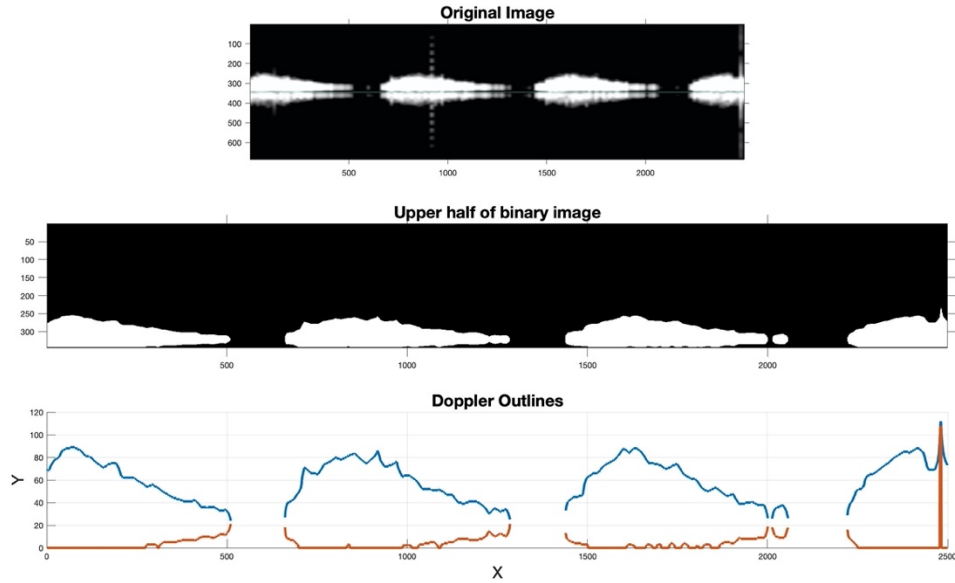
Figure 2.6 – Ultrasound Doppler measurement of flow. *Top panel shows the original image obtained from the Butterfly iQ probe. Middle panel shows the conversion of the flow signal to a binary image. Bottom panel shows the extraction of the flow waveform (blue).*
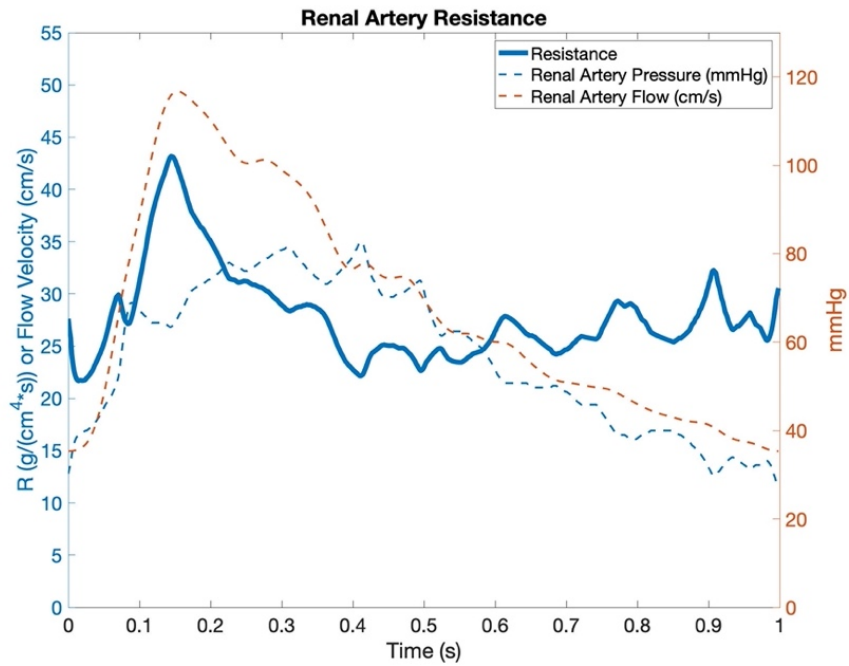
Figure 2.7 – Renal artery resistance plot*. Dotted lines represent measured pressure (blue) and flow (red). Flow is measured using the doppler probe as described above. Solid line represents the calculated resistance using an ohmic relationship.*

2.2.3 Mechanical Support Device

The flow loop is versatile and permits the implantation of one or more MCS devices. Initially an Impella CP (Abiomed Inc., Danvers, MA) was introduced through the femoral artery and threaded into the LV. The Impella was connected to the automated Impella controller (AIC) and operated normally. CO calibration algorithm (**Figure 2.8**) was used and was accurately able to measure flow in the system.
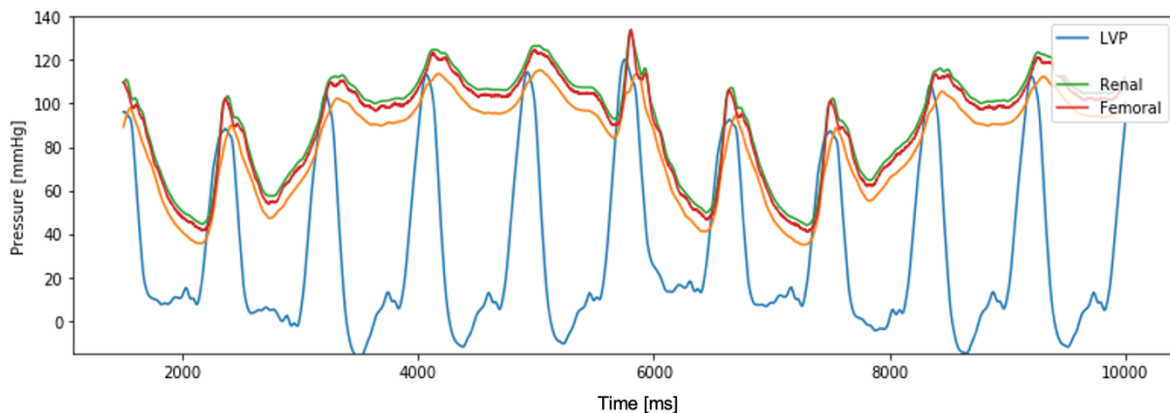
Figure 2.8 - Cardiac output calibration mode in the Impella was successfully achieved in the loop.
Demonstrating stability of the generated signals in the loop as well as parameters within physiologic range – calibration process uses pressure, systemic resistance, and compliance to calculate flow. If any of the parameters are out of range calibration fails. Alternating pressure signals are caused by the calibration algorithm.

An ECMO circuit (Medtronic BioMedicus 550 Centrifugal Pump) was then used in VA-ECMO configuration. A withdrawal cannula was place in the reservoir and a return cannula was introduced through the femoral artery. Initial "native" CO was set, followed by adjustment of ECMO RPM to achieve a predetermined total circulatory flow (net CO *plus* ECMO). Once ECMO is initiated, "native" CO might decrease due to the increased afterload in the system, and the ViVitro Superpump's gain is adjusted accordingly.

Boluses of dye were injected continuously into the return line for visualization of the mixing zone (MZ) region. A Straight tip pressure catheter was advanced into the descending aorta to record pressure waveforms proximally and distally from the MZ. Outlet resistances were adjusted, and flow visualization was repeated. Experiments were repeated at multiple native CO to ECMO flow ratios.

Lastly, a proof-of concept Ecpella (VA-ECMO circulatory support and LV venting with Impella) showing the ability to implant and operate both MCS simultaneously was successful. A pressure-volume catheter was placed in the LV for PV loop generation. Future studies will use this capability for the quantification of the effect LV venting cardiac and vascular mechanics.

2.3 Results

2.3.1 Left Ventricular Waveform and Hemodynamic Control

Careful interrogation of the recorded waveforms, and numerous design iterations, led to the achievement of desired arterial waveforms. Experiments were then done to fine tune specific hemodynamic features. These included the incisura in the aortic pressure waveform, which arises with proper closure of the aortic valve, and an upslope in LV pressure during diastole, due to filling of the ventricle and an atrial "kick". The former is of importance when using cardiac output calibration in the Impella CP and the analysis of reflected pressure waves, and the latter would affect LVEDP estimation and diastolic assessment algorithms. **Figure 2.9** displays output pressure waveforms recorded in the model with reduced CO and ECMO support. Systolic pressure in the distal arteries is amplified possibly due to reflected waves, and A dicrotic notch is evident in the proximal vessels.

Further interrogation of the flow loop, while working on titrations of pressures and flows to specific experimental set points, revealed the complex dynamics of the loop's input parameters, motivating a systematic study. Key findings revealed:

- HR (BPM) is the strongest determinant of LV and proximal aortic pressure waveform shape (**Figure 2.10**). The dynamics of compliance and capacitance impose limitations on the system, and these limitations have a physiological basis. Specifically, heart rate plays a crucial role in the cardiac cycle, regulating the balance between diastole and systole. It significantly impacts diastolic filling, whereas its impact on systolic ejection is relatively minimal.

- Outlet resistance, particularly at the proximal outlets (aortic arch), has second most dominant effect (**Figure 2.11**).

- Systole duration (percent of total beat cycle) has only modest effect.

- "Inotropy" (max motor forward speed at systole) has only modest effect.

- SV is not directly determined by the length of motor piston draw. Instead, controlled by the factors governing LV waveform, i.e. LV compliance, HR, systole duration, and inotropy.
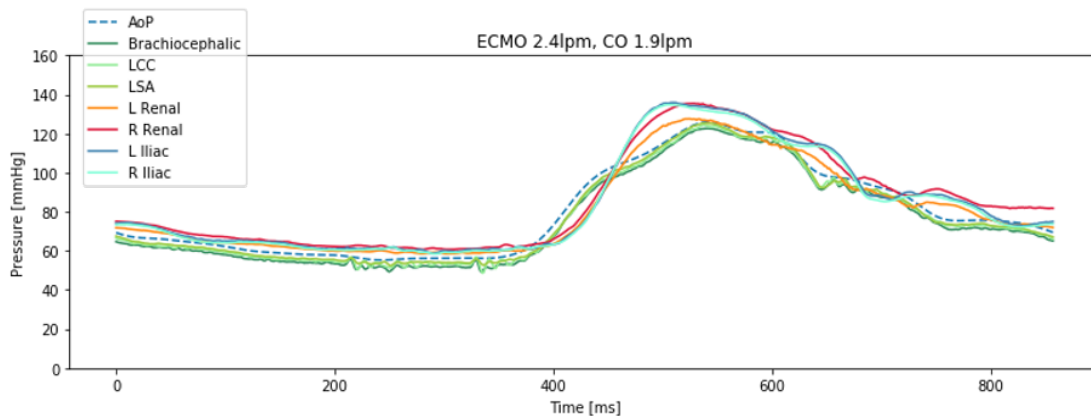
Figure 2.9 – Recorded pressure waveforms with reduced cardiac output and VA-ECMO support. *AoP – aortic pressure; LCC – left common carotid; LSA – left subclavian artery; L/R renal – left and right renal arteries; L/R iliac – left and right iliac arteries.*
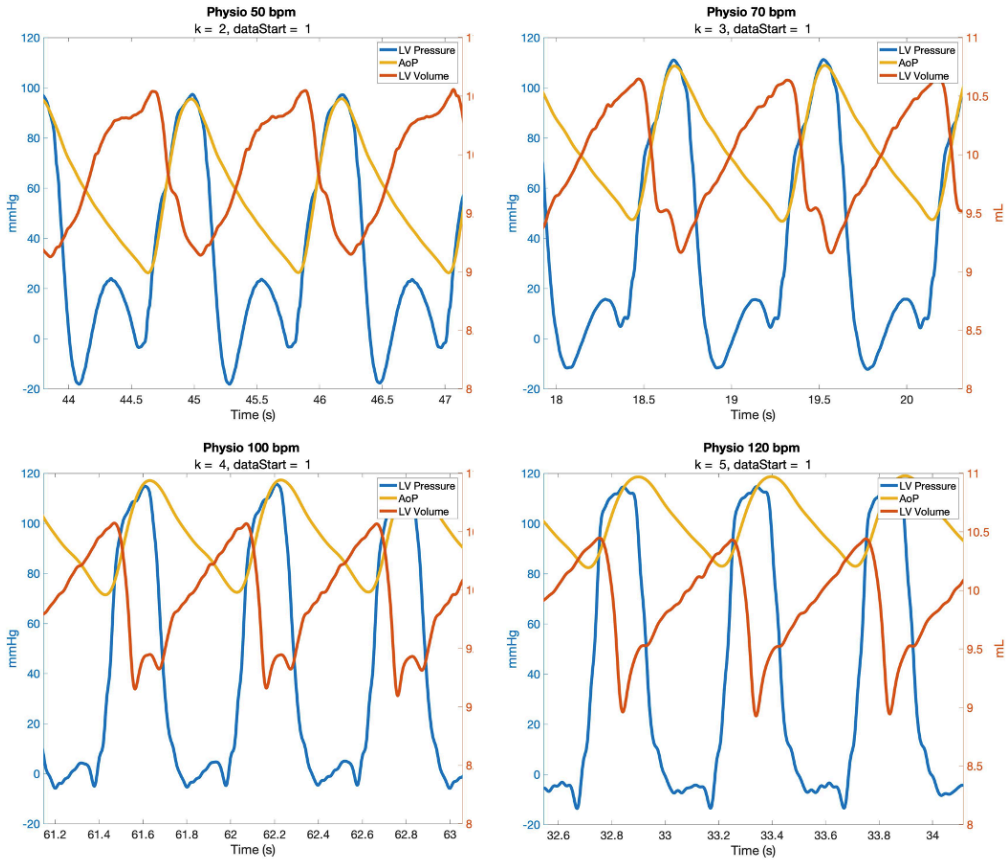
Figure 2.10 – Effect of heart rate frequency (BPM) on pressure and volume waveforms. *Left ventricular pressure (blue) and volume (red); Aortic pressure (yellow). The 4 panels show change in frequency alone (top left – min frequency, bottom right – max frequency) and its effect on ventricular and vascular dynamics.*
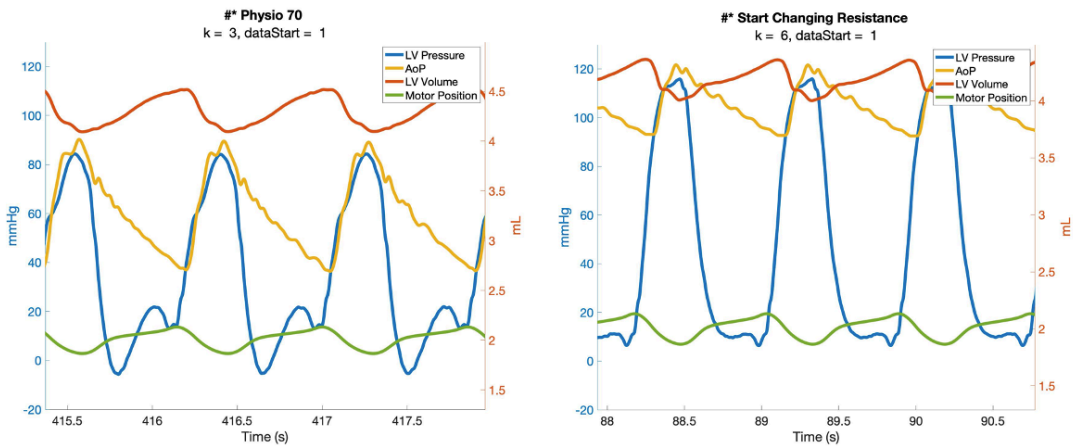
Figure 2.11 – Effect of proximal outlet resistance on pressure and volume waveforms. *Left panel – low resistance; Right panel – high resistance.*

2.3.2 Mixing Zone Region Dynamics

In a series of studies using VA-ECMO configuration with reduced CO, the mixing zone (MZ) region consistently landed in bifurcation regions. Specifically in our model, at the Renal arteries or the proximal arteries (in higher ECMO flow rates) bifurcating from the aortic arch. Initially, native CO and ECMO flow were set to 2 lpm each, and, using flow visualization, the MZ region was observed at the renal arteries (**Figure 2.12**). Next, CO was reduced and ECMO flow was increased at ~0.5 lpm intervals, keeping total flow constant, the MZ region remained in the renal arteries. Only when reaching ~85% of total flow with ECMO the MZ moved to the proximal arteries. MZ did not locate at any point in the descending aorta.
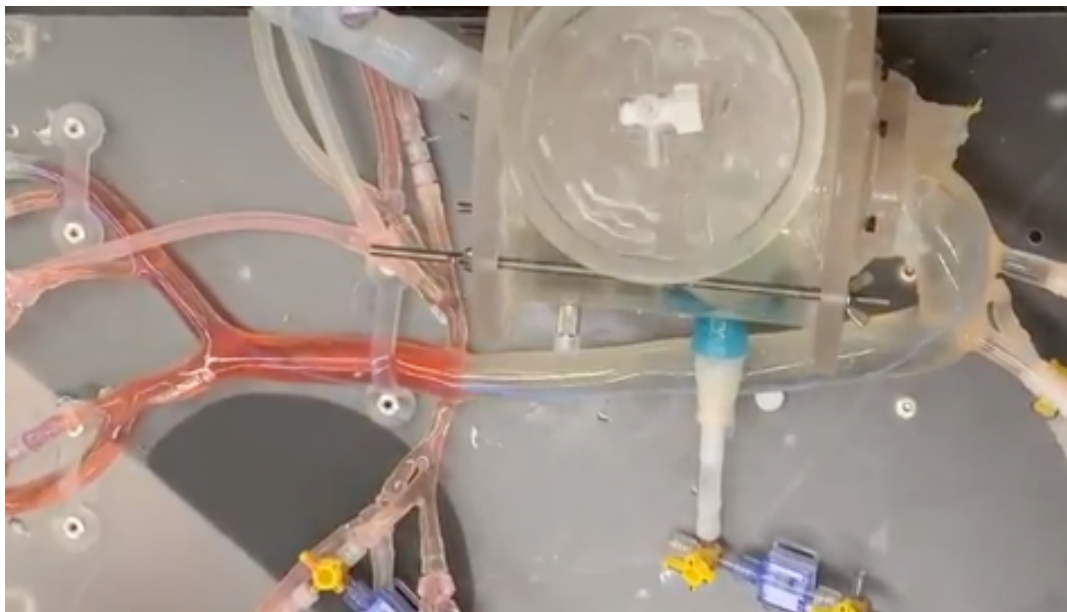
*Figure 2.12 – **Mixing zone (MZ) visualization**. Residual native CO driving forward flow, and ECMO inflow introduced through the femoral artery creating a MZ in the renal arteries. Clear fluid is native CO and red colored fluid is the oxygenated flow coming from the ECMO.*

A following study was performed, repeating the fractional flows that were measured in the initial study, with increased renal arteries resistance. The tube resistors created an obstruction to flow of ~50% of the original lumen. In this configuration, VA-ECMO fractional flow of as low as 40% led to MZ location in the aortic arch (**Figure 2.13**).
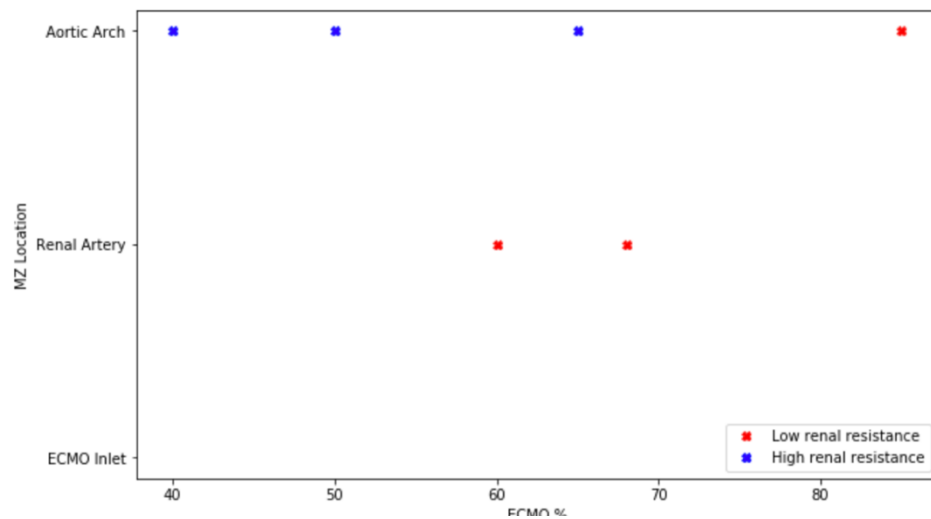
Figure 2.13 – Mixing zone (MZ) location as a function of ECMO fractional flow and renal artery outlet resistance.

In comparison to a CFD study done in our lab (**Figure 2.14**), with similar flow input parameters (ECMO flow fraction), the same pattern was noticed (47). This result raised the hypothesis that the MZ region is strongly affected by anatomy, and thus with similar flow configuration different patients can get different resulting perfusion patterns.
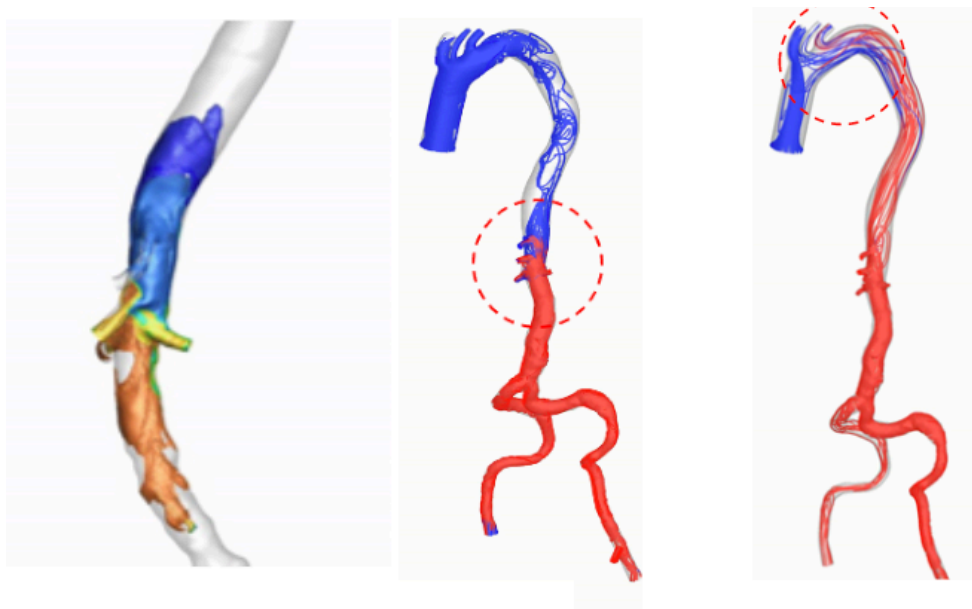
Khodaee et al, CBM, 2021

Figure 2.14 – *Computational fluid dynamics confirm mixing zone (MZ) dynamics.* *In these studies, MZ also appears in bifurcations, and is dependent on ECMO fractional flow and vessel anatomy.*

2.4 Discussion

Using a benchtop model of an anatomic ventricle and aortic tree, with VA ECMO support at varying native CO, we found that MZ region resides in arterial bifurcations. The MZ specifically settle at points of flow separation and are not seen along a continuum. Moreover, vessel anatomy and **resistance** are main determinants of MZ location. Our model includes 2 possible regions for the MZ to settle in – renal arteries or the aortic arch. By experimentally modifying outlet resistance with steady VA-ECMO fractional flow, we were able to show how MZ location is binary (in this case, due to model anatomy) and not a linear continuous phenomenon.

The MZ region arises with the use of VA-ECMO when some native pulsatility is preserved, and forms when retrograde flow from the return cannula into the aorta collides with the forward flow from native CO. In patients, the blood arriving from the ECMO circuit is oxygenated, and the

blood coming from the native heart might be de-oxygenated due to an underlying pulmonary condition. As such, if the MZ resides distally, in the descending aorta, the brain (and upper torso) might not be getting oxygenated blood. The differences in oxygenation provide variegation in appearance of the skin reflected in the terms North-south or Harlequin syndrome. The location of the MZ is not well understood clinically, but since it affects aortic pressure patterns, and thus perfusion, it is critical to understand the mechanisms that govern this phenomenon.

Our benchtop model enabled a mechanistic and simplified opportunity to interrogate the behavior of the MZ. Owing to the fraction of aortic bifurcations compared to human anatomy, it became clear that our initial hypothesis, of a linear relation between fractional ECMO flow to MZ location, was disputed. In this set of experiments, we varied the fractional flow coming from the native heart vs. the ECMO circuit. While Total volumetric flow was preserved, the ratio between flow sources was changed by 0.5 lpm increments in each flow source setting (i.e. 3.5 lpm native heart and 0.5 lpm ECMO, 3 lpm native heart and 1 lpm ECMO, and so on). Using bulk flow visualization, the MZ was visualized in each fractional flow setting. The visualizations revealed that the MZ does not move linearly through the aorta depending solely on fractional flow ratio. The MZ consistently emerges in bifurcations and moves in a stepwise fashion between adjacent bifurcations when a threshold is met. In a subsequent set of experiments, fractional flows were repeated with an increased renal artery resistance (50% lumen obstruction). As before, MZ location was noted to move in a stepwise fashion, however the threshold for the movement between the renal arteries and the aortic arch arrived earlier, at 40% ECMO flow.

These data confirm that MZ emerges at a location of flow separation, that allows for release of the increased mass and pressure by **venting through an outlet** (**Figure 2.13**). **Thus, MZ location is dependent on anatomy and vessel resistance.** The MZ is stationary when titrating ECMO flow, and there exists a threshold for the movement of the MZ to the next anatomical

bifurcation. These results were also shown in a CFD model (Figure 2.14). We hypothesize that in mammalian anatomy, having many bifurcations, the MZ location will behave likely **Figure 2.15**, in
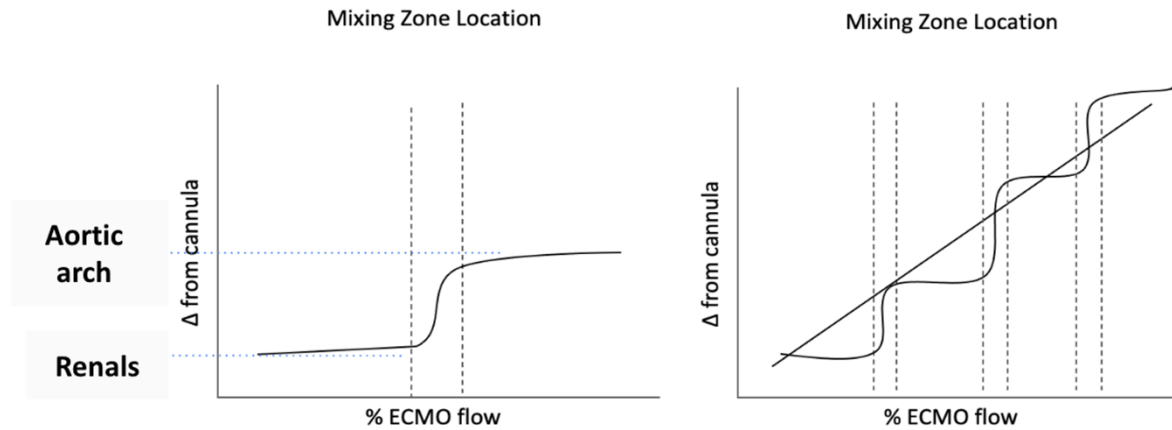
Figure 2.15 - Schematic of mixing zone (MZ) location as a function of ECMO fractional flow. Left panel – results in the flow loop or a computational fluid dynamics simulation, where the modeled geometry includes two regions of bifurcations. Right panel – projected MZ behavior in a section of interest in an anatomical vessel, with multiple bifurcations.

a stepwise manner including more frequent steps.

Furthermore, **resistance** is inversely proportional to the 4th power of the radius (Hagen Poiseuille principle), thus we hypothesize that small bifurcating arteries will not play a major role in providing a relief of pressure in the MZ. These results will need to be validated in an animal model.

When examining the control volume depicted in Figure 2.16 – total in-flow **Error! Reference source not found.**is given by:

$$Q_{ECMO} + Q_{CO} = Q_{outlets}$$

Total flow out of the control volume is given by:

$$Q_{outlets} = Q_1 + Q_2 + Q_3$$

Using lumped parameter model for the dynamic boundary conditions - the following equation relates pressure and flow rate at the outlets:

$$Q_{ECMO} + Q_{CO} = Q_1 + Q_2 + Q_3 = \frac{dp_1}{dt} + \frac{p_1}{C_1 R_{d1}} + \frac{dp_2}{dt} + \frac{p_2}{C_2 R_{d2}} + \frac{dp_3}{dt} + \frac{p_3}{C_3 R_{d3}} =$$

Figure 2.16 - Control volume (dashed red) for flow analysis. Inlet flows - Q_{1i} is pulsatile CO input; Q_{2i} is constant ECMO flow. 1,2,3 (red) outlet flows.
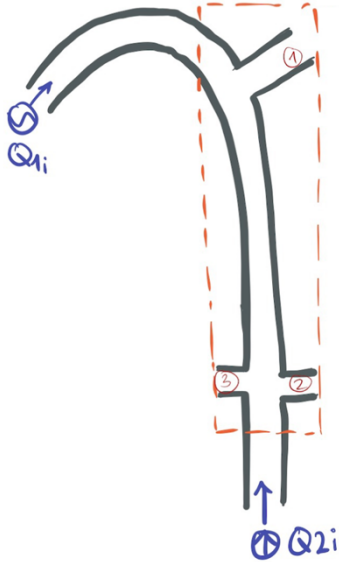
$$\frac{Q_1}{C_1}\left(1 + \frac{R_{p1}}{R_{d1}}\right) + R_{p1}\frac{dQ_1}{dt} + \frac{Q_2}{C_2}\left(1 + \frac{R_{p2}}{R_{d2}}\right) + R_{p2}\frac{dQ_2}{dt} + \frac{Q_3}{C_3}\left(1 + \frac{R_{p3}}{R_{d3}}\right) + R_{p3}\frac{dQ_3}{dt}$$

Where Q – flow, C – compliance, Rp – proximal resistance, Rd – distal resistance.

The last equation shows the dependence of flow on both proximal and distal outlet resistance, explaining, as expected, how the location of the MZ (venting of the two colliding input flows) is affected by vessel resistance.

The study and results described above provide an example of the capabilities a benchtop flow model can provide for studying, in a mechanistic way, complex physiological phenomena. The limitations of each model need to be clearly stated and the question at hand needs to be specified in a manner that its results are not skewed by the limitations and assumptions of the model.

For example, our in-vitro ECMO studies were coupled with CFD simulations in our lab, aiming to harness the advantages of each model and to validate the CFD. Specifically, the study sought to quantify the effects of hybrid flow on cardiac load. However, the benchtop aortic model is compliant while the CFD has rigid walls. Ventricular and vascular energetics are deeply altered by arterial elastance and as such, the assumptions and limitations of the two modeling techniques do not agree. Further studies will be conducted, to iteratively solve an optimization problem for

the CFD's boundary conditions, to create the proper lumped compliance and resistance to recreate the mock loop resulting hemodynamics.

2.5 Conclusion

The design of this flow loop, enabling replication of physiological and pathological hemodynamics in an anatomically correct compliant aorta, provides a testbed for quantification of changes in aortic perfusion with and without MCS devices. Our flow loop also enabled testing of hemodynamic patterns emerging from the use of other implantable devices (e.g. soft robotic sleeve mimicking aortic stenosis) – where accurately capturing pressure waveforms is crucial (62).

MZ location is determined by **flow fraction (native heart and MCS flow), anatomy,** and **vessel resistance.** A systematic evaluation of the MZ with varying flow fraction in an animal model is needed to verify these trends in a mammalian aortic anatomy. Moreover, the effects of vasoactive drugs (vessel resistance changes) on the location of the MZ could be quantified and are of clinical relevance. Further studies in the benchtop flow loop will be essential for quantifying the associated changes in perfusion proximally and distally from the MZ and its implications. Ultimately with the goal of predicting the location of the MZ based on measured signals in the VA-ECMO console (changes in machine afterload, pressure and flow).

Additional MCS mechanistic studies with specific questions that harness the flow loop's advantages, and agree with its limitations, will benefit from the ability to tightly regulate system inputs independently. It enables quantification of hemodynamic changes with initiation or titration of MCS devices. As well as provide "noise-free" environment to interrogate device signals for the development of advanced clinical evaluation metrics. The use of MCS for support while gaining insight into cardiovascular state at the same time, can assist in optimizing device use, predict end-organ perfusion and support hemodynamic stability.

Chapter 3: Effects of Continuous-Flow Mechanical Circulatory Support Devices on Ventricular-Vascular Coupling

Abstract

In this chapter we examine the effects of mechanical, pharmaceutical interventions and pathophysiologic states, on ventricular-vascular coupling (VVC) using a porcine cardiogenic shock model. Motivated by the hypothesis that by determining the optimal VVC for a given state, could reduce load on the failing heart, we evaluated changes in end-systolic pressure-volume relationship (ESPVR), arterial elastance (Ea), stroke work (SW) and load-dependent contractility.

A range of inotropic and vascular states were studied through pharmacological and mechanical interventions which showed that continuous flow intracardiac devices reduce preload, LVEDP, SV, SW, end-systolic pressure, and ESPVR, and its slope Ees show minimal response, as expected. However, arterial elastance increases with initiation of support. In state of CS we observed reduction in SV, SW, end-systolic pressure and Ees with increased LVEDP all commensurate with reduced contractility and increased arterial elastance slope. Thermodynamic efficiency of the LV was severely impacted and reduced.

VVC metrics might be a helpful framework by which to evaluate and optimize the degree of pharmacological in combination with mechanical support for a given CS state. Evaluation of VVC remains challenging in a clinical setting, and further development of VVC metrics, from MCS signals could greatly aid in decision making.

3.1 Introduction

In health, the heart and the vasculature are coupled to provide optimal energetic transfer between the heart - specifically the LV's work - and vascular blood flow. With aging and in pathological states this relationship is altered, making the LV work harder than the resulting output that is needed to get adequate systemic perfusion (63–66). When introducing mechanical circulatory support (MCS) which, by virtue of its function deeply alters hemodynamics, it further decouples the heart and the vasculature. Specifically, it decouples classical supply and demand - augments supply, and based on the modality, might alter demand as well. Better understanding of hybrid hemodynamics and device titration might be beneficial for utilizing MCS to shift the system towards a healthier coupling state, with or without concomitant pharmaceutical intervention.

Classically, Ventricular vascular coupling (VVC) considers the aorta as a 3rd chamber, creating one chamber with the LV during systole, and decoupling during diastole.

*Figure 3.1 - **Pressure Volume loop and bounding curves.** EDPVR - end diastolic pressure volume relationship (green curve) – ventricular compliance; ESPVR – end systolic pressure volume relationship (orange curve) and its slope Ees – end systolic elastance, considered an index of contractility; Ea – arterial elastance.*

Ventricular function is constrained by elastance of the ventricle and the arterial system, and arterial elastance is determined by vascular tone (resistance and compliance). Put together, Cardiac performance is dependent on ventricular-vascular coupling (67). The pressure-volume (PV) loop

(Figure 3.1), depicting cardiac function in a thermodynamic framework, is bound by 3 curves. These curves represent the envelope in which the ventricle operates: end systolic pressure-volume relationship (ESPVR), end diastolic pressure-volume relationship (EDPVR), and arterial elastance (Ea). The ratio Ea/ESPVR is a measure of VVC, and in health |Ea/Ees|--> 1.

We hypothesize that by optimizing VVC for a given state, through hemodynamic optimization and ventricular energetics, we could reduce load on the failing heart and thus favor LV recovery. Although VVC has been studied extensively in health and in the ageing cardiovascular system (66,68), the effects of shock (39), and the implantation of MCS on these metrics have been rarely described. They can provide a framework to determine cardiovascular state and describe changes in arterial elastance with initiation of support. All of which might inform afterload management for CS patients - determine degree of support with or without pressors using VVC metrics. This set of studies aim to show mechanistically what might be beneficial for a given patient state, increase of support and/or drug intervention.

Towards this goal, we used a CS porcine model to evaluate the effects of different physiologic states on VVC and how the initiation of MCS further alters VVC in these states. The model included pharmacologic interventions (Table 3.1) mimicking a range of pathologic and therapeutic states, which were then repeated in presence of an MCS. Changes in ESPVR, Ea and VVC were quantified as well as stroke work (SW) and load-dependent LV contractility.
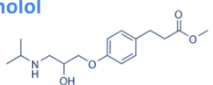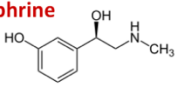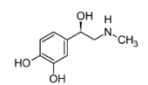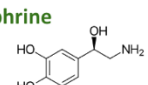
Drug	α - Vasoconstrict	$\beta1$ - ↑Contractility	$\beta2$ - Vasodilate
Esmolol	0	Blocker - - -	0
Phenylephrine	++++	0	0
Epinephrine	++	++++	++
Norepinephrine	++++	+++	0

Table 3.1 – Pharmacological interventions used in the animal model. Except for Esmolol (a beta blocker) that was used to induce further inotropic compromise, all other drugs are vasoactive/inotropes used in the clinic for CS support.

3.2 Materials and Methods

We used an acute porcine cardiogenic shock (CS) model that was developed in our laboratory (69,70). This model is utilized for research which mainly focuses on quantifying the effects of MCS implantation on shock physiology and optimizing methods to monitor physiology with indwelling devices.

In this chapter I will bring together results from multiple sets of studies, to study the effects of mechanical and pharmaceutical interventions, as well as pathophysiologic states on VVC. All studies start with an acute CS porcine model, but subsequent interventions vary.

3.2.1 Porcine Cardiogenic Shock Model

~70 kg young adult male Yorkshire swine were used for the assessment of cardiovascular response and quantification of changes in the cardiovascular system induced by MCS implantation. All animals were maintained in accordance with National Institutes of Health (NIH) and

Association for Assessment and Accreditation of Laboratory Animal Care (AAALAC) guidelines (CBSET, Lexington, MA); body temperature, oxygen saturation, and electrocardiogram were continuously monitored for the duration of the studies. Anesthesia was induced via intramuscular injection of Telazol (6 mg/kg) and maintained using inhaled isoflurane after intubation.

A pressure–volume catheter (Millar, Houston, TX), placed via the left carotid artery, measured continuous LVP and volume. Additional catheters and sheaths were introduced for pressure monitoring – including aortic, pulmonary artery, central venous, femoral artery. Measurements of cardiovascular state (e.g. LV pressure, LV volume, EKG, aortic pressure, central venous pressure) were recorded continuously and monitored in real time through a data acquisition system (ADInstruments, Dunedin, New Zealand). Contractility, LV energetics and vascular metrics were calculated retrospectively. Once animal setup is completed, a set of baseline measurements is done, used for calibrations and quantification of the change in physiologic state when the animal reaches CS state.

A balloon catheter was introduced through the right femoral vein and into the inferior vena cava to enable a mechanical occlusion in the vein, which causes a quick preload reduction leading to a change in loading conditions on the LV. These data are used during post-processing for extrapolation of V_o, which is then used to calculate end systolic pressure volume relationship (ESPVR).

CS was achieved through induction of permanent local ischemia mainly in the left heart region. A Judkins guide catheter was advanced into the left anterior descending (LAD) coronary artery via the left femoral artery. Hydropearl microbeads (45-105 um in diameter; Terumo, Inc., Tokyo, Japan) were instilled in boluses (0.25 mL of microspheres mixed with 10 mL of isotonic saline and 10 mL of contrast) followed by re-assessment of the animal's cardiovascular function.

Microbead instillation was continued until left ventricular end diastolic pressure (LVEDP) exceeded 16 mm Hg and either the mean arterial pressure (MAP) decreased below 50 mm Hg, mixed venous oxygen saturation (MvO_2) was less than 55% or the TDCO was less than 50 ml/kg/min, or with clear evidence of LV decoupling. Upon reaching this physiological state, a new experimental baseline was established for each animal.

3.2.2 Mechanical Circulatory Support

An Impella CP was placed into the left ventricle via the right femoral artery. Appropriate placement and aortic valve competency were monitored via fluoroscopy. Each condition was assessed at two Impella speeds - P-3 and P-6, which are commonly used to avoid suction from high flow rates and retrograde flow during diastole. After desired level of support is set, real time monitoring was done to ensure hemodynamic stability and collection of data in the new steady state. Once hemodynamically steady, consecutive two minutes of data are recorded and labeled to be analyzed retrospectively.

For the studies which results are described in section 3.3.2 and 3.3.3 in this chapter, please see modification of MCS regime methods in chapters 4.2 and 5.3 respectively.

3.2.3 Pharmacological Interventions

A range of inotropic and vascular states were studied in this set of experiments, achieved by pharmacological and mechanical interventions. Aiming to quantify and studying VVC response in pathophysiological conditions, and specifically the effects of MCS implantation on this ratio. Pharmacological interventions include mainly drugs that are commonly used in the clinic for CS patients with the goal of hemodynamics stabilization, without or in conjunction with MCS. Table

3.1: Phenylephrine – a vasoconstrictor, Epinephrine – a beta 1 agonist, causing an increase in inotropy as well as an alpha receptor agonist causing vasoconstriction and beta 2 agonist leading to a vasodilatory effect, and Norepinephrine – mainly alpha and beta 1 agonism leading to vasoconstriction and an increase in contractility. Lastly, Esmolol – a beta blocker, causing a decrease in inotropy (decrease in contractility) was used as a mean to simulate a depressed cardiac state. The Pharmaceutical interventions were delivered via the femoral venous sheath, during baseline, CS, and circulatory support. These interventions were repeated at the three states in order to capture the change in response. The drugs were delivered in boluses, dosing 1 µg/kg to induce positive inotropic and 1.8 mg/kg negative inotropic effects. Drugs were administered in baseline and at shock state at two levels of Impella support (P3 and P6). Between different drug bolus, proper washout was ensured by waiting according to the proper half-life, as well as hemodynamically monitoring for return to established baseline for each section.

3.2.4 Data Analysis

Recorded hemodynamic (pressures), ventricular pressure-volume data, electrocardiogram signals were imported to a custom python script developed for the analysis of cardiovascular state and thermodynamic analysis of LV energetics. Impella signals (motor speed, motor current, pressure) recorded during the studies were retrieved and time-synced to the recorded physiologic data. At each physiologic state, pressure-volume loops were plotted at end expiration to ensure consistency, and VVC metrics were calculated including end-systolic pressure volume relationship, arterial elastance, end-diastolic pressure-volume relationship. LV thermodynamic energetics were also calculated including stroke work, potential energy, and pressure volume area. For hemodynamic beat-to-beat calculations, two consecutive respiratory cycles were analyzed, and results were averaged.

3.3 Results

The effects of different MCS regimes on VVC metrics including, mechanical (pVAD) with and without pharmacological interventions (positive and negative Inotropes and vasopressors), retrograde constant flow circulatory support (VA-ECMO) and LV unloading in the setting of VA-ECMO support, with two unloading mechanisms.

3.3.1 Inotropic, Vascular, and Mechanical Interventions Effects on VVC

VVC metrics, specifically end-systolic pressure-volume relationship (ESPVR) and its slope (Ees), arterial elastance (Ea), VVC ratio and stroke work (SW) were calculated in the pressure-volume (PV) domain. Additional LV metrics including load-dependent LV contractility (dP/dt $_{max}$) and LVEDP were calculated from hemodynamic recordings for the corresponding beats. The metrics were evaluated in a range of physiologic conditions (induced pharmacologically and mechanically), and cardiovascular response was evaluated, examining fold-change from established baselines for each condition. The following data are plotted for a representative subject.
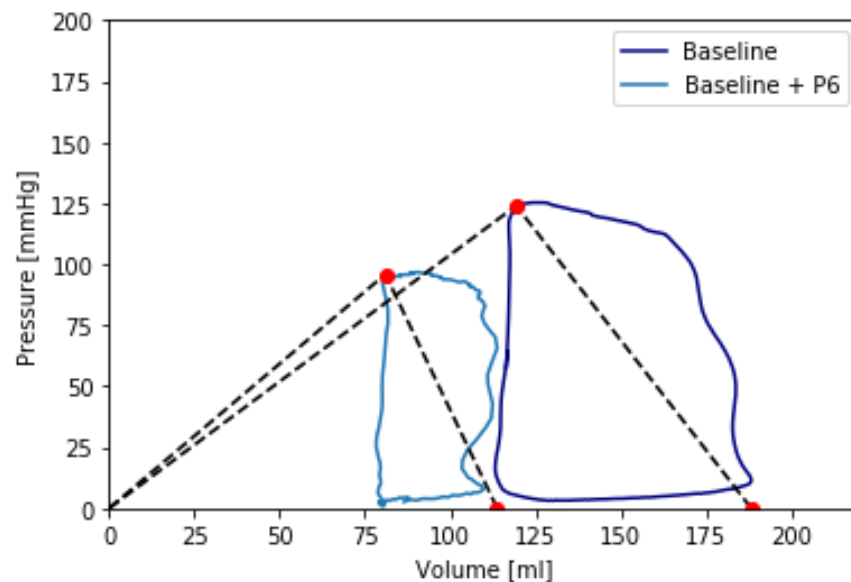
Figure 3.2 – Baseline pressure-volume loops. Plotted with ESPVR and Ea. Baseline (dark blue) and Baseline with Impella support at P6 (light blue).

In the intact cardiovascular system (Figure 3.2, Figure 3.5), initiation of continuous flow intracardiac device decreases preload, LVEDP, SV, SW, and end-systolic pressure. ESPVR, and its slope Ees show minimal response, as expected. However, arterial elastance increases by 22% with initiation of support (P3) and by 66% compared to baseline when augmenting to P6. Taken together, VVC ratio increases with increase of support. dP/dt_{max} mildly decreases with an increase of mechanical support. Examining baseline response to pharmaceutical interventions (Figure 3.3, Figure 3.4) reveals that increased support is neutral on contractility while increasing coupling ratio via arterial elastance changes.
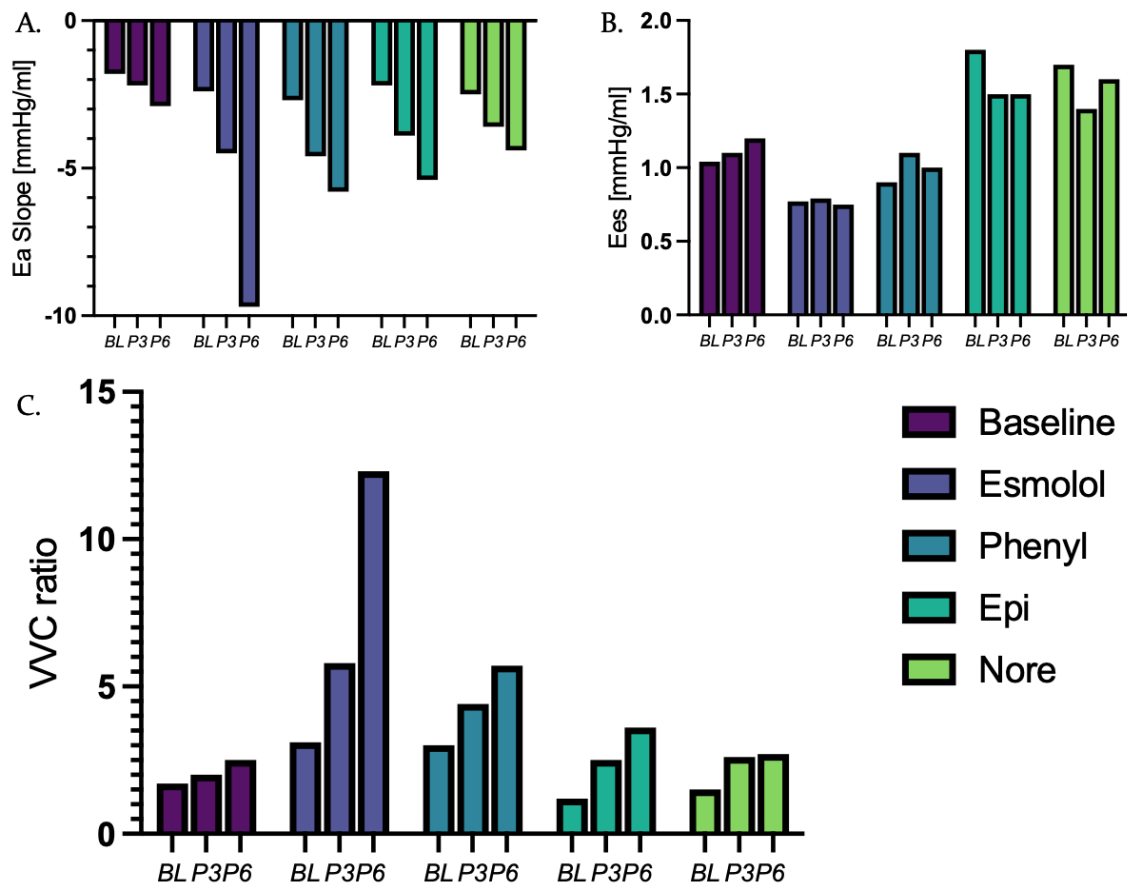
Figure 3.3 – Baseline VVC metrics response to increase of support, with pharmacological interventions in a representative animal. *A. Arterial elastance slope; B. ESPVR slope, Ees; C. Resulting VVC ratio.*
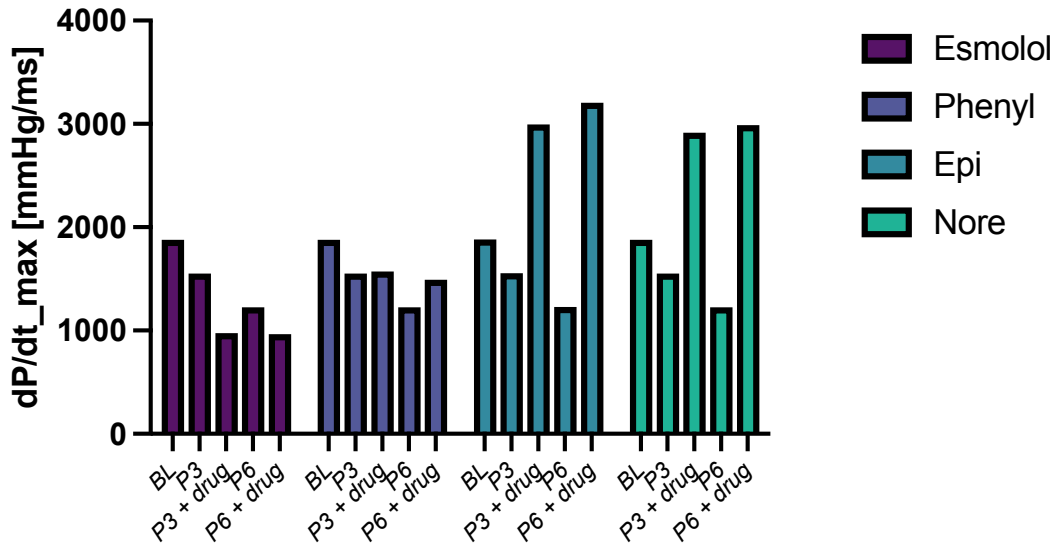
Figure 3.4 – Baseline load-dependent ventricular contractility response to increase of support with pharmacological interventions.
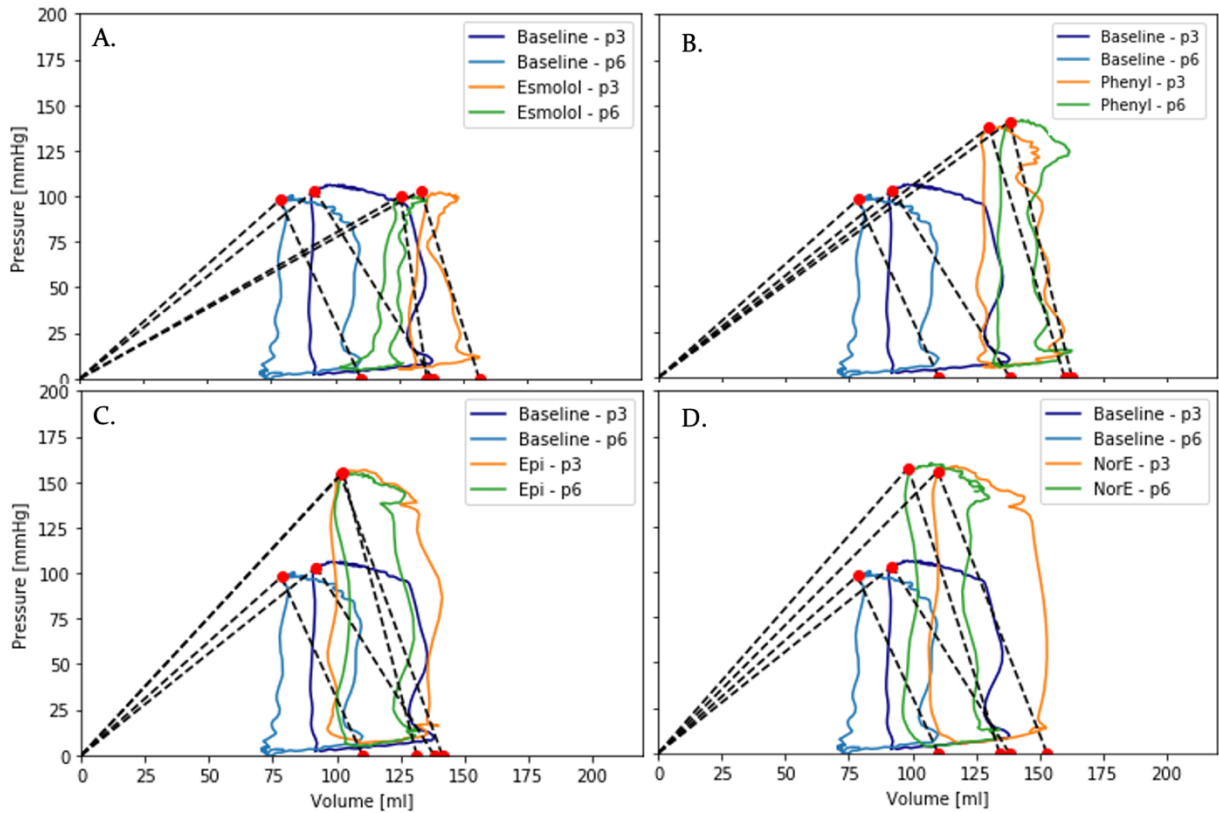
Figure 3.5 – Baseline pressure-volume loops for a representative animal at two support levels, and with pharmacologic interventions at the corresponding support levels. Changes in ESPVR, Ea, SV, SW and LVEDP are appreciated within each ramp for a given state.

In state of CS (Figure 3.6), SV, SW, end-systolic pressure and Ees decrease, contractility decreases and arterial elastance slope and LVEDP increases. The thermodynamic efficiency of the LV is severely impacted and reduced. When ramping Impella support from P3 to P6 there is an appreciable reduction in LVEDP and SV, affecting arterial elastance as well. However, Ees remains unchanged. In comparison to baseline, when Inotropes and vasoactive drugs are administered in shock state, an increase in support reduces contractility and loading and increases coupling ratio (Figure 3.7, Figure 3.8).
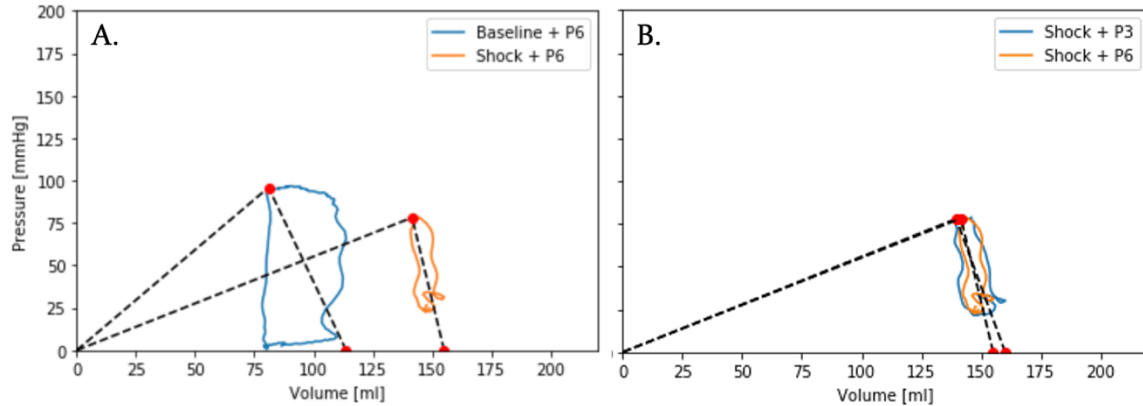
Figure 3.6 – Baseline and cardiogenic shock pressure-volume loops. *A. Baseline with support (blue) and shock with support (orange). B. Cardiogenic shock with low support (blue) and high support (orange).*
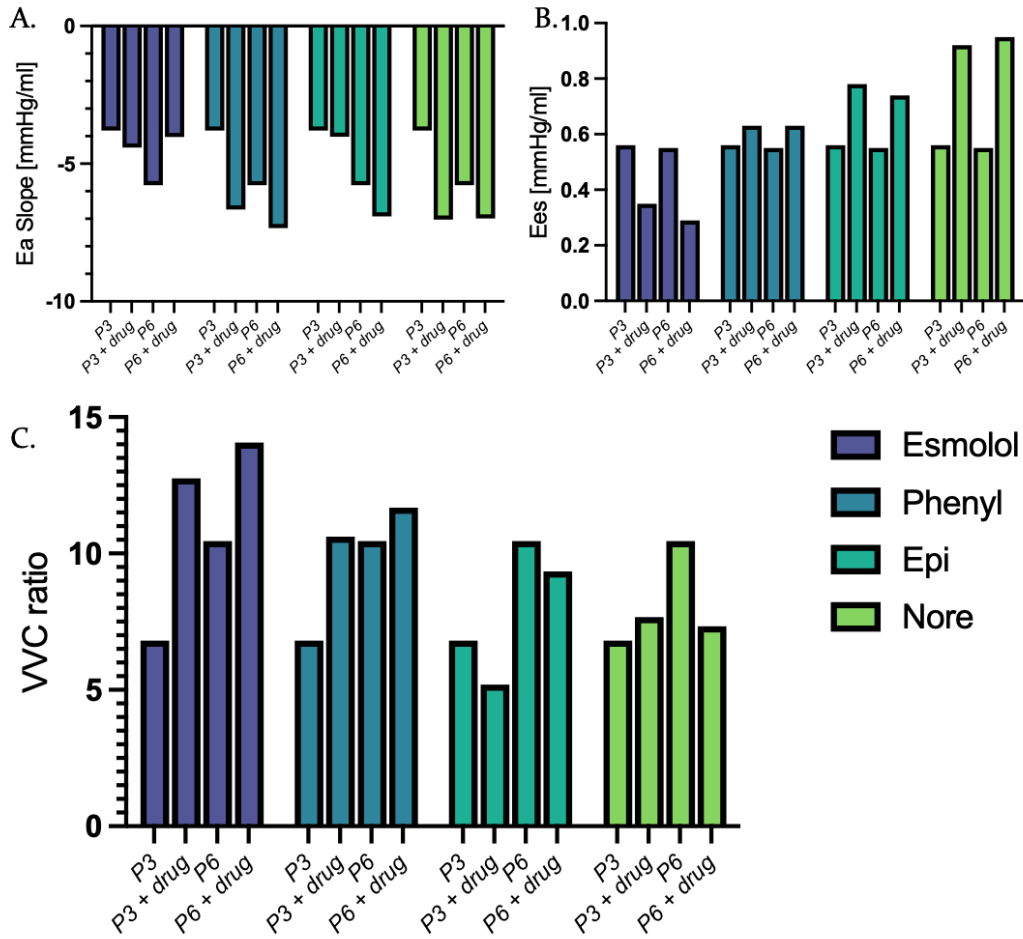
Figure 3.7 – Cardiogenic shock VVC metrics response to increase of support, with pharmacological interventions in a representative animal. *A. Arterial elastance slope; B. ESPVR slope, Ees; C. Resulting VVC ratio.*
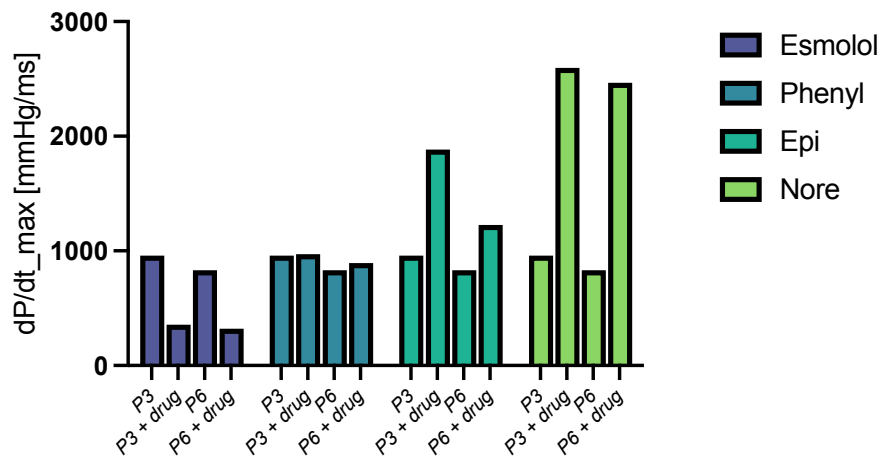
Figure 3.8 – Cardiogenic shock load-dependent ventricular contractility response to increase of support with pharmacological interventions.

3.3.2 VA-ECMO Effects on VVC

VA-ECMO effects on ventricular energetics metrics – in particular ESPVR, Ea, VVC and dp/dt $_{max}$ are displayed in Figure 3.9. As discussed in chapter 4 (physiologic response to VA-ECMO initiation and titration), the effect of ECMO initiation on VVC are variable among subjects. The changes in the metrics of interest varied depending on the cardiovascular state of the subject.

Interestingly, within the profound shock subjects (animals 3,4,6), VA-ECMO titration has little effect on VVC ratio. Within the mild CS group ECMO increases this ratio. We see a decrease in Ea slope as ECMO flow is titrated up in all animals to a certain degree.
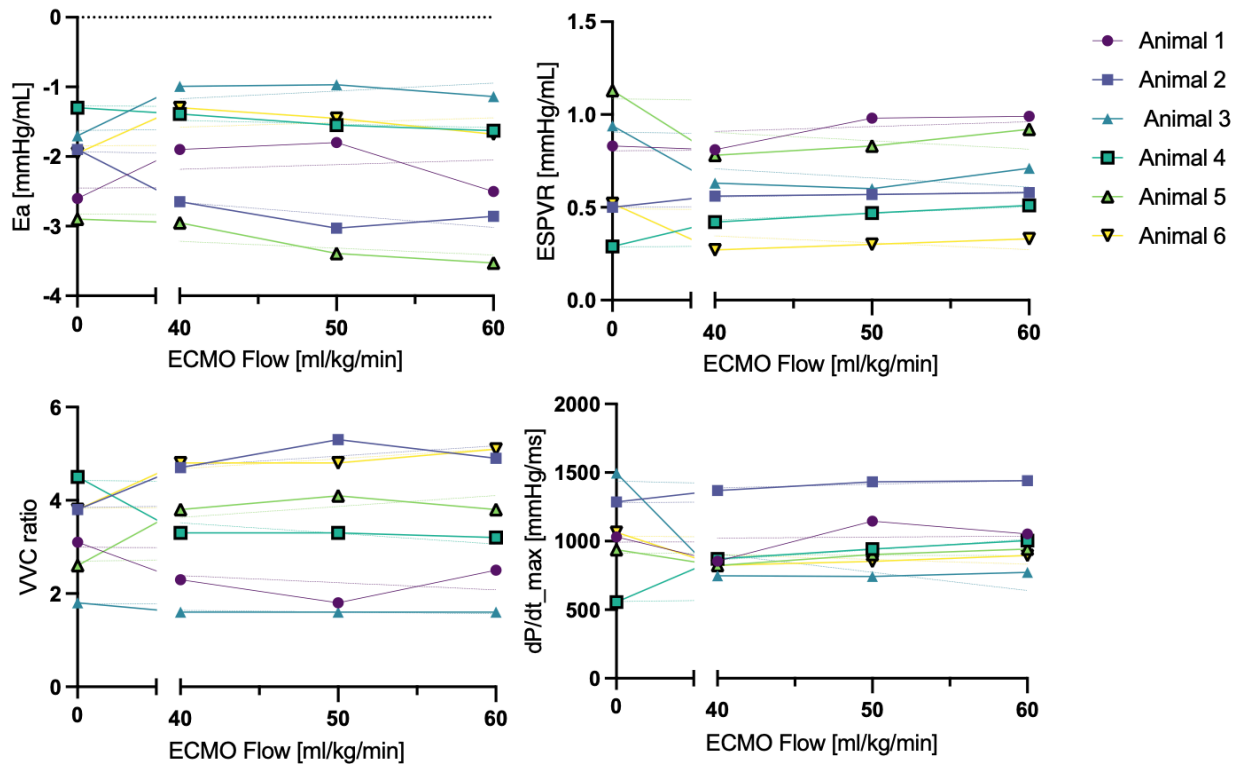
Figure 3.9 – Cardiogenic shock VVC metrics and load-dependent contractility. ECMO flow – 0, the origin denotes shock state with no support. 40-50-60 ml/kg/min are support ramps.

3.3.3 VA-ECMO mechanical unloading effects on VVC

VVC metrics were quantified and compared between VA-ECMO only support and VA-ECMO with two different LV unloading strategies – IABP and a pVAD (Impella CP). IABP showed to decrease VVC ratio overall mildly (Figure 3.10), driving VVC values lower towards more physiological values, decreasing by -9.5±3.5% from ECMO alone state. Results were uniform within the 3 subjects.

In the Impella group, results were dependent on initial shock state (further discussion in chapter 4). Overall, as support level increased, VVC values increase, showing once again a decoupling effect Figure 3.11 A. For all animals, Figure 3.11 B. shows that regardless of initial state, as P levels increase VVC increases (within a P level ramp). However, in this group the variability of the effect on VVC was greater - in one of the subjects, the initiation of Impella reduced VVC values in all ECMO states when initiating Impella using P2 through P6. When reaching P8, highest level of support studied in this experiment, VVC increased by 6-36%. In the two other subjects, VVC increased by 13-40% and by 48-180%.
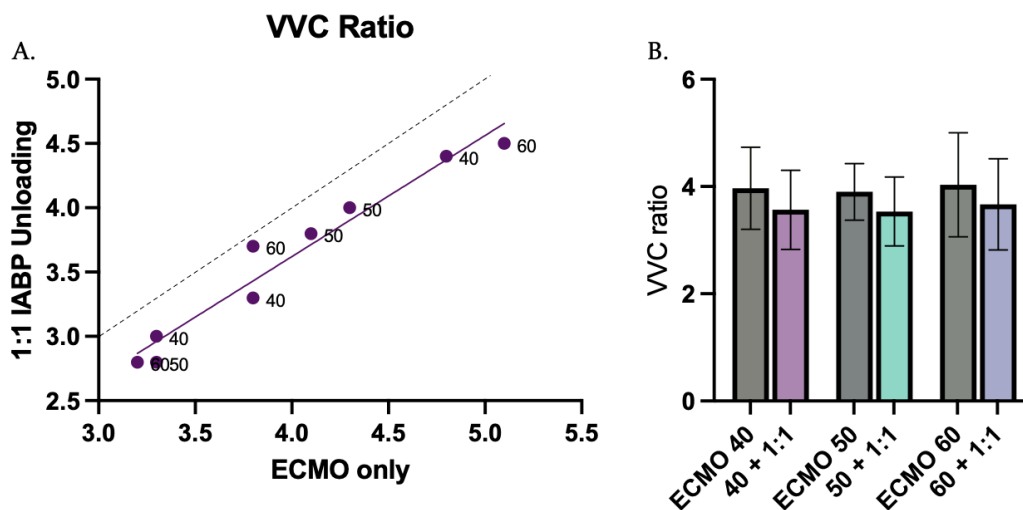
Figure 3.10 – VVC ratio changes with IABP unloading. *A. Dashed line represents y=x slope. Best fit line* y = 0.9414*x - 0.1453; R2 = 0.9519. *B. Change in VVC ratio comparing ECMO alone (grey) to IABP unloading with 40-50-60 ml/kg/min (pink, turquoise and purple respectively).*
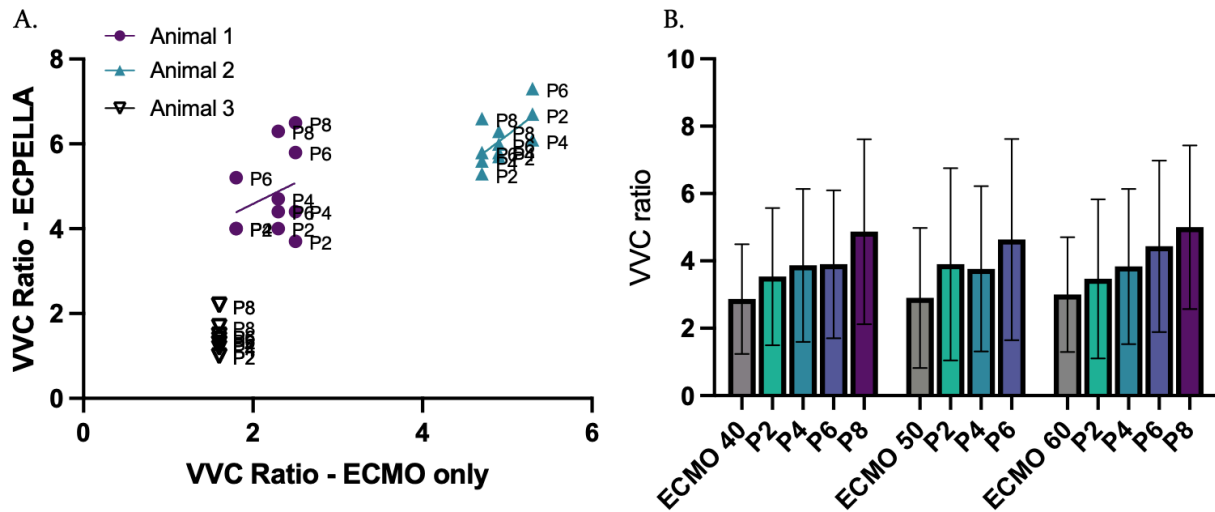
Figure 3.11 – VVC changes with Impella unloading. A. Response to unloading is dependent on initial state, however increasing support increases decoupling regardless of initial state. B. VVC ratio change from initial ECMO only support (40-50-60ml/kg/min) to Impella unloading at 4 P levels.

3.4 Discussion

The initiation of circulatory support for CS patients remains a complex clinical decision, and guidance on device selection and combination with inotropes and vasopressors is far from optimal. MCS devices are implanted in the circulatory system, and the dynamics of the system are a function of VVC - the interaction between the heart and the vasculature. We could therefore optimize the usage of these devices if those dynamics were better understood. VVC metrics provide a framework by which the contribution of each intervention can be evaluated, and work towards optimizing drug and device usage and combination. This study enables us to inspect the effects of different pharmacological and mechanical interventions on metrics of ventricular efficiency in health and in disease. The ability to separate the interventions and measure response to each intervention separately, enables us to appreciate the contribution of each intervention when preformed simultaneously. As established, in health VVC ratio is ~1. We hypothesize that, whenever possible, an attempt to reduce VVC ratio, as close as possible to 1, will have favorable myocardial implications by optimization of energetic demand.

Impella and pharmacological interventions – in the intact LV, with state changes by pharmacological interventions, increase in support is neutral on contractility but increases coupling ratio. When CS state is achieved, an increase in support reduces contractility and loading and increases coupling ratio. Specifically inspecting the combined response to a drug and level of support can help inform the titration for a given state – e.g. increase in support might be marginally beneficial but could increase cardiac inefficiency, and a combination of drug intervention is needed or vice-versa. Afterload management for these patients remains challenging and further understanding of the interplay of tools at hand of the clinician are needed.

VA-ECMO, profoundly affects afterload by virtue of its mode of insertion and operation, had a mixed response within subjects. Similar to the findings reported in chapter 4, cardiovascular response to the initiation of this mode of circulatory support is highly dependent on shock severity and deviation from the subject's baseline. Arterial elastance slope, which is closely related to afterload, increases with increase in ECMO support (absolute value). However, VVC shows a differential response within the graded degrees of shock, due to variable Ees changes. These results can be of clinical importance for afterload management - choosing proper mode of support with medical therapy (pressors). Further studies are needed for establishing these predictions.

LV unloading had minor effects on VVC. Unloading with IABP uniformly showed benefit in afterload reduction – which is the device property, leading to a decrease in arterial elastance slope and thus drove VVC lower overall, improving VVC index. The Impella cohort, although starting at very different VVC values in CS, showed increase in coupling ratio within each individual P level ramp. Uniformly, the higher P levels (P6 and P8) drove coupling ratio higher than ECMO alone, regardless of initial state. This means that the higher P levels increase coupling ratio, further decoupling ventricular-vascular function.

3.5 Conclusion

Combining these observations, the interplay between experimental cardiac metrics and the search for a metric by which to optimize CS treatment (therapeutic and circulatory support) remains challenging. The state of the subject should be evaluated considering first and foremost the intended outcome of an intervention and specific case limitations. VVC metrics give us another tool to factor in when assessing treatment options.

Further studies are needed to better understand the trends of VVC with greater power and to determine the set of parameters that are desirable for optimization of treatment for a given state. Specifically for afterload management, VVC metrics might be a helpful framework to evaluate and optimize the degree of pressors in combination with support for a given CS state. Still, evaluation of VVC is challenging in a clinical setting, and further development of VVC metrics, from MCS signals could greatly aid in decision making.

(This page was intentionally left blank)

Chapter 4: Effects of Retrograde Continuous-Flow Mechanical Support on Left ventricular Function

Abstract

VA-ECMO provides high degree of circulatory support during cardiogenic shock, however it is a highly invasive therapy and carries high risk of adverse effects. In this study we investigated and quantified cardiovascular metrics of VA-ECMO physiology in a porcine cardiogenic shock model, aiming to better understand which patients might benefit and which patients might have little or negative effect from this invasive treatment.

Cardiogenic shock was induced through microbead embolization of the left anterior descending artery. Animals (n=6) underwent VA-ECMO at different levels of support, and hemodynamic measurements, LV pressure-volume loops, and carotid artery blood flow were evaluated.

The results suggest that ECMO operates on a functional continuum of cardiovascular health, disease, and intervention. The study revealed that a combination of severe decrease in CO with the highest increase in LVEDP were able to best identify the subgroup that benefited most from ECMO initiation and titration. These subjects demonstrated the highest positive effect in ventricular efficiency metrics, possibly due to the contribution of significant increase in coronary perfusion. The study supports this finding by the linear trends showing changes in ventricular contractility and relaxation linearly correlate with changes in coronary perfusion.

While the response to ECMO support initiation and titration varied among subjects, the quantifiable responses lay on a functional continuum. The linear trend that emerged might

ultimately help predict which subjects will show the greatest benefit from VA-ECMO support in the setting of cardiogenic shock.

4.1 Introduction

Cardiogenic Shock (CS) is a deadly condition where a severely impaired left ventricle (LV) results in decreased cardiac output (CO) leading to systemic hypotension and thus poor tissue perfusion and eventually end-organ damage. With inadequate acute treatment, diminished CO starts a self-perpetuating process, where the coronary arteries do not receive adequate blood flow, further damaging myocardial tissue and decreasing CO [71].

Patient stabilization can be achieved through prompt medical care including treatment to augment CO and blood pressure and revascularization. Medical treatment includes fluid administration, vasopressors, and inotropes - classically meant to increase cardiac and systemic blood supply. When the shock is refractory to medical treatment, care can be escalated to mechanical circulatory support (MCS). Different MCS modalities exist, with varying levels of invasiveness and support, and usually focus on decreasing demand or increasing supply. Veno-arterial membrane oxygenator (VA ECMO), is an MCS with the ability to provide dramatic increase in supply [20].

Despite rapidly growing adoption to provide circulatory support, ECMO is highly morbid with reported patient mortality over 50% [9,72,73]. Complications intrinsic to ECMO support – such as thromboembolism, bleeding, altered hemodynamics, and impaired left ventricle (LV) ejection, limit its clinical efficacy and are a barrier to improved patient outcomes [22,74,75]. In severe cardiac impairment, inadequate forward flow may lead to blood stasis within the LV and result in the catastrophic complication of LV thrombosis [22].

Deployed as an MCS device, ECMO shunts venous blood through an oxygenator via a centrifugal pump to return oxygenated blood to the systemic arterial circulation (20). In its common implementation, a vascular cannula is placed in the femoral artery and advanced to the iliac artery to provide retrograde blood flow from the ECMO circuit into the distal aorta. Increased afterload produced by ECMO-generated retrograde perfusion stresses the LV, restricting aortic valve opening and forward flow while simultaneously increasing end diastolic pressures and causing pulmonary congestion (76).

Studies to mechanistically evaluate the effects of VA ECMO on cardiopulmonary state are lacking, specifically of interest, guidance on escalation of care as well as optimization of ECMO titration. Using a porcine CS model, the cardiovascular response at different CS states can be evaluated and quantified. This study aims to shed light on the dynamic cardiovascular response to VA ECMO support and titration in varying initial pathophysiologic states. Specifically monitoring and quantifying cardiovascular metrics through health, shock and circulatory support, these data can ultimately aid in understanding the range of physiologic responses to ECMO support and to determine the potential benefit for an individual.

4.2 Materials and Methods

4.2.1 Animal Preparation and Data Acquisition

The effect of VA-ECMO titration on cardiac and vascular state was evaluated in a porcine model of CS. Experimental procedures were conducted on six young adult castrated male Yorkshire swine (60-80 kg, mean 67 kg) in accordance with NIH and AAALAC guidelines (CBSET, Inc., Lexington, MA). Animals underwent induction anesthesia with intramuscular tiletamine-zolazepam (4-6 mg/kg) injection followed by endotracheal intubation. A 20-gauge catheter was

placed in the ear vein and a continuous infusion of propofol (0.2 to 0.4 mg/kg/min) was administered and titrated to maintain deep sedation. The animals were then initiated on mechanical ventilation with a Puritan Bennett 840 Ventilator (Medtronic, Inc., Dublin, Ireland) using volume control mode with a tidal volume of 8 ml/kg actual body weight, positive-end expiratory pressure of 5 cm H_2O, and a fraction of inspired oxygen of 50%. Body temperature, oxygen saturation, end-tidal carbon dioxide, and electrocardiogram were monitored throughout the experiment.

Vascular access was obtained via percutaneous insertion of catheters (6 to 9 Fr) in the right and left femoral arteries and veins, right and left jugular vein, and right carotid artery (Figure 1). A Swan-Ganz catheter (Edwards Lifesciences, Inc., Los Angeles, CA) was inserted into the pulmonary artery through the right jugular vein for continuous recordings of central venous and pulmonary artery pressures and to obtain thermodilution cardiac output measurements. A sheath was inserted into the right jugular vein through which a Millar pressure catheter (Millar, Inc., Houston, TX) was advanced into the pulmonary artery to obtain high fidelity measurements of pulmonary arterial pressure less susceptible to catheter motion artifact. A second Millar pressure catheter was placed in the aortic arch via the femoral artery to measure proximal systemic arterial pressure while a fluid-filled pressure transducer was used to measure femoral arterial pressure via the side port of the vascular catheter.

A Millar Ventri-Cath 507 pressure-volume (PV) catheter was advanced via the right carotid artery into the left ventricular. A second Millar Ventri-Cath 507 PV catheter was advanced via the left jugular vein into the right ventricle. The PV catheters provided continuous measurement of biventricular pressure and volumes throughout the cardiac cycle. All catheters were placed using fluoroscopic guidance to confirm intended positioning. Following skin incision in the left neck, the left carotid artery was exposed with blunt dissection and an FME-series carotid flow probe

(Transonic, Inc., Ithaca, NY) was placed around the outside of the vessel to provide continuous measurement of blood flow through the carotid artery. One animal experienced carotid artery injury during dissection which precluded flow measurement.

Following catheter placement, baseline measurements and arterial and mixed venous blood gases were obtained. The ventilator rate was titrated to maintain a baseline partial pressure of carbon dioxide of 35 to 45 mm Hg confirmed on serial arterial blood gas assessment. A Coda balloon catheter (Cook Medical, LLC, Bloomington, IN) was inserted via the femoral vein and advanced to the proximal inferior vena cava. The balloon was serially inflated and then deflated to obtain end-systole pressure volume relationships and baseline ventricular volume measurements for PV catheter calibration. The animals then underwent serial (triplicates) thermodilution cardiac output (TDCO) measurements.

4.2.2 Porcine Model of Cardiogenic Shock

CS was induced using a previously described method (77–79) to induce diffuse microvascular ischemia in the left ventricle. Briefly, a guide catheter was advanced into the left anterior descending coronary artery via the left femoral artery. Hydropearl microbeads (45-105 um in diameter; Terumo, Inc., Tokyo, Japan) were instilled in aliquots followed by re-assessment of the animal's cardiovascular function. Microbead instillation was continued until left ventricular end diastolic pressure (LVEDP) exceeded 16 mm Hg and either the mean arterial pressure (MAP) decreased below 50 mm Hg, mixed venous oxygen saturation (MvO_2) was less than 55% or the TDCO was less than 50 ml/kg/min. Upon reaching this physiological state, a new experimental baseline was established for each animal.

4.2.3 Mechanical Circulatory Support

VA-ECMO support was provided by the OXY-1 System (Abiomed, Inc., Danvers, MA) consisting of a centrifugal pump, oxygenator, and device controller. The system was primed with normal saline at the beginning of each experiment. Following achievement of CS, the animal underwent cannulation and initiation of VA-ECMO support. An Amplatz extra stiff guidewire (Boston Scientific, Marlborough, MA) was inserted into the left femoral vein through a vascular catheter which was then removed. Following serial dilation, a 21 French Bio-Medicus multistage cannula (Medtronic, Inc., Dublin, Ireland) was advanced to the inferior venal caval-right atrial junction under fluoroscopic guidance. Using the same method, a 15 French Bio-Medicus arterial cannula was inserted via the left femoral artery with the distal cannula tip terminating at the junction of the iliac artery and distal aorta. The vascular cannulas were then connected to the ECMO circuit with pump RPMs gradually increased to achieve a flow of 50 ml/kg/min while sweep gas of 100% O_2 was initiated at 2 L/min. Sweep gas flow rate was then titrated to maintain a target partial pressure of carbon dioxide of 35 to 45 mmHg in the post-oxygenator as determined by serial blood gas assessment. VA-ECMO flow rates were then decreased to 40 ml/kg/min and maintained until steady-state was achieved after which hemodynamic data was obtained. Pump RPMs were then increased to achieve an ECMO flow rate of 50 ml/kg/min and then increased to 60 ml/kg/min. At each ECMO flow rate, hemodynamic data was obtained once the animal achieved steady-state conditions as determined by stable MAP and LV pressure over 40 respiratory cycles. At least 20 minutes elapsed between state changes to assure return to baseline hemodynamics.

4.2.4 Data Analysis

Venous and arterial hemodynamics, EKG and PV data for both ventricles were recorded continuously throughout the study. Data were analyzed with custom Python scripts. Volume

calibration (Millar catheter LV volume signal) was done using triplicate thermodilution (TD) at baseline state paired with Inferior-Vena Cava (IVC) balloon occlusion. Average CO from TD measurements with HR at the corresponding time were used for the calculation of stroke volume (SV) using the following relationship – CO = HR x SV. The value of minimum LV volume during peak IVC occlusion was then used along with calculated SV, in order to determine DC offset and scaling factor for conversion of raw volume signal (volts) to a usable volume signal in ml.

For each state analyzed, parameters were calculated for corresponding beats, beat by beat, during two full respiratory cycles to account for respiratory variation. Each of these parameters were averaged over the two respiratory cycles. Individual PV loops were taken at end-expiration. The calculated metrics included ventricular energetics and state, carotid flow data and arterial hemodynamics (Table 4.2, Table 4.3, Table 4.4 respectively).

With the output raw values for the calculated metrics, fold change and delta change for from the established CS baseline were calculated (Table 4.5) (calculated as: [*100*(metric $_{ECMO}$ – metric $_{cs}$)/ metric $_{cs}$, and Δ = metric $_{ECMO}$ – metric $_{cs}$*, respectively].

4.2.5 Statistical Analysis

All calculated cardiac metrics are presented in absolute values, as well as fold change from established CS baseline is calculated for each metric.

Statistical analysis was performed using Prism (GraphPad Software, San Diego, CA). Correlation matrices were used to find linear correlations between CS metrics, and subsequently for grouping of subject's shock state severity.

4.3 Results

4.3.1 Physiologic Response to Cardiogenic Shock Model

Despite using set threshold determinants of shock state in real time, the subjects revealed a profoundly differential response to the induction of CS. During data analysis, shock state was evaluated by examining absolute values and fold change from baseline in the following metrics: CO, LVEDP, coronary perfusion (CP) and MAP (Table 4.1, Figure 4.2).

For evaluation of LV thermodynamic energetic response, pressure-volume (PV) loops were analyzed (Figure 4.1). In these representative PV loops, the variable response to shock is evident, shown by the change from the baseline loop (green) to the CS loop (black). The additional PV loop in each panel reveals the response to VA-ECMO initiation (blue). It is evident that the response to initiation of circulatory support varied, based on baseline and mostly on CS state.

However, SW significantly reduced for all subjects with an average reduction of -64 ± 11.3%, and LVEDP increased by 118 ± 50.7 %. Hemodynamically, mean arterial pressure (MAP) universally decreased, averaging -35 ± 14.6%, and pulse pressure (PP) decreased as well by -38 ± 10.9%. However, analysis of the thermodynamic response in the PV domain, revealed a nuanced physiologic presentation, corresponding to the degree of shock. Probably responsible for a differential response in LV energetic and hemodynamic parameters.

Correlation matrices (**Error! Reference source not found.**) were used to visualize the relationship between the calculated parameters for all animals. Considering the data presented in Table 4.1 and using it to categorize the animals by shock severity, the matrices were plotted again for a subset of animals. When plotting just the subjects identified as profound shock (**Error! Reference source not found.** Rt panel), strongest correlations were revealed, validating the parameters that were chosen to evaluate shock state.
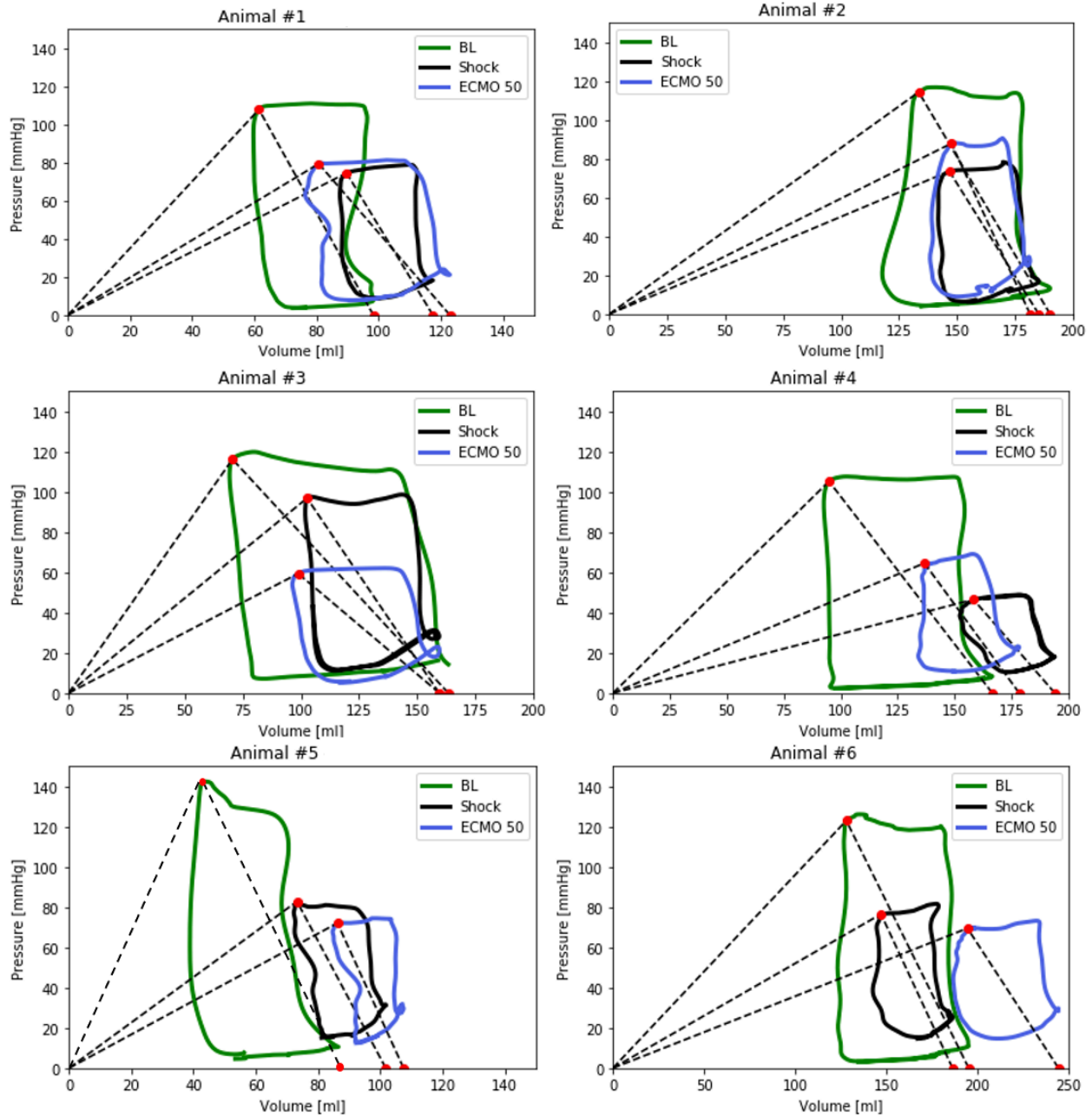
*Figure 4.1 - **Representative pressure-volume loops for the 6 subjects.*** *BL = baseline loop (green); shock (black) and ECMO initiation (blue). Dashed lines are end-systolic pressure-volume relationship and arterial elastance.*
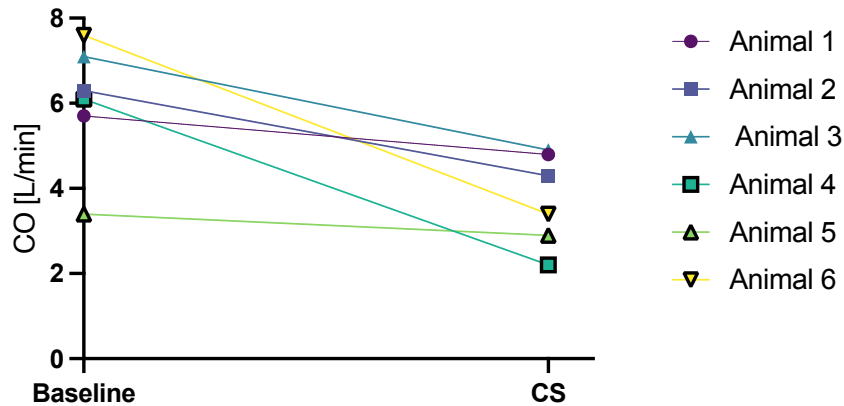
Figure 4.2 – Cardiac output change from baseline to induced cardiogenic shock (CS) state.

	Animal	1	2	3	4	5	6
CO [L/min]	BL	5.7	6.3	7.1	6.1	3.4	7.6
	Shock	4.8	4.3	4.9	2.2	2.9	3.4
	Delta	**-0.9**	**-2**	**-2.2**	**-3.9**	**-0.5**	**-4.2**
	% Reduction	**-16**	**-32**	**-31**	**-64**	**-15**	**-55**

	Animal	1	2	3	4	5	6
LVEDP [mmHg]	BL	9.72	15.54	12.9	9.33	11.5	12.8
	Shock	21.13	21.59	32.9	19.36	33.03	25.63
	Delta	**11.41**	**6.05**	**20**	**10.03**	**21.53**	**12.83**
	% Increase	**117**	**39**	**155**	**108**	**187**	**100**

	Animal	1	2	3	4	5	6
MAP [mmHg]	BL	110.49	107.96	111.8	97.87	130	116.69
	Shock	74.53	71.74	97.3	40.47	79	76.28
	Delta	**-35.96**	**-36.22**	**-14.5**	**-57.4**	**-51**	**-40.41**
	% Reduction	**-33**	**-34**	**-13**	**-59**	**-39**	**-35**

	Animal	1	2	3	4	5	6
CP [mmHg]	BL	48.5	57.1	62.8	56	71.3	63.1
	Shock	28.1	33.7	44.8	8.8	34.5	29.4
	Delta	**-20.4**	**-23.4**	**-18**	**-47.2**	**-36.8**	**-33.7**
	% Reduction	**-42**	**-41**	**-29**	**-84**	**-52**	**-53**

Table 4.1 – Shock state evaluation parameters presented for 6 animals. Baseline (BL), shock, delta (calculated as shock – BL) and % reduction/increase from BL to shock. CO = cardiac output; LVEDP = left ventricular end diastolic pressure; MAP = mean arterial pressure; CP = coronary perfusion pressure.

4.3.2 VA-ECMO Retrograde Flow Effects – Initiation and Titration

In the following section, the response to circulatory support initiation is analyzed. Metrics are presented as absolute values (Table 4.2-4.4) and fold change (%) for each animal from the established CS baseline (Table 4.5). Finally, ECMO titration effects are quantified, similarly calculating metrics for 40, 50 and 60 ml/kg/min support level.

Given the different severity of initial cardiovascular compromise among animals, the response to circulatory support initiation and titration elicited a differential response within
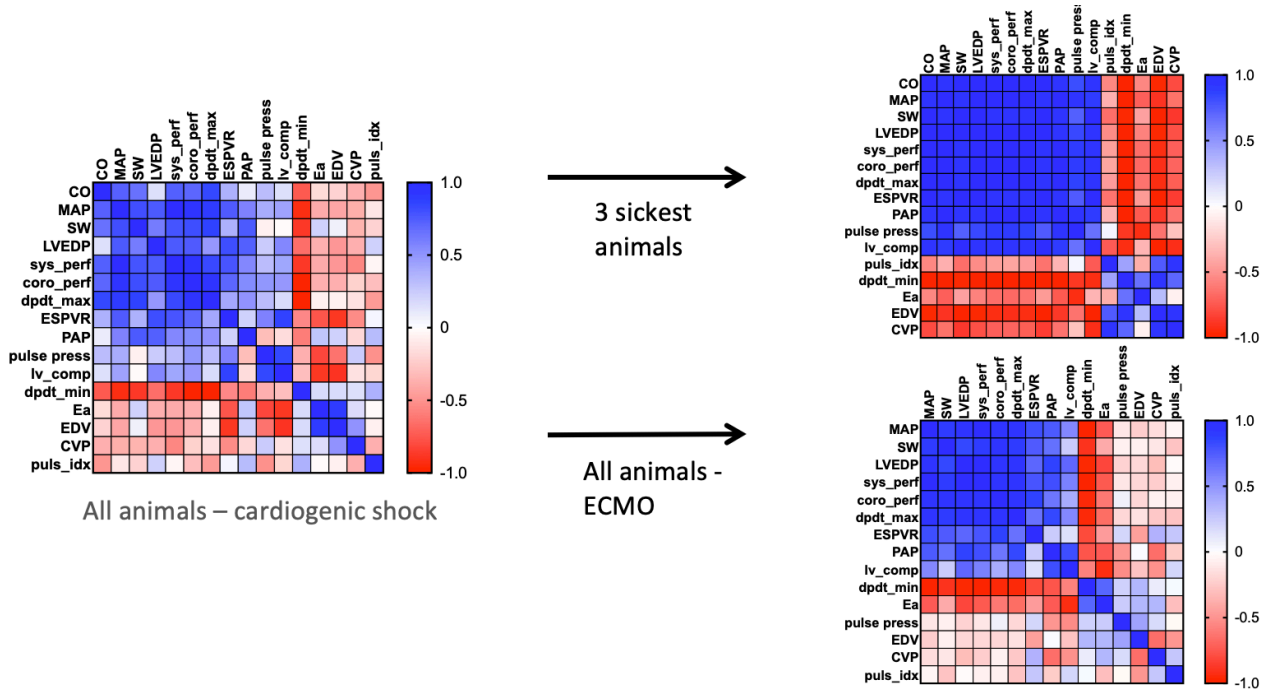
Figure 4.3 – Correlation matrices with cardiogenic shock metrics. Left panel – all 6 animals. Right top panel –animals 3, 4, 6.Right bottom panel – all 6 animals with ECMO.

animals (Figure 4.4). These representative PV loops display CS state (black), along with 3 additional loops depicting a support ramp – 40-50-60 ml/kg/min (purple, blue, turquoise respectively). In all animals the change within the ramp is evident, showing an expected increase in LVEDP, SW and end-systolic pressure (ESP).
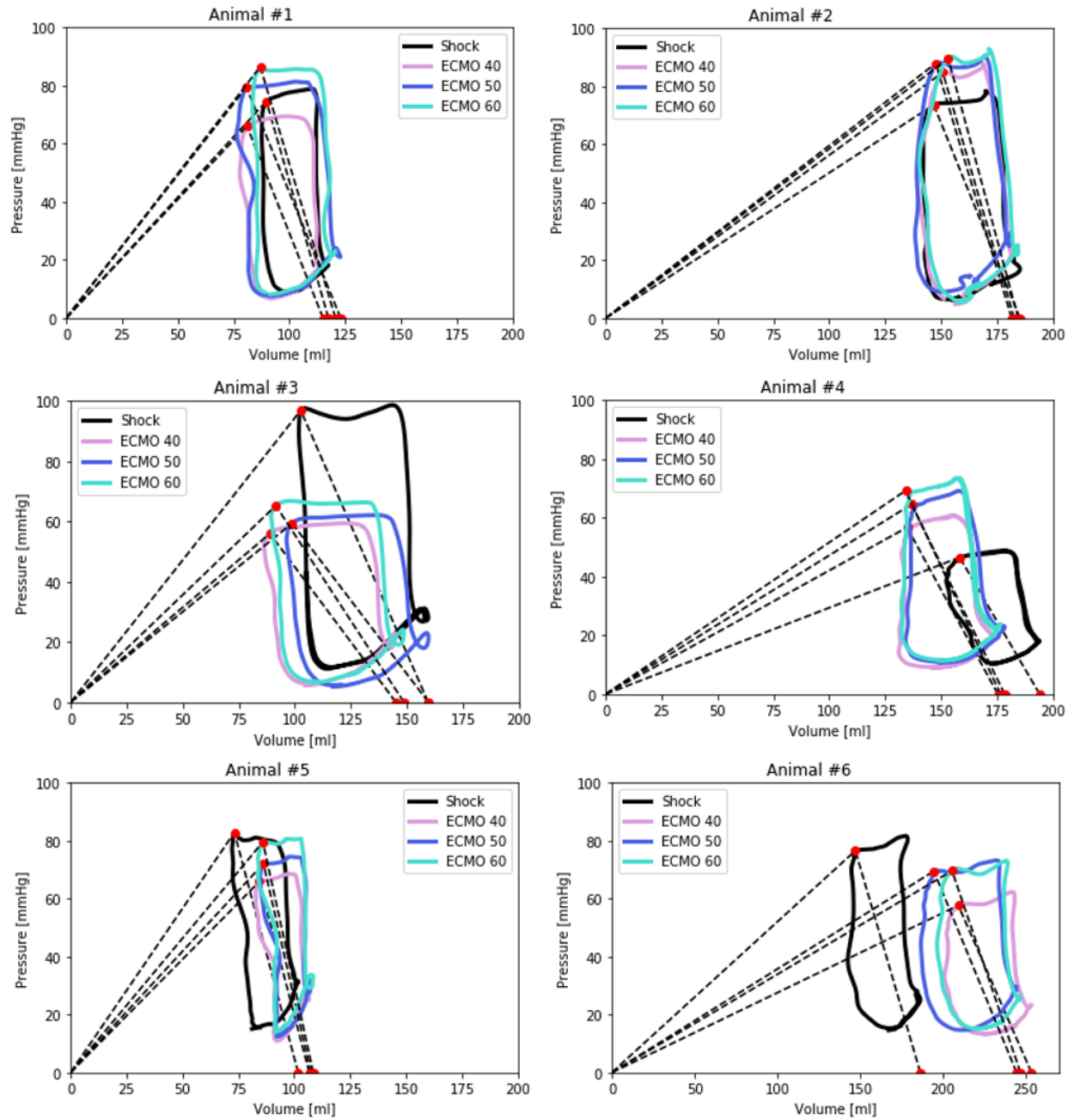
Figure 4.4 - ECMO titration - representative pressure-volume loops for the 6 subjects. *Shock (black) and ECMO flow ramp 40, 50 and 60 ml/kg/min (pink, blue and turquoise respectively). Dashed lines are end-systolic pressure-volume relationship and arterial elastance.*

Figure 4.5 and Figure 4.6 present values and change (respectively) in metrics of cardiovascular response to support titration, including initial CS (ECMO = 0 data point), followed by 40-50-60 ml/kg/min ramps. The flow rate ramps revealed a linear response in most metrics, with varying slope magnitude depending on subject's CS severity. SW, systemic perfusion pressure, coronary perfusion, load-dependent contractility (dP/dt $_{max}$) and LVEDP showed a linear positive correlation with the increase in ECMO flow. Pulsatility index (carotid) and LV relaxation (dP/dt $_{min}$) showed an inverse linear response.

Carotid artery flow, measured as a surrogate of cerebral perfusion, decreased in all subjects by an average of 33 ± 19% in CS, but uniformly increased with ECMO initiation, equating, or surpassing pre-shock values (90 ± 62%). However, pulsatility index initially increased in CS (+92 ± 63%), followed by a linear decrease when ramping ECMO flows (-52± 15%; -61 ± 15%; -71 ± 15%). Interestingly, for the profound shock group, pulsatility index values are half fold baseline values, but reach baseline values in the remaining subjects.

Figure 4.6 shows how the response to ECMO flow increase creates a linear response that its slope magnitude is modified by severity of shock. Figures 4.7 and 4.8 show the change and absolute values (respectively) of two independent metrics for all 6 subjects. Illustrating the relationship between contractility and relaxation as a function of coronary perfusion for the different physiologic states. The plotted relationship creates a linear continuum throughout health and disease, with a higher R^2 value at higher stress states. Regardless of initial state of the subject and severity of shock, datapoints create a linear functional continuum.
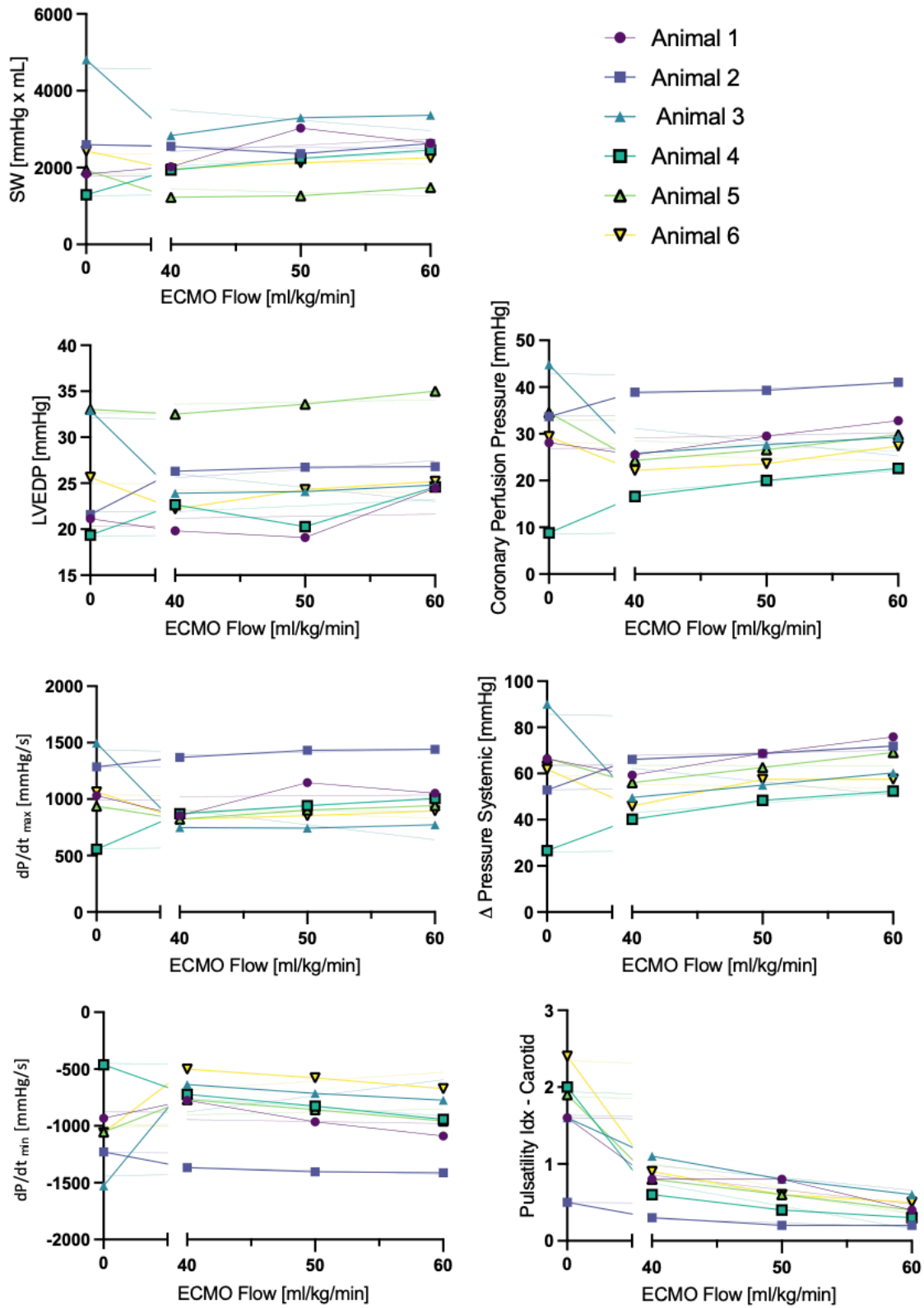
Figure 4.5 – Subject's response to ECMO initiation and titration of flow. *0 ECMO flow denotes cardiogenic shock without support. SW = stroke work; LVEDP = left ventricular end diastolic pressure.*
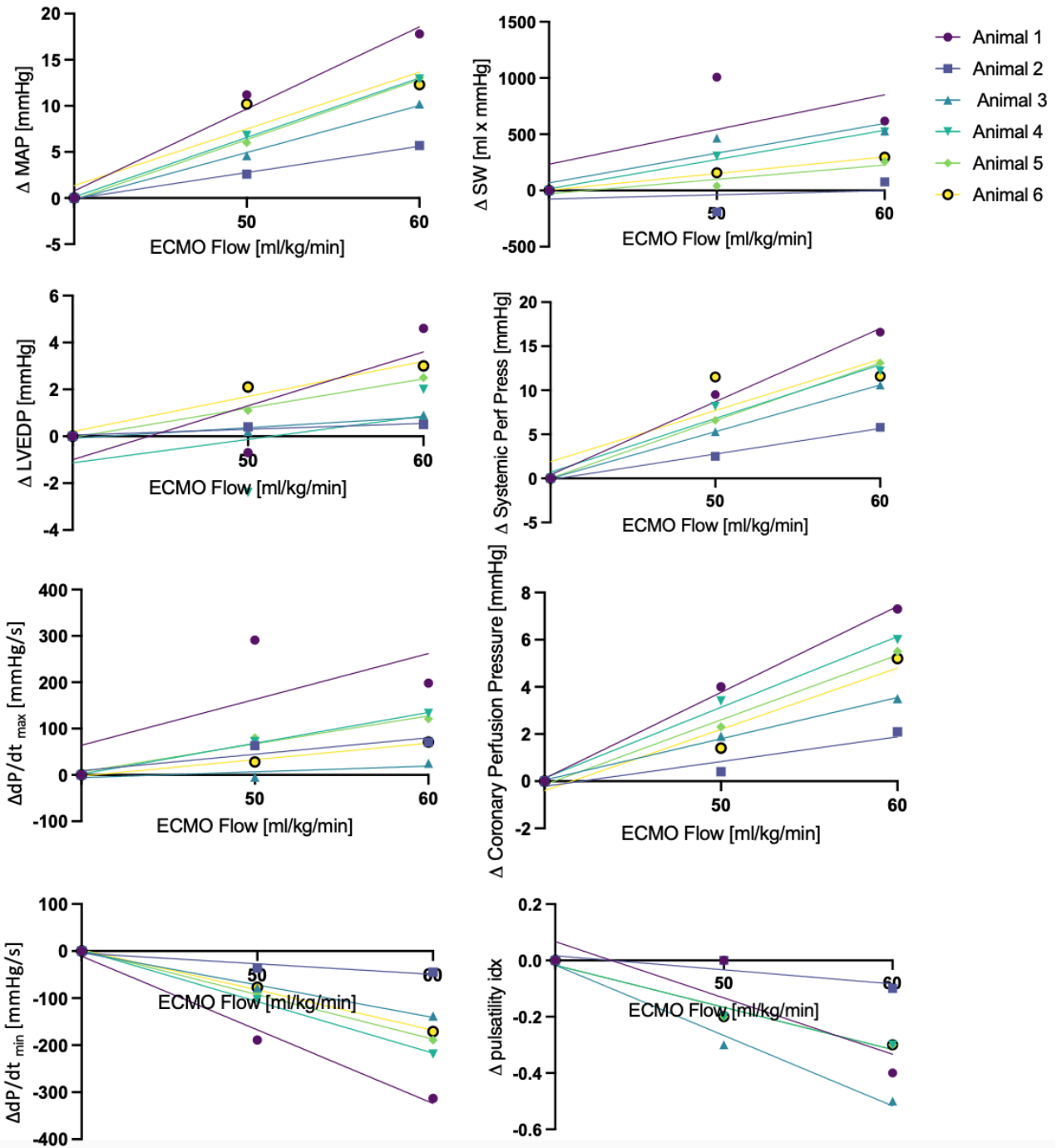
Figure 4.6 – Change in cardiovascular metrics with ECMO flow titration. *Resulting slopes represent subject's response. 0 point (origin of graph) is ECMO at 40 ml/kg/min, data points 50 and 60 ml/kg/min represent the delta between the corresponding flow rate and measured value at 40 ml/kg/min.*
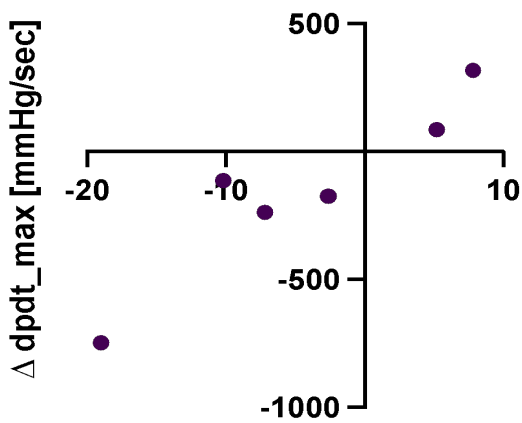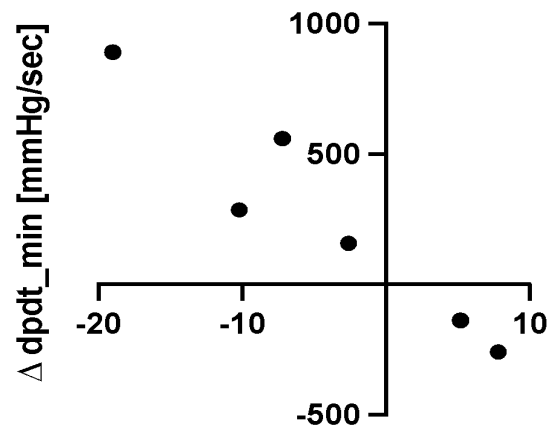
*Figure 4.7 - **Changes in contractility (left panel) and relaxation (right panel) as a function of changes in coronary perfusion.** Deltas are calculated as the change between the metric measured in cardiogenic shock minus ECMO initiation. Each data point represents one subject.*
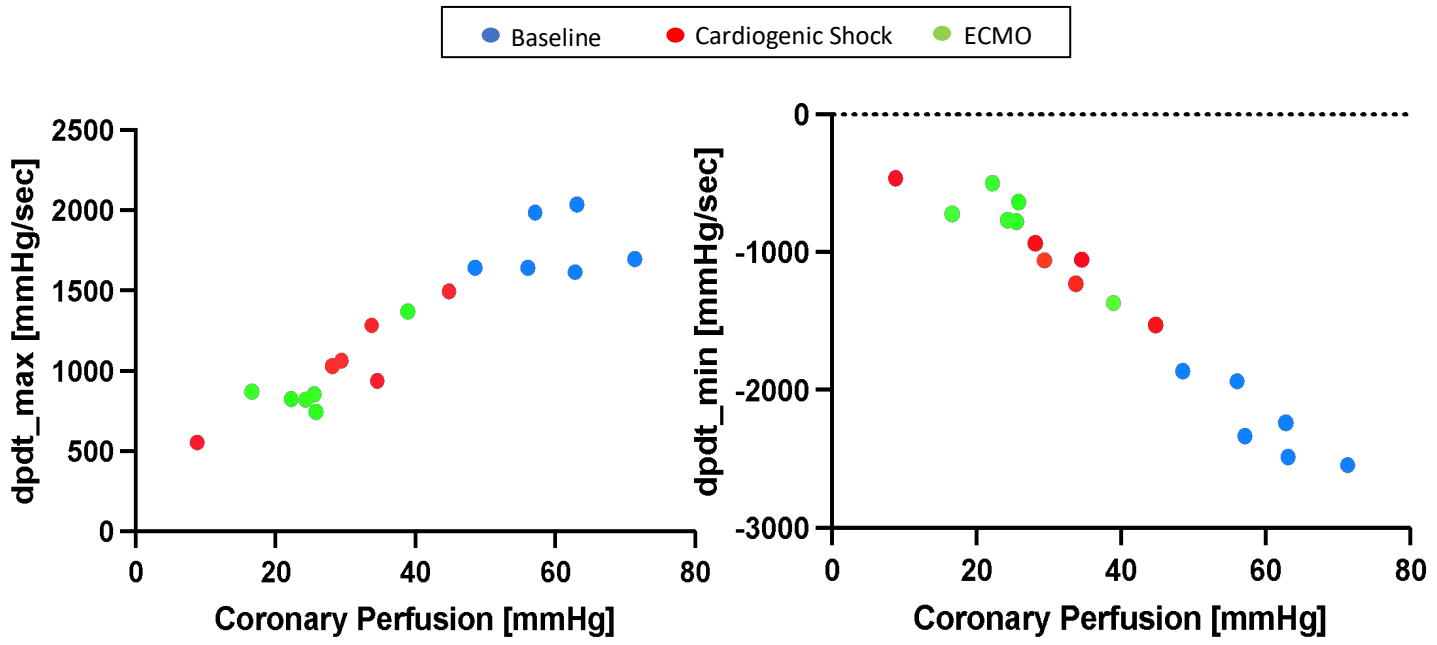
*Figure 4.8 – **Absolute values of contractility (left) and relaxation (right) as a function of coronary perfusion.** Datapoints represent the different subjects and color represents state (blue – baseline, red – CS, green – ECMO). Left panel - R^2 = 0.86, right panel - R^2 = 0.95.*

	Animal #	1	2	3	4	5	6
SW [mmHg x ml]	BL	3838.7	6260	10714	7378	6020	8056
	Shock	1831.18	2597	4806	1294	1933	2432
	ECMO 40	2020.6	2554	2831	1936	1225	1964
	ECMO 50	3028.4	2363.37	3297	2241	1266	2121
	ECMO 60	2638.7	2629	3360	2456	1480	2259
dp/dt max [mmHg/s]	BL	1644	1987	1615	1643	1700	2037
	Shock	1030	1285	1496	556	938	1064
	ECMO 40	854	1369	747	871	822	824
	ECMO 50	1145	1432	742	943	902	852
	ECMO 60	1052	1440	772	1004	943	895
dp/dt min [mmHg/s]	BL	-1862	-2332	-2237	-1936	-2545	-2487
	Shock	-933	-1230	-1527	-463	-1054	-1059
	ECMO 40	-776	-1368	-636	-723	-769	-501
	ECMO 50	-965	-1404	-714	-826	-858	-578
	ECMO 60	-1089	-1413	-774	-942	-958	-672
ESPVR (Ees) [mmHg/ml]	BL	1.7	0.85	1.64	1.1	3.32	0.96
	Shock	0.83	0.5	0.94	0.29	1.13	0.52
	ECMO 40	0.81	0.56	0.63	0.42	0.78	0.27
	ECMO 50	0.98	0.57	0.6	0.47	0.83	0.3
	ECMO 60	0.99	0.58	0.71	0.51	0.92	0.33
LVEDP [mmHg]	BL	9.72	15.54	12.9	9.33	11.5	12.8
	Shock	21.13	21.59	32.9	19.36	33.03	25.63
	ECMO 40	19.83	26.31	23.9	22.65	32.5	22.2
	ECMO 50	19.1	26.73	24.1	20.29	33.6	24.3
	ECMO 60	24.47	26.8	24.8	24.6	35	25.2
Ea [mmHg/ml]	BL	-2.9	-2	-1.22	-1.46	-3.2	-1.83
	Shock	-2.6	-1.9	-1.7	-1.3	-2.9	-1.95
	ECMO 40	-1.9	-2.65	-0.99	-1.39	-2.95	-1.3
	ECMO 50	-1.8	-3.03	-0.97	-1.55	-3.39	-1.45
	ECMO 60	-2.5	-2.86	-1.14	-1.63	-3.53	-1.68
Coronary perfusion pressure [mmHg]	BL	48.5	57.1	62.8	56	71.3	63.1
	Shock	28.1	33.7	44.8	8.8	34.5	29.4
	ECMO 40	25.5	38.9	25.8	16.6	24.3	22.2
	ECMO 50	29.5	39.3	27.7	20	26.6	23.6
	ECMO 60	32.8	41	29.3	22.6	29.8	27.4

PVA [mmHg x ml]	BL	7043.5	13632	14703	12260	8926	15733
	Shock	4785.58	7536	9140	4160	4415	6989
	ECMO 40	4422	8583	5069	5152	3545	6616
	ECMO 50	5924.1	8603.47	5975	5924	3836	7224
	ECMO 60	6041.2	9060	6050	6337	4304	7872
EDV [ml]	BL	98.27	190.11	165.2	166.53	86.55	195.2
	Shock	117.4	185.2	158	193.97	101.74	186.33
	ECMO 40	115	182.58	145.08	175.31	106.71	253.44
	ECMO 50	122.89	180.69	159.6	178.34	107.45	250.48
	ECMO 60	120.51	184.42	148.66	176.49	108.49	246.83
LV compliance [ml/mmHg]	BL	0.17	0.21	0.10	0.10	0.16	0.14
	Shock	0.45	0.40	0.38	0.25	0.63	0.28
	ECMO 40	0.39	0.67	0.33	0.34	0.97	0.20
	ECMO 50	0.27	0.75	0.31	0.23	1.00	0.25
	ECMO 60	0.49	0.68	0.32	0.31	0.94	0.25

Table 4.2 – Ventricular metrics calculated for 6 animals at baseline (BL), shock and ECMO 40,50,60 ml/kg/min. SW = stroke work; ESPVR (Ees) = the slope of end systolic pressure-volume relation; LVEDP = left ventricular end diastolic pressure; Ea = arterial elastance; PVA = pressure volume area; EDV = end diastolic volume.

ECMO retrograde flow effects on cerebral perfusion

	Animal #	1	2	3	4	5	6
Carotid flow [ml/min]	BL	448.09	75.23	276	455.19	372	282.02
	Shock	352.63	52.8	268	214.66	185	171.37
	ECMO 40	441.22	75.52	460	456.45	346	512.38
	ECMO 50	453.97	81.84	539	513.73	426	655.6
	ECMO 60	578.58	82.95	609	576.55	454	651.84
Pulsatility index (carotid)	BL	0.7	0.4	1.5	0.8	0.8	1.2
	Shock	1.6	0.5	1.6	2.0	1.9	2.4
	ECMO 40	0.8	0.3	1.1	0.6	0.8	0.9
	ECMO 50	0.8	0.2	0.8	0.4	0.6	0.6
	ECMO 60	0.4	0.2	0.6	0.3	0.4	0.5

Table 4.3 – Brain perfusion surrogate metrics calculated for 6 animals at baseline (BL), shock and ECMO 40,50,60 ml/kg/min. Flow in animal #2 was obtained from a branching vessel due to technical issues.

ECMO retrograde flow effects on arterial hemodynamics

	Animal #	1	2	3	4	5	6
MAP [mmHg]	BL	110.49	107.96	111.8	97.87	130	116.69
	Shock	74.53	71.74	97.3	40.47	79	76.28
	ECMO 40	67.45	83.34	57.71	54.37	66	57.99
	ECMO 50	78.6	85.99	62.29	61.13	72	68.22
	ECMO 60	85.26	89.03	67.9	67.26	79	70.28
Systemic perfusion [mmHg]	BL	104.32	91.47	105.61	87.67	122.13	105.78
	Shock	66.39	52.84	90.06	26.66	66.61	61.79
	ECMO 40	59.29	66.16	49.66	40.17	56.04	45.91
	ECMO 50	68.74	68.65	54.96	48.39	62.61	57.42
	ECMO 60	75.91	71.91	60.25	52.39	69.13	57.52
Pulse pressure [mmHg]	BL	21.69	27.4	26.3	23.55	31.8	29.76
	Shock	17.57	18.72	15.07	13.04	19.34	15.14
	ECMO 40	14.23	16.93	13.51	10.64	13.58	15.05
	ECMO 50	16.01	16.41	13.72	9.31	13.39	15.71
	ECMO 60	14.64	16.42	12.5	9.09	12.59	13.96
coronary perfusion pressure	BL	48.5	57.1	62.8	56	71.3	63.1
	Shock	28.1	33.7	44.8	8.8	34.5	29.4
	ECMO 40	25.5	38.9	25.8	16.6	24.3	22.2

[mmHg]	ECMO 50	29.5	39.3	27.7	20	26.6	23.6
	ECMO 60	32.8	41	29.3	22.6	29.8	27.4
PAP [mmHg]	BL	10.6	19.0	21.6	18.8	20.8	23.1
	Shock	14.1	19.1	31.7	19.3	22.7	27.4
	ECMO 40	11.0	20.4	22.1	20.0	25.8	24.8
	ECMO 50	12.8	20.3	22.7	21.8	27.8	26.5
	ECMO 60	13.5	20.4	22.9	21.9	28.9	26.5
PAP$_{sys}$ [mmHg]	BL	18.9	27.7	31.4	27.4	32.1	32.0
	Shock	22.1	28.5	40.5	25.9	35.6	36.7
	ECMO 40	18.1	29.4	31.7	28.2	33.6	33.1
	ECMO 50	21.1	28.9	32.6	29.9	34.7	34.9
	ECMO 60	21.2	28.7	33.1	30.2	35.7	34.6
PAP$_{dia}$ [mmHg]	BL	2.7	11.7	11.9	10.4	11.2	13.1
	Shock	5.7	11.3	21.1	13.9	7.2	19.1
	ECMO 40	5.2	13.5	14.5	13.7	18.5	18.5
	ECMO 50	5.8	12.7	14.9	15.0	21.3	19.2
	ECMO 60	6.3	13.2	14.6	15.1	22.5	19.8
CVP [mmHg]	BL	6.18	16.49	6.19	9.63	8.37	10.9
	Shock	8.13	18.9	7.23	13.01	12.55	14.48
	ECMO 40	8.17	17.18	8.04	13.14	9.96	12.08
	ECMO 50	9.85	17.33	7.33	13.25	10.21	12.25
	ECMO 60	9.351	17.11	7.65	13.8	10.59	12.75

Table 4.4 - Hemodynamic metrics calculated for 6 animals at baseline (BL), shock and ECMO 40,50,60 ml/kg/min. MAP = mean arterial pressure; Pap = pulmonary artery pressure; Pap$_{sys}$ = systolic pulmonary artery pressure; Pap$_{dia}$ = diastolic pulmonary artery pressure; CVP = central venous pressure.

PERCENT CHANGE							
[%]	ECMO [ml/kg/min]	animal 1	animal 2	animal 3	animal 4	animal 5	animal 6
MAP	40	-9.5	16.2	-40.7	34.3	-16.5	-24.0
	50	5.5	19.9	-36.0	51.1	-8.9	-10.6
	60	14.4	24.1	-30.2	66.2	0.0	-7.9
SW	40	10.3	-1.7	-41.1	49.6	-36.6	-19.2
	50	65.4	-9.0	-31.4	73.2	-34.5	-12.8
	60	44.1	1.2	-30.1	89.8	-23.4	-7.1
dp/dt$_{max}$	40	-17.1	6.5	-50.1	56.7	-12.4	-22.6
	50	11.2	11.4	-50.4	69.6	-3.8	-19.9
	60	2.1	12.1	-48.4	80.6	0.5	-15.9
dp/dt$_{min}$	40	-16.8	11.2	-58.3	56.2	-27.0	-52.7
	50	3.4	14.1	-53.2	78.4	-18.6	-45.4
	60	16.7	14.9	-49.3	103.5	-9.1	-36.5
ESPVR	40	-2.4	12.0	-33.0	44.8	-31.0	-48.1
	50	18.1	14.0	-36.2	62.1	-26.5	-42.3
	60	19.3	16.0	-24.5	75.9	-18.6	-36.5
LVEDP	40	-6.2	21.9	-27.4	17.0	-1.6	-13.4
	50	-9.6	23.8	-26.7	4.8	1.7	-5.2
	60	15.8	24.1	-24.6	27.1	6.0	-1.7
Ea	40	-26.9	39.5	-41.8	6.9	1.7	-33.3
	50	-30.8	59.5	-42.9	19.2	16.9	-25.6
	60	-3.8	50.5	-32.9	25.4	21.7	-13.8
Systemic perfusion	40	-10.7	25.2	-44.9	50.7	-15.9	-25.7
	50	3.5	29.9	-39.0	81.5	-6.0	-7.1
	60	14.3	36.1	-33.1	96.5	3.8	-6.9
Pulse pressure	40	-19.0	-9.6	-10.4	-18.4	-29.8	-0.6
	50	-8.9	-12.3	-9.0	-28.6	-30.8	3.8
	60	-16.7	-12.3	-17.1	-30.3	-34.9	-7.8
Coronary perfusion	40	-9.3	15.4	-42.4	88.6	-29.6	-24.5
	50	5.0	16.6	-38.2	127.3	-22.9	-19.7
	60	16.7	21.7	-34.6	156.8	-13.6	-6.8
Carotid flow	40	25.1	43.0	71.6	112.6	87.0	199.0
	50	28.7	55.0	101.1	139.3	130.3	282.6
	60	64.1	57.1	127.2	168.6	145.4	280.4
PVA	40	-7.6	13.9	-44.5	23.8	-19.7	-5.3
	50	23.8	14.2	-34.6	42.4	-13.1	3.4

	60	26.2	20.2	-33.8	52.3	-2.5	12.6
EDV	40	-2.0	-1.4	-8.2	-9.6	4.9	36.0
	50	4.7	-2.4	1.0	-8.1	5.6	34.4
	60	2.6	-0.4	-5.9	-9.0	6.6	32.5
LV complianc e	40	-14.5	68.9	-15.3	33.7	53.3	-27.5
	50	-39.6	87.5	-18.7	-9.1	58.0	-11.9
	60	7.7	69.7	-16.2	23.7	48.8	-12.4
Pulsatility index (carotid)	40	-45.9	-42.7	-30.4	-70.1	-57.9	-63.5
	50	-48.8	-49.3	-46.4	-80.6	-70.2	-73.4
	60	-72.1	-54.5	-60.9	-84.9	-76.4	-78.0
PAP	40	-22.0	7.1	-30.3	3.6	13.6	-9.5
	50	-8.9	6.6	-28.4	13.0	22.4	-3.2
	60	-4.5	6.8	-27.9	13.6	27.3	-3.1
PAP$_{sys}$	40	-17.9	3.4	-21.7	9.1	-5.8	-9.9
	50	-4.3	1.6	-19.5	15.6	-2.6	-5.1
	60	-4.1	0.7	-18.3	16.9	0.3	-5.7
PAP$_{dia}$	40	-9.7	19.3	-31.2	-1.4	157.9	-3.1
	50	0.7	12.7	-29.6	8.1	196.5	0.4
	60	10.3	17.2	-30.6	9.0	212.4	3.7
CVP	40	0.4	-9.1	11.2	1.0	-20.6	-16.6
	50	21.1	-8.3	1.4	1.8	-18.6	-15.4
	60	15.0	-9.5	5.8	6.1	-15.6	-11.9

Table 4.5 – Fold change from shock state for 6 animals at 40,50,60 ml/kg/min ECMO flow rate. MAP – mean arterial pressure; SW- stroke work; ESPVR (Ees) = the slope of end systolic pressure-volume relation; LVEDP = left ventricular end diastolic pressure; Ea = arterial elastance; PVA = pressure volume area; EDV = end diastolic volume; PAP = pulmonary artery pressure; PAP$_{sys}$ = systolic pulmonary artery pressure; PAP$_{dia}$ = diastolic pulmonary artery pressure; CVP = central venous pressure.

4.4 Discussion

At face value it might seem that ECMO is of binary value – protective in some and of minimal or even negative value in others. Such thinking has prompted some to look for means of augmenting ECMO in those whose benefit is not evident. Our work suggests that ECMO operates on a functional continuum of cardiovascular health from polar forms of health and cardiogenic shock, with extent of shock as well as how reversible it is driving the potential benefit of ECMO. This functional continuum of cardiac health and compromise is evident as contraction and relaxation followed an equal and opposite linear relationship (figure 4.7 and 4.8) with coronary perfusion for all subjects and physiologic states (i.e. baseline, CS and ECMO support). Indeed, the extension to stress and ECMO states added fidelity to this continuum as the fit became better not only with additional data points but over an extended range. It is also seen in the correlation matrices of cardiovascular dynamics (Fig 4.3) which include other cardiovascular metrics.

While VA-ECMO provides circulatory support through e.g. enhanced coronary perfusion there are distinct negative effects. Retrograde flow augments afterload, and increases LV stress. Thus, using correlation matrices we were able to show how serial stress modulation caused homogenization of changes in cardiovascular metrics. Clustering the sickest animals as well as examining ECMO induced stress increases parameter correlations - the system is pushed towards a more homogeneous state. While ECMO is a therapeutic intervention and restores systemic perfusion, it is evident that it stresses the cardiovascular system (ECMO correlation matrix, Figure 4.3).

More specifically, a thermodynamic efficiency analysis in the pressure-volume domain revealed a nuanced response to VA-ECMO initiation. Leading to the observation that response is dependent on the initial cardiovascular state and the severity of induced CS (mild, moderate, or profound). The data in Table 4.1 indicates that a combination of severe CO decrease with highest

increase in LVEDP, were able to best identify the subgroup that benefitted most from ECMO initiation and titration. These subjects demonstrated highest positive effect (fold increase) in ventricular efficiency metrics, **possibly due to the contribution of significant increase coronary perfusion**. This is also supported by the linear trends depicted in Figure 4.7 showing the changes in ventricular contractility and relaxation linearly correlate with changes in coronary perfusion.

During flow titration, ramping 40 – 50 – 60 ml/kg/min revealed linear trends for cardiac and vascular metrics including SW, LVEDP, coronary perfusion pressure, systemic perfusion pressure, contractility (dp/dt $_{max}$) with a positive slope with increase in ECMO flow. Carotid pulsatility index and ventricular relaxation (dp/dt $_{min}$) revealed an inverse linear trend.

Carotid artery flow response, surrogate of cerebral perfusion, showed that while bulk average flow is substantially higher with initiation of ECMO, pulsatility index varies with shock state degree. In the profound shock group, indices are down ~50-70% from baseline, begging a discussion and future studies of optimal brain perfusion strategy and chronic effects in prolonged use of VA-ECMO.

Studying the slopes of the response to flow titration (Figure 4.5, Figure 4.6), subjects 3,4, and 6 had a similar response, confirming the correlation showed in the initial CS state analysis. For these subjects, we could then predict the trajectory of flow titration, its effects on systemic hemodynamic metrics (e.g. MAP, systemic perfusion pressure) and LV state metrics. Conversely, the subject identified in mild CS state, showed a minimal benefit to ECMO initiation and titration minimal increase in CP and systemic perfusion with initiation, with no effect for titration, with an increase in LVEDP.

4.5 Conclusions

This study highlights two main themes – first, the importance of the definition of proper experimental CS state for the study of MCS intervention and its effects on cardiovascular state, and second, an evaluation of the effects of VA-ECMO flow titration on cardiac and vascular metrics in the setting of CS. With the goal of finding an optimum of support for a given CS state.

While the results of this study are preliminary, they illustrate the breadth of physiologic response to CS state and to the initiation of circulatory support. These data suggest that while a proportion of subjects benefit from VA-ECMO support initiation and titration, others might not benefit from this specific mode of support. And lastly, another subset of subject might not have an appreciable physiologic response to titration.

Further studies are needed to provide a larger experimental set, for quantifying the response of the different CS severity subgroups to type and degrees of circulatory support. Specifically, to quantify effect on key metrics such as LVEDP, systemic and coronary perfusion, SW and pulsatility index. These studies can aid in establishing key metrics for the assessment of benefit from VA-ECMO initiation in the clinic. Better understanding of the dynamic physiologic response can inform patient selection for treatment invasive as VA ECMO. And once initiated, can inform support titration for minimal LV strain while maximizing beneficial increase in prefusion, ultimately towards better outcomes for these patients.

(This page was intentionally left blank)

Chapter 5: Steady Flow Left Ventricle Unloading is Superior to Pulsatile Pressure Augmentation for VA ECMO Support of Cardiogenic Shock

5.1 Abstract

Objectives: The aim of this study was to compare two mechanical methods for left ventricle (LV) venting during VA-ECMO support.

Background: VA-ECMO restores end-organ perfusion in circulatory failure but simultaneously increases afterload that may impede LV ejection. To maintain flow across the aortic valve, secondary mechanical circulatory support (MCS) devices are increasingly employed to vent the LV. Uncertainty of the optimal combined MCS strategy motivates the need to advance mechanistic understanding to guide device selection and improve patient outcomes.

Methods: Cardiogenic shock was induced in swine through microbead embolization of the left anterior descending artery. Animals underwent VA-ECMO (N=6) followed by either intra-aortic balloon pump (IABP) (N=3) or percutaneous ventricular assist device (pVAD) (N=3) to perform mechanical LV venting. Hemodynamic measurements, LV pressure-volume loops, and carotid artery blood flow were evaluated at three different levels of VA-ECMO support (40, 50, and 60 ml/kg/min) before and after LV venting.

Results: LV venting withe IABP produced negligible decreases in LV end diastolic pressure (LVEDP) with average values ranging from 20 to more than 30 mm Hg. By comparison, the pVAD reduced LVEDP to 8 to 22 mmHg depending on the level of pVAD support. Overall, the pVAD led

to lower LV stroke work, higher coronary and systemic perfusion gradients, and higher carotid blood flow rates across all ranges of ECMO flow rates in comparison to LV venting with IABP.

Conclusions: LV venting with a pVAD provides improved unloading of the ventricle in comparison to that provided by an IABP. Afterload, preload, and contractility metrics alone overlook the profound benefits of mechanical LV unloading. Metrics such as thermodynamic pressure-volume representation of ventricular energetics more accurately describe ventricular and vascular response. Device outcomes should be analyzed to capture the benefits of unloading and to be able to better select the patients that will benefit from this highly invasive care.

5.2 Introduction

Veno-Arterial Extracorporeal Membrane Oxygenation (VA ECMO) provides circulatory or pulmonary-circulatory support, and yet the attendant retrograde aortic flow increases afterload on the already compromised left ventricle (LV)(20,80). The increased afterload stresses the LV, restricting aortic valve opening and forward flow while simultaneously increasing end diastolic volumes and pressures and pulmonary congestion (81). Simultaneously then further stressing the heart and compromising distal perfusion as well as promoting lethal clotting and embolism formation in the LV.

Combined mechanical circulatory support (MCS) modalities can increase ECMO support and are presumed to protect the LV and the vasculature from deleterious effects by venting the LV, reducing blood pressures and volumes, leading to greater chance of myocardial recovery. Most published studies of LV venting rely on retrospective data, anecdotal patient outcomes or computational studies (82–84). Often, patient care is dependent on the center and physician's preference and experience rather than clear guidance as to which patients would benefit or not

from the increased invasiveness and extra support modality. Hence, a mechanistic understanding of the cardiovascular response are urgently needed for patient selection and titration of care (85).

Herein we compare unloading using pulsatile pressure augmentation from an intra-aortic counterpulsation balloon (IABP) device to continuous flow constant impeller motor speed device for optimizing VA ECMO use in the setting of cardiogenic shock.

5.3 Materials and Methods

5.3.1 Physiologic Measurements and Data Acquisition

6 young adult castrated male Yorkshire swine (ranging 60-80kg, mean 67kg) were maintained in accordance with NIH and AAALAC guidelines (CBSET, Lexington, MA).

Animals underwent induction anesthesia with intramuscular tiletamine-zolazepam (4-6 mg/kg) injection followed by endotracheal intubation. A 20-gauge catheter was placed in the ear vein and a continuous infusion of propofol (0.2 to 0.4 mg/kg/min) was administered and titrated to maintain deep sedation. The animals were then initiated on mechanical ventilation with a Puritan Bennett 840 Ventilator (Medtronic, Inc., Dublin, Ireland) using volume control mode with a tidal volume of 8 ml/kg actual body weight, positive-end expiratory pressure of 5 cm H_2O, and a fraction of inspired oxygen of 50%. Body temperature, oxygen saturation, end-tidal carbon dioxide, and electrocardiogram were monitored throughout the experiment.

Vascular access was obtained at both femoral arteries and veins, left jugular vein, and left carotid artery (***Error! Reference source not found.***). A guide catheter was introduced through the left femoral artery and into the left ascending (LAD) coronary artery for execution of the cardiogenic shock model (detailed below). After Shock state was achieved, the guide catheter was replaced by the ECMO return cannula.

In the unloading phase an Impella CP (Abiomed Inc., Danvers, MA) or an IABP (Datascope CS300, Maquet 40cc Intra-Aortic Balloon Pump) was introduced through the right femoral artery and advanced to position under fluoroscopy. The Impella is a constant motor speed continuous flow transvalvular MCS whereas IABP is counterpulsation with retrograde pulsatile augmentation of aortic diastolic pressure and reduction in systolic pressure. Transonic clamp-on flow meter (MAxPSB, TS420 Module, Transonic Systems, NY) was placed around the left carotid artery. A pressure–volume catheter (Millar, Houston, TX) was advanced from the contralateral carotid artery into the LV through a 6-9 Fr introducer. Venous access was achieved in the right and left jugular veins for the placement of a pulmonary artery catheter (TD Swan), and a Millar pressure sensor for pulmonary artery pressure. A 14 Fr femoral venous introducer sheath enabled placement of a 10 cc occluder balloon in the inferior vena, to be used for volume signal calibration, which was later replaced by the ECMO withdrawal cannula. Each device was tested in three pigs.

Baseline arterial hemodynamics and dual ventricular pressure-volume measurements were taken. Triplicate thermodilutions were done, promptly followed by inferior vena cava occlusion for volume signal calibration. The following data were recorded continuously for the reminder of the study: HR, AoP, CVP, PAP, femoral pressures, LV and RV pressures and volume, SpO_2 and $ETCO_2$ with periodic mixed venous O_2 saturation.

5.3.2 Porcine Model of Cardiogenic Shock

CS state was induced using microbead (45-105 um) embolic occlusion (described in more detail in Ch.4 – methods), of the LAD and if needed, the circumflex coronary artery. CS state was achieved when: LVEDP exceeded 16 mmHg and/or MAP dropped below 50 mmHg, and/or SvO2

was <55% or CO <50 mL/kg/min (per TD). Once CS stage was achieved a new experimental

baseline was established for each of the animals.
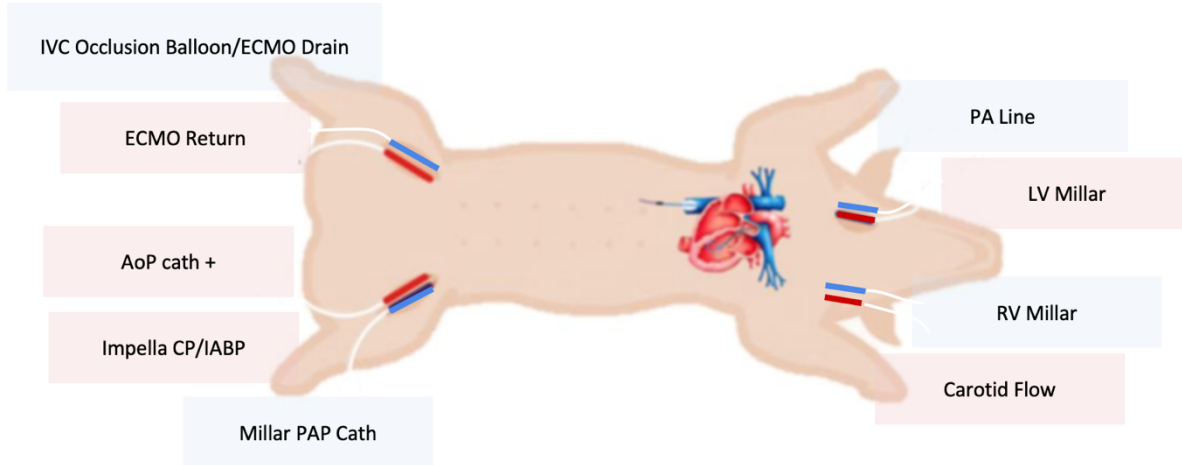
Figure 5.1 - Experimental set-up. Red sheath represents arterial access, blue sheath represents venous access. IVC = inferior vena cava; AoP = aortic pressure; IABP = intra-aortic balloon pump; PAP = pulmonary artery pressure; PA = pulmonary artery; LV = left ventricle; RV = right ventricle.

5.3.3 Mechanical Circulatory Support

VA ECMO setup was primed in advance and initiated at 50 ml/kg/min once the withdrawal

cannula was confirmed in the femoral vein and return cannula in the left femoral artery. Once

hemodynamics reached steady state, ECMO was titrated to 40 ml/kg/min and, hemodynamic data

were obtained, followed by repeat measurements for 50 ml/kg/min and 60 ml/kg/min. At each level

of ECMO support hemodynamics were monitored in real time to define a steady state and baseline

for subsequent analysis, where MAP and LVP remained within a set range over multiple respiratory

cycles (min. waiting time >2min), as the Impella spanned performance levels from P2 to P8 and

IABP from 1:3-1:1. At least 20 minutes elapsed between state changes to assure return to baseline

hemodynamics.

5.3.4 Data Analysis

Venous and arterial hemodynamics, EKG and PV data for both ventricles were recorded continuously throughout the study. Data were analyzed with an in-house Python algorithm. For each state analyzed, parameters were calculated for corresponding beats, beat by beat, during two full respiratory cycles to account for respiratory variation. Each of these parameters were averaged over the two respiratory cycles. Individual PV loops were taken at end-expiration. The calculated metrics included ventricular energetics and state, arterial hemodynamics, and carotid flow data.

5.3.5 Statistical Analysis

Statistical analysis was performed using Prism (GraphPad Software, San Diego, CA). One-way ANOVA were performed to compare the effects of unloading on LV and vascular mechanics. Plots are presented as mean with standard deviation for each experimental group.

5.4 Results

Six animals underwent the study protocol and were initiated on VA-ECMO support and subsequent placement of the specified secondary mechanical venting support device. All animals reached the target parameters used to define CS prior to initiation of extracorporeal circulatory support resulting in decreased systemic pressure and increased LVEDP. After initiation of VA-ECMO support, animals underwent combined MCS with either pVAD (N=3) or IABP (N=3).

5.4.1 LV State

Impella unloading enabled significant reduction in left ventricular end diastolic pressure (LVEDP) while IABP elicited only minimal response (Figure 5.2 B., C., Figure 5.4 A.). Moreover, absolute LVEDP values during Impella unloading were closer to normal physiologic values, even when initial baseline support LVEDP was higher as post unloading values were as low as 8.2 and only as high as 22.6mmHg for the Impella and almost 20 and more than 30 mmHg for the IABP.

Reduction in contractility, dP/dt $_{max}$, was noted in both groups but was more substantial in the Impella group (Figure 5.5). Stroke Work (SW) changes (Figure 5.6) showed opposite trends with the two unloading modalities – significantly reduced for the Impella and increased for the IABP at all three levels of ECMO support.

5.4.2 Arterial Hemodynamics

Changes in systolic blood pressure (SBP) were consistent across the IABP cohort (Table 5.1) – showing, as expected, a mean reduction of -11-(-13) % when unloaded with the IABP (Figure 5.3 A.). Interestingly, SBP reduction is not dampened in the setting of ECMO when compared to the use of IABP alone (86). The Impella response was more nuanced (Figure 5.3 B.), dependent on cardiovascular state. Diastolic Augmented Pressure (AP) for the IABP cohort showed a linear

relation to the degree of ECMO support (Table 5.1), animals showed the same response with a trend line slope mean 0.58 ± 0.04, with an R^2 mean of 0.95.

5.4.3 Coronary Perfusion Pressure

Coronary prefusion pressure (CP) was calculated using two methods – Initially,

[*diastolic blood pressure (DBP)] – [LVEDP]* in the Impella cohort, and as [*augmented pressure] – [LVEDP]* in the IABP group. This method is used for clinical estimation due to limitations in measurement in the clinic. However, it provides a skewed result, taking into consideration only a specific timepoint in the cardiac cycle. Having continuous pressure measurements in the LV and aorta simultaneously, enable the following calculation [*AOP – LVP]* during diastole.

CP improved with both unloading modalities (Figure 5.7 A.) but more significantly in the Impella cohort, with 1.5-fold improved mean perfusion when unloading with Impella P2 (lowest level of support) compared to IABP. Impella cohort demonstrated a linear increase in coronary perfusion as support level increased, reaching ~50% improvement for all ECMO states when unloading with P4 and higher. IABP showed least benefit for the highest ECMO flow – an insight that, when validated, can be valuable in a clinical setting when choosing an unloading device for a patient on high ECMO flows.
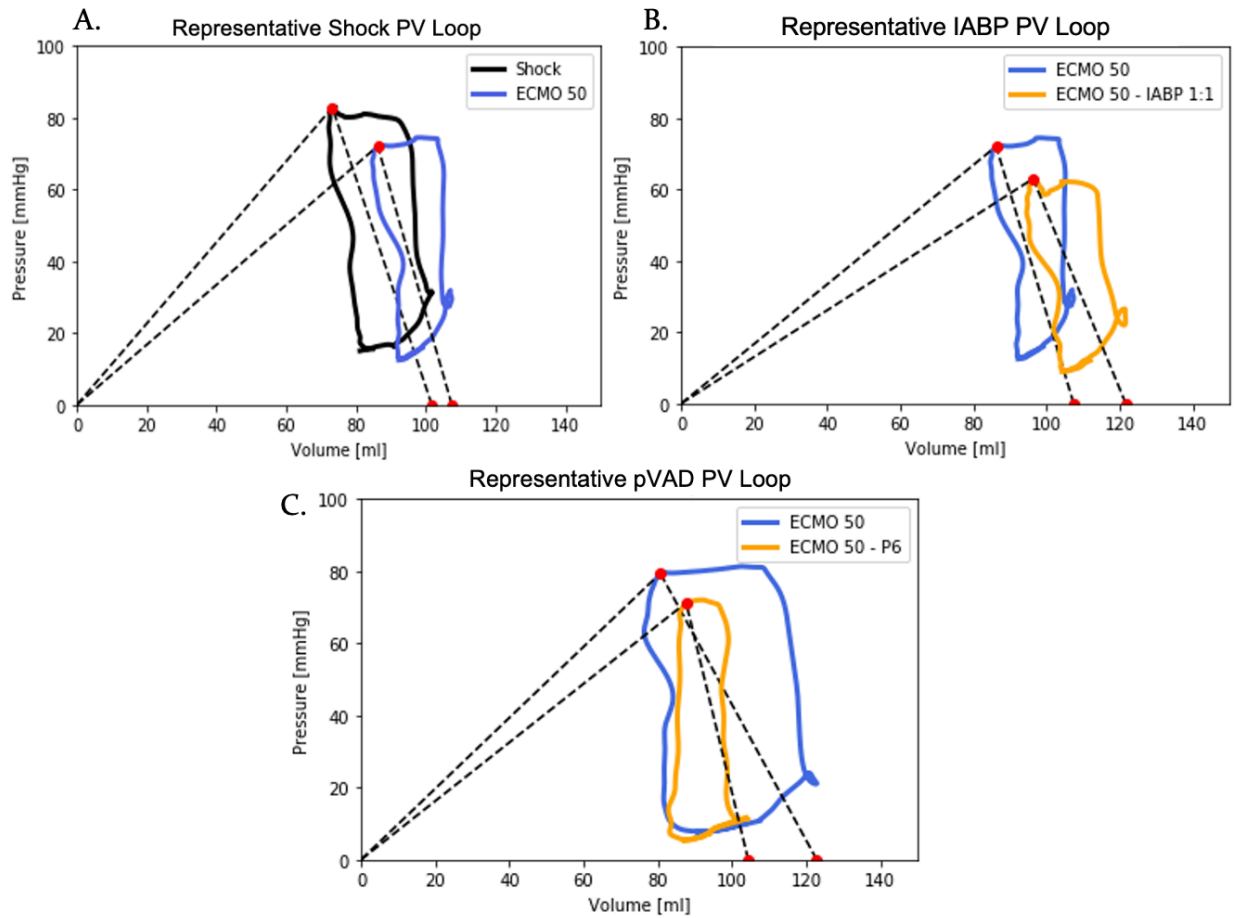
Figure 5.2 – *Representative pressure-volume loops of cardiogenic shock, VA-ECMO support and unloading modalities.* *A. Loop at cardiogenic shock (black) and after VA-ECMO initiation (blue). B. Loop during VA-ECMO support before and after IABP. C. PV loop during VA-ECMO support before and after pVAD.*
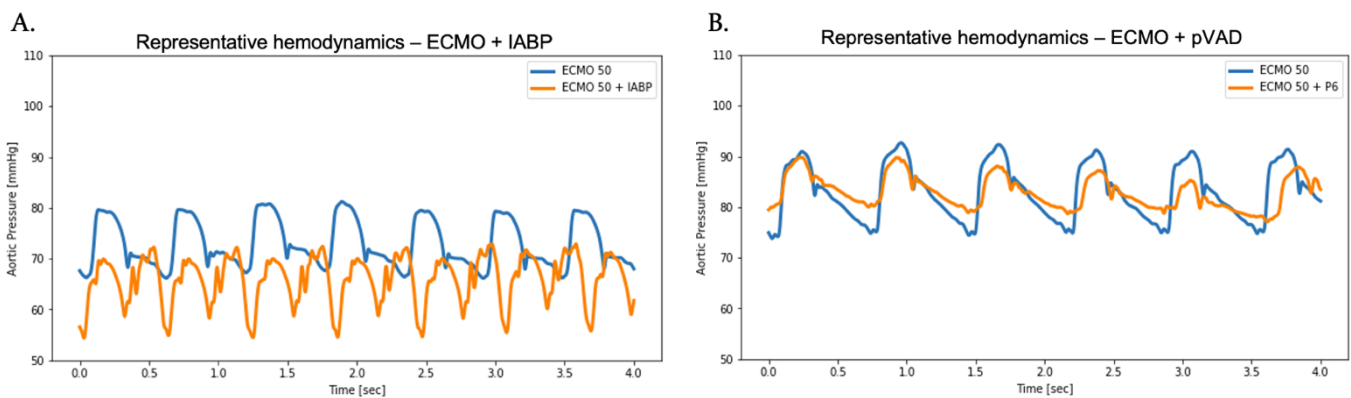
Figure 5.3 – *Representative hemodynamic tracings.* *A. Systemic arterial blood pressure during VA ECMO support and following introduction of IABP in a representative animal. B. Systemic arterial blood pressure during VA ECMO support and following introduction of pVAD in a representative animal.*
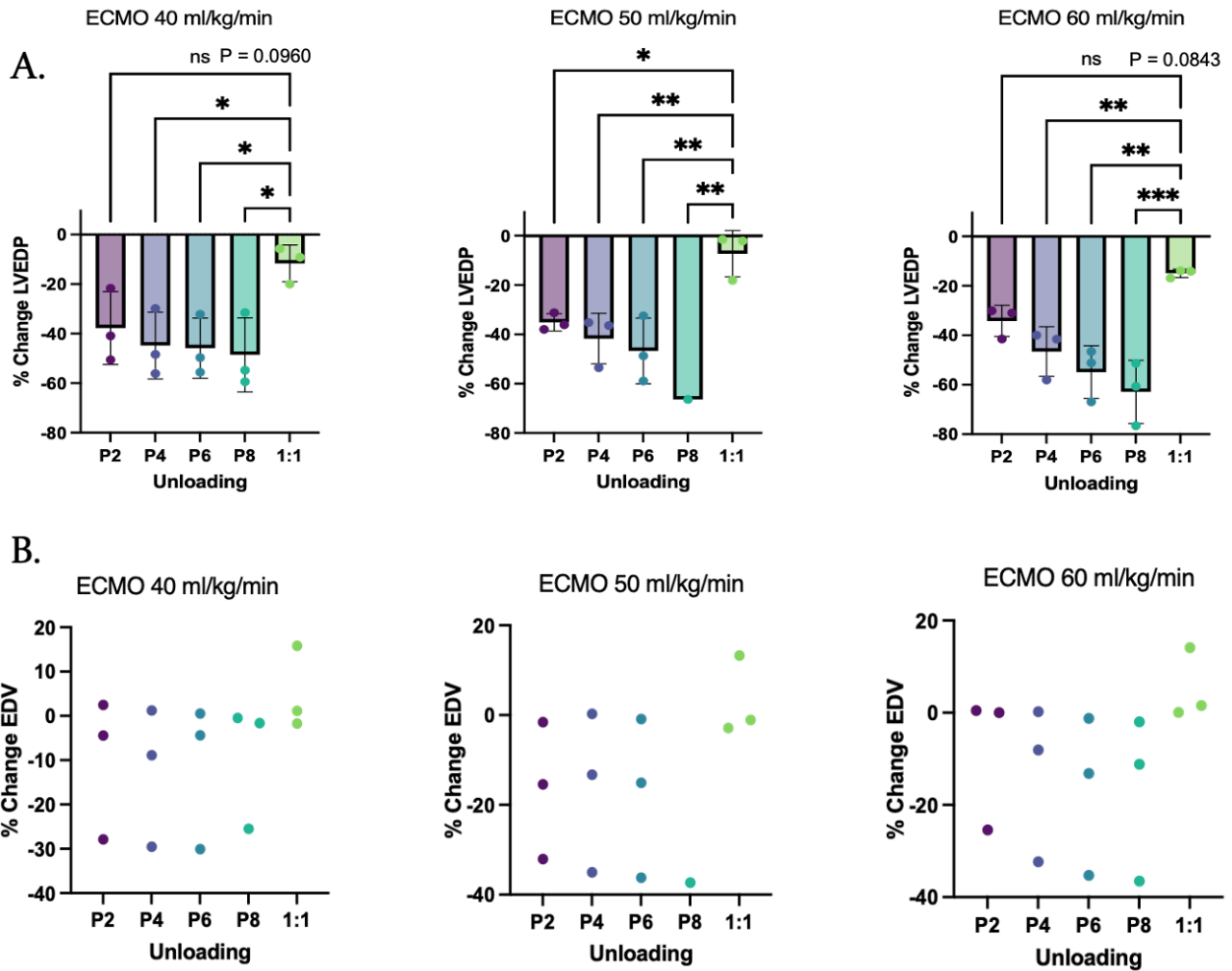
Figure 5.4 - Percent change from VA-ECMO alone for 3 flow rates*. A. LVEDP: VA-ECMO 40 -37.7 - -48.5% vs.-11.6%, VA-ECMO 50 -35.1 - -66.4% vs. -7.2%, VA-ECMO 60 -34.2 - -62.8% vs. 14.9%, mean range given for P2-P8 unloading vs. IABP at 1:1, for all ECMO states. B. EDV change is state dependent showing overall reduction in the Impella cohort, and overall increase in the IABP cohort.*
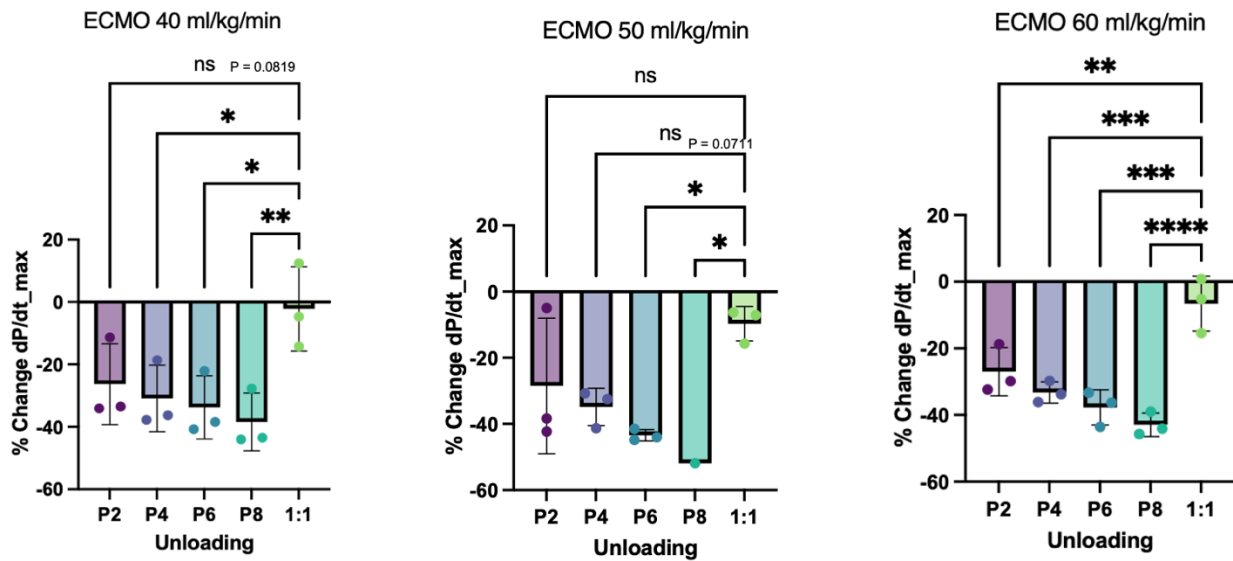
Figure 5.5 - Contractility percent change from VA-ECMO alone for 3 flow rates. *VA-ECMO 40 -26.3 - -38.4% vs. -2.8%, VA-ECMO 50 -28.5 - -51.8% vs. -9.7%, VA-ECMO 60 -26.9 - -42.9% vs. 6.6%, mean range given for P2-P8 unloading vs. IABP at 1:1 for all ECMO states.*
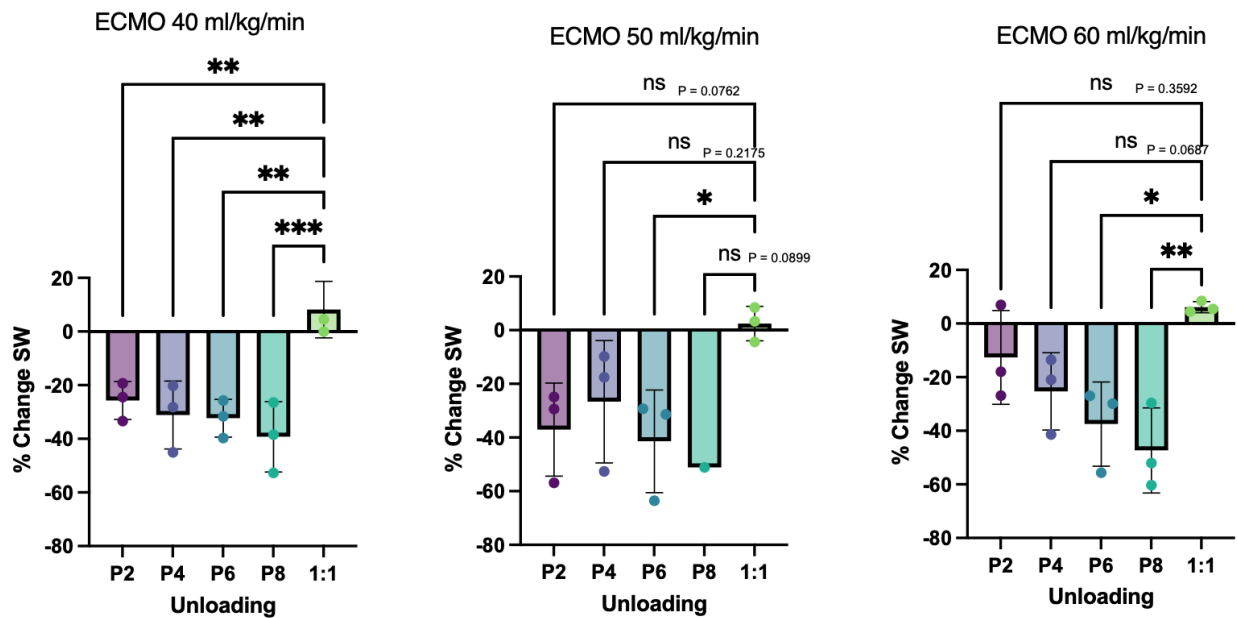
Figure 5.6 - SW percent change from VA-ECMO alone for 3 flow rates. *VA-ECMO 40 -25.7 - -39.2%, VA-ECMO 50 -26.6 - -51.1%, VA-ECMO 60 -12.6 - -47.3%, mean range given for P2-P8 unloading for all ECMO states), while using IABP a slight increase in SW was recorded across ECMO flow rates (2.4-8.2%).*
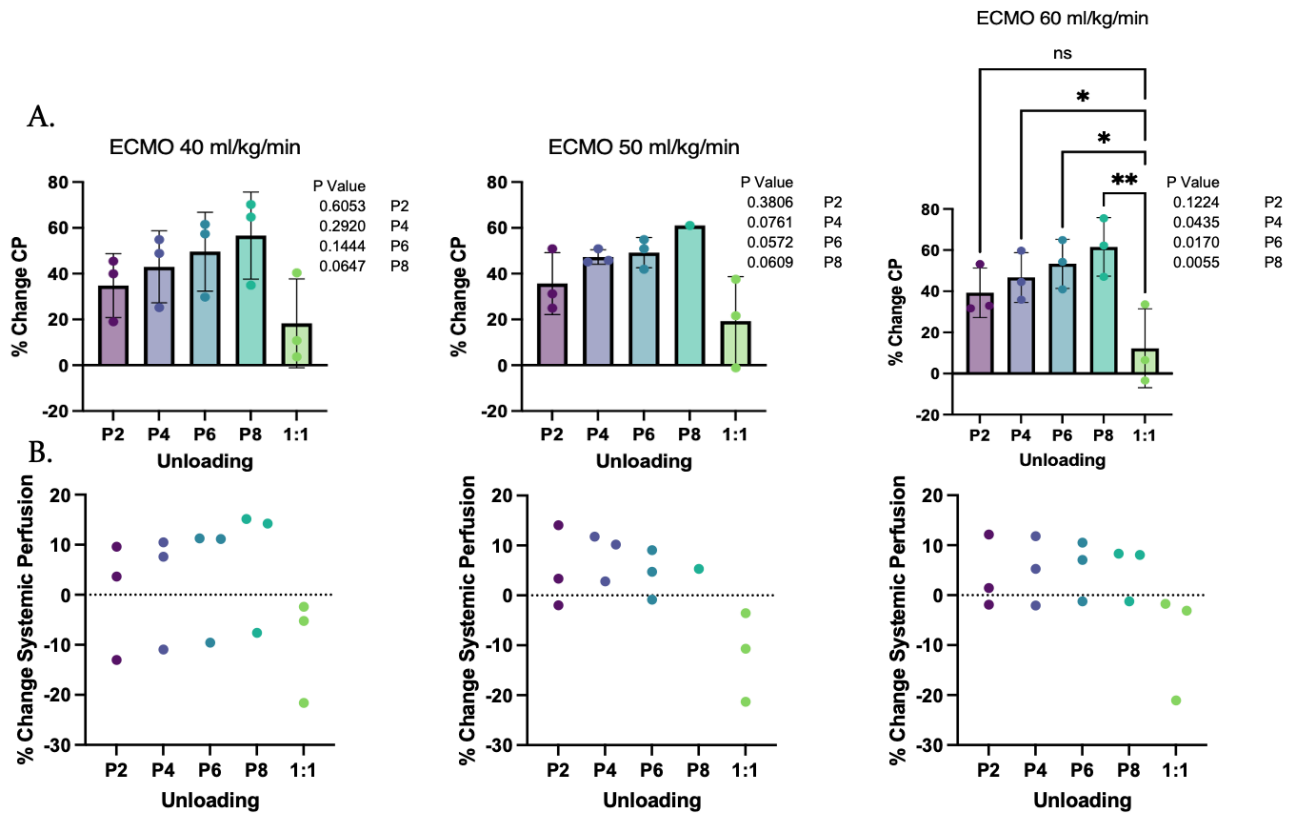
Figure 5.7 – Changes in coronary and systemic prefusion pressures. *A. CP = Coronary perfusion pressure percent change from VA-ECMO alone for 3 flow rates. VA-ECMO 40 34.8-56.6%, VA-ECMO 50 35.6-61%, VA-ECMO 60 39.2-61.6%, mean range given for P2-P8 unloading for all ECMO states, while using IABP ECMO 40,50,60 perfusion pressure increased 18.3%, 19.3% and 12.3% respectively. B. Systemic perfusion pressure.*
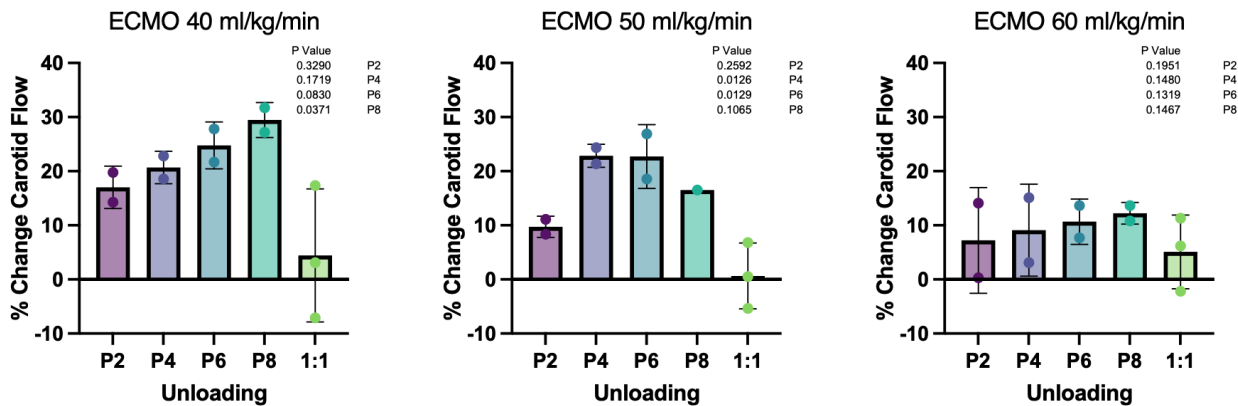
Figure 5.8 - Changes in Carotid flow at each ECMO flow rate.

% Change from CS	40	50	60
HR	-7.0 (6.7)	-9.4 (4.3)	-9.6 (7.4)
SBP	-11.1 (1.6)	-13.2 (0.8)	-12.1 (0.9)
DBP	-20.9 (5.9)	-17.9 (4.6)	-14.1 (1.6)
Augmented DBP [mmHg]	65.93 (3.3)	71.15 (2.9)	77.48 (3.7)
MAP	-4.3 (1.7)	-6.5 (2.9)	-6.1 (2.6)
PA sys	0.3 (11.6)	-6.7 (5.0)	-6.5 (11.1)
PA dias	6.0 (29.6)	-9.0 (13.5)	-10.7 (15.4)
PA mean	5.0 (16.1)	-6.7 (5.9)	-7.4 (11.6)

Table 5.1 - Percent change in each hemodynamic parameter for combined MCS with IABP operating at 1:1 and VA-ECMO (n=3) compared to baseline state of cardiogenic shock supported on VA-ECMO only at each specific ECMO flow rate [ml/kg/min]. All values unless specified otherwise are % change. Negative values reflect reduction. STDEV is in parenthesis. HR = heart rate; SBP = systolic blood pressure; DBP = diastolic blood pressure; MAP = mean arterial pressure; PA = pulmonary artery pressure (systolic, diastolic, and mean).

ECMO % Change	40 [ml/kg/min]				50 [ml/kg/min]				60 [ml/kg/min]			
	P2	P4	P6	P8	P2	P4	P6	P8	P2	P4	P6	P8
HR	-5.5	-8.2	-5.5	-3.3	0.0	-2.2	-6.7	-6.7	-4.4	-4.4	-4.4	-2.2
	(8.2)	(3.1)	(8.2)	(5.4)	(6.7)	(7.7)	(13.3)		(3.8)	(3.8)	(3.8)	(3.8)
SBP	-4.6	-4.0	-3.2	-1.8	-1.1	4.3	-0.4	-5.7	-0.3	-0.9	-1.4	-2.8
	(8.0)	(7.1)	(7.3)	(7.8)	(7.9)	(2.0)	(4.8)		(6.0)	(4.7)	(3.6)	(2.7)
DBP	2.0	5.4	8.2	12.4	5.9	15.2	13.1	12.9	3.4	6.1	7.7	8.7
	(10.2)	(10.2)	(10.9)	(12.2)	(10.4)	(3.1)	(9.9)		(7.8)	(7.0)	(6.3)	(5.2)
MAP	-1.6	0.4	2.1	4.7	-1.7	5.0	1.4	2.8	1.0	1.6	1.7	1.5
	(11.0)	(11.0)	(11.2)	(12.2)	(10.8)	(4.4)	(5.1)		(6.6)	(6.0)	(5.3)	(5.0)
PA sys	-1.0	-0.9	-0.1	0.2	-13.9	-6.1	-7.8	-12.7	-10.6	-13.0	-13.7	-12.7
	(16.7)	(16.5)	(16.0)	(15.9)	(3.5)	(9.9)	(5.7)		(3.6)	(3.0)	(6.2)	(6.5)
PA dias	13.5	11.5	15.7	5.1	-24.6	12.7	-1.9	-19.8	-8.2	-17.8	-21.2	-21.2
	(43.3)	(45.0)	(52.7)	(35.6)	(10.5)	(47.4)	(18.6)		(14.4)	(5.7)	(4.8)	(7.8)
mPAP	8.7	8.1	8.6	6.4	-15.0	0.9	-3.5	-14.3	-7.6	-12.5	-14.4	-15.5
	(27.8)	(28.9)	(30.2)	(26.4)	(2.1)	(23.7)	(12.6)		(8.8)	(6.5)	(9.8)	(10.4)

Table 5.2 - Percent change in each hemodynamic parameter for combined MCS with pVAD and VA-ECMO (n=3) compared to baseline state of cardiogenic shock supported on VA-ECMO only at each specific ECMO flow rate for a given pVAD P-level. All values % change from baseline obtained during VA-ECMO support unless other specified. Negative values reflect reduction from baseline. STDEV is in parenthesis. HR = heart rate. SBP = systolic blood pressure. DBP = diastolic blood pressure. MAP = mean arterial blood pressure. PAS = pulmonary artery systolic pressure. PAD = pulmonary artery diastolic pressure. mPAP = mean pulmonary artery pressure.

5.5 Discussion

VA-ECMO bypasses the heart providing high flow and systemic perfusion but strains the LV by increasing afterload (Figure 5.2 A.), increasing SW and thus, myocardial oxygen demand. The addition of hybrid MCS devices might alleviate these challenges and yet it is not clear which cardiovascular parameters are aimed to be modified. The advantages of focusing on a specific metric (e.g. afterload reduction with IABP), vs. titrating treatment to drive multiple thermodynamic determinants are yet to be established in clinical practice.

Classically, the use of an IABP, a device external to the LV, provided afterload reduction and as such was of interest when trying to battle the negative effects of ECMO. By virtue of residing in the aorta, it affects primarily the vasculature and not the ventricle, where reduction in afterload reduces systolic and mean arterial pressure, impeding forward flow, and increasing ventricular volumes.

Conversely, in this study we were able to show how an intracardiac indwelling device affects thermodynamic work parameters and by virtue of residing in the LV, alters multiple cardiovascular parameters while preserving forward flow, concurrently beneficial for systemic perfusion and prevention of lethal thromboembolisms. While providing superior forward flow, it reduces EDV and pressures and is highly titratable, cumulatively with the ability to fine-tune ECMO flow. It provides the ability to dynamically adjust in response to cardiovascular state as well as ECMO titration, compared to an extracardiac device, can be only turned on/off, and does not allow the freedom to fine tune to a desirable unloading state.

Thermodynamic Myocardial Work

Impella reduced SW for all animals while IABP had no effect or slight increase (Figure 5.6), suggesting that while the Impella does provide reduction of load on the LV and venting, the IABP is beneficial for a different subset of patients. Statistical significance demonstrated for the higher Impella unloading states (P6 and P8) in the higher VA ECMO level of support, indicating that, as expected, the higher the load on the LV with greater ECMO flow, higher degree of mechanical unloading needs to be provided for reduction of myocardial O_2 demand.

dP/dt $_{max}$ is also used for the evaluation of contractility, and thus myocardial work. While a reduction in contractility is noted for both study groups, a more significant reduction is noted with the Impella, and more profoundly with higher P levels (P6, P8). In the IABP group, the reduction in dP/dt $_{max}$ is most likely linked to the reduction in SBP, an expected target of this device.

While both SW and dP/dt $_{max}$ are metrics of LV work, the latter is tied more closely to changes in blood pressure. SW is calculated from the area enclosed by the PV loop making it dependent both on LV volume state (SV) as well as the pressure generated by the LV. Thus, it provides a more accurate way to quantify changes in LV work.

Reduction in LV End Diastolic Pressure

LVEDP is the pressure in the LV at the end of filling phase, right before contraction begins. Clinically, LVEDP is used to assess LV state in both acute and chronic heart failure, and changes in LVEDP provide insight into the cardiovascular state, efficacy of an intervention or disease progression. Elevated LVEDP is a marker of increased volumes and congestion and loss of ventricular compliance.

The results of this study show a profound reduction in LVEDP in all levels of mechanical unloading with Impella (Figure 5.4 A.). In most cases, the Impella was able to reduce pressures to near normal physiologic range. IABP cohort also demonstrated a reduction in comparison to VA ECMO alone albeit minimal, leaving LVEDP at 19-30 mmHg, elevated values out of the normal range. When targeting LVEDP reduction, unloading with an Impella, at any P levels equal or greater than P4 proved statistically significant benefit over the IABP. Moreover, in the Impella cohort, the ability to fine tune LVEDP reduction is evident across all levels of ECMO flow – with a linear trend showing greater LVEDP reduction as P level is increased. The change (i.e. greater reduction with P level increase) is more significant as ECMO flow increases. This comes in comparison to IABP where unloading with a counter pulsation of 1:1 provides an on/off option for unloading without the ability to further titrate the amount of LV unloading to the patient's state.

Changes in EDV

The change in EDV was variable among the subjects (Figure 5.4 B.), with a negative (reduction) overall trend for the Impella cohort, and a slightly positive trend for the IABP cohort. The Impella's results varied among animals, suggestive of a CS state response. Overall, when aiming to reduce LV volumes, the Impella is the adequate device to use, as it continuously propels blood from the LV into the aorta, both during systole and diastole, leading to a reduction in preload (Figure 5.2 C.).

Coronary Perfusion Pressure

Mechanical unloading increased CP in both groups when compared to ECMO alone. The improvement is driven by the main determinants of coronary perfusion pressure – *[aortic diastolic pressure] - [LV diastolic pressure]*. Due to an increase in arterial diastolic pressure and a decrease in LV diastolic pressure in both groups, the resulting pressure gradient which drives coronary flow is increased.

In the IABP cohort, CP showed better improvement over ECMO alone at lower ECMO flows, suggesting that for higher afterload states, IABP does not provide enough diastolic pressure augmentation and LVEDP reduction.

Impella's cohort CP increased steadily as P levels were increased, owing this improvement both to an increase in DBP, due to constant flow through the Impella throughout the cardiac cycle, as well as a significant reduction in LVEDP. As such, the benefits of mechanical unloading for myocardial metabolism are two-fold – reducing demand (SW, contractility reduction) as we all increasing the supply by augmenting diastolic coronary perfusion pressure.

A larger spread was observed in the fold increase in CP, suggesting a greater dependence on native cardiac state. E.g. in the Impella cohort, the animal with the lowest improvement in CP, was the animals in mildest CS state (maintain relatively high SBP and DBP post CS and on ECMO alone). Similarly, the animal in most profound CS state, showed the greatest benefit of 50-75% fold improvement in CP. A 50% improvement was shown even with an Impella level as low as P2.

5.6 Conclusions

ECMO provides support during CS, but profoundly alters hemodynamics, increases afterload, and impedes forward flow from the LV. Mechanical unloading is used for LV venting, and proposed to favor myocardial recovery for CS patients, but mechanistic studies are lacking.

A CS porcine model was leveraged to quantify unloading effects on cardiovascular parameters. Unloading with a percutaneous continuous flow intracardiac unloading showed superiority in all metrics tied to LV state improvement including LVEDP, SW, contractility, CP. CP improves with increase of intracardiac unloading due to improvement of both DBP and LVEDP (reduction).

The choice of a secondary device for unloading should be tailored to specific patient's state and target intended effect by understanding the mechanism of action of each unloading approach. Extracardiac vs. intracardiac hybrid MCS – the ability to control single, vascular parameter, vs. multiple cardiac parameters – thermodynamic work and efficiency.

5.7 Limitations and Future Work

The experimental results detailed in this study are derived from a porcine model of acute CS. While this model provides many similarities to clinical patient care, the severity of shock does not capture the range of pathology encountered clinically. It is important to note that the model generated primarily isolated LV failure and is not a model of biventricular dysfunction. Additionally, all animals maintained systemic pulsatility on initiation of VA-ECMO throughout titration of support. Clinical patients undergoing LV venting often experience loss or near-loss of systemic pulsatility motivating placement of a secondary MCS device. The modest benefits of

combined MCS with IABP in this study may understate the benefit in clinical settings of severe failure where IABP placement has been observed to promote aortic valve opening. Future experimental work will investigate an expanded range of shock severity and further variation in patterns of cardiac dysfunction.

Chapter 6: Conclusions and Future Directions

Overview and Challenges

The work presented in this dissertation aims to mechanistically investigate mechanical circulatory support (MCS) devices:Cardiovascular interactions in the setting of cardiogenic shock (CS). CS rates have been on the rise over the past two decades, and despite advances in therapeutics and interventions, mortality rates remain devastatingly high. Advanced MCS devices and support modalities are introduced in the setting of shock, but their use is limited by an incomplete understanding of their interaction with the failing heart and vascular system. Clinical treatment for these patients remains extremely complex, requiring big multidisciplinary teams and tremendous resources. With a gap in mechanistic understanding of MCS:cardiovascular interactions, there are no clear guidelines on care optimization, and approaches vary between centers and among clinicians.

Research is limited by the severity and multifactorial effects of CS pathological spiral. Most studies to date are based on retrospective clinical data, confounded by very ill patients, and lack of standard metrics by which to evaluate patient state, initiation, and titration of care. Moreover, MCS devices are highly invasive, but do not provide insight about patient state, requiring additional invasive hemodynamic measurements.

My long-term goal focused on studying MCS induced hemodynamics, as a framework to better understand the emerging flow patterns which can help utilize MCS devices to their full potential. Using a benchtop flow loop model and an in-vivo model, we aimed to identify key metrics for prediction and real time evaluation of cardiac and vascular response to MCS implantation and titration.

Key takeaways and future work –

Designing, fabricating, and validating a flow loop (chapter 2) proved to be a long process through which the understanding of modeling approaches and limitations crystalized. The resulting in-vitro set up enables investigation of questions spanning from MCS ventricular-vascular coupling (VVC) effects, changes in pulsatility to results of ventricular "remodeling" on downstream perfusion and more. This model is most reliably used when quantifying the **change** an intervention elicits rather than absolute values. It is useful for investigating macro-scale (pressure and perfusion) fluid dynamics phenomena, in a controlled and reproducible manner - an endeavor that remains challenging in an in-vivo setting due to profound variances in physiologic response.

Next steps include validating the results of mixing zone patterns in an animal model, left ventricular (LV) unloading studies in the loop, validation of CFD studies using boundary conditions optimization function. Lastly, interrogation of device signals in a controlled environment aiming to identify metrics for device usage optimization and real-time insight into patient's cardiovascular state.

For the study of MCS devices effects on VVC and cardiovascular thermodynamic efficiency (chapters 3-5) in an in-vivo model of CS, we were able to create expertise as a team and obtain a library with a wealth of data, improving with each study we executed. Our animal model is stable and reliable and produces high fidelity clean data.

The limitation that remains, as in every in-vivo study, is the intrinsic inter-subject variability. The number of specimens in these large animal studies is limited by cost and complexity of the studies. In chapter 4, I showed the dependence of the response to veno-arterial extracorporeal membrane oxygenation (VA-ECMO) support on the initial state of the animal as well as the individual's response to shock induction. This highlighted the heterogeneity of responses both to

the shock model as well as support initiation. Interestingly, we found that this heterogeneity lies on a functional continuum. Moreover, the more we stress the system (baseline → CS → ECMO) we get a better linear trend on this continuum. In the clinic, some subjects benefit greatly from high degree of VA-ECMO support, and benefit from support titration, other subjects do not. Further studies are needed to validate this functional continuum finding, specifically validate the metrics by which we can predict if initiation of support will be beneficial. Lastly, these results highlighted the need for creation of a score for shock staging while maintaining pulsatility in the in-vivo model.

The VVC study, showed how increase of percutaneous ventricular assist device (pVAD, an Impella CP) support increases decoupling and decreases loading and contractility. Which can ultimately inform clinical selection of device and support level in combination of pressors – as afterload management remains challenging, and further understanding of the interplay between tools at hand of the clinician are needed.

In chapter 5 I demonstrated superiority of a pVAD over extracardiac pulsatile afterload reduction (IABP) for unloading the LV in the setting of VA-ECMO support during CS. The Impella decreased LV end-diastolic pressures, volumes, and stroke work (SW) while simultaneously maintaining coronary perfusion pressure and systemic perfusion pressure gradient. Based on these experimental findings, combined MCS with VA-ECMO and pVAD provide a means to sustain end-organ perfusion while simultaneously decreasing LV preload and promoting forward flow across the aortic valve. Future work is required to investigate the effects of combined MCS in a broader range of shock severity and to determine optimal titration of dual support.

Taken together, this dissertation explores novel frameworks to mechanistically evaluate the coupling of MCS:cardiovascular system, and suggests findings towards optimization of device

selection, initiation, and titration during CS. Further studies and clinical data evaluation will be done for validation of the trends, metrics and key findings presented in this thesis.

Once validated, these insights can be leveraged towards closed-loop real-time optimization of care that utilize device signals as well as additional external measurements. These insights can also incorporate guidance on optimization of concomitant drug and device support. Using real-time close-loop monitoring can help ultimately predict patient trajectory and aid in weaning or optimize for goals of cate (e.g. bridge to recovery optimization vs. bridge to transplant).

Moreover, by identifying metrics of interest for dynamic representation of LV and vascular state, devices can be designed to incorporate the ability to sense, rendering additional invasive measurements redundant and thus increase patient safety. For example – incorporating a volume measurement catheter on an indwelling pVAD and using the derivative of the change in LV volume to quantify flow. Using accurate flow and pressure measurements, vascular impedance can be easily calculated and monitored.

Continued development of the above findings, validation with clinical data and eventually translation to the clinic, in form of both mechanistic understanding and device development, can have measurable impact and ultimately lead to better outcomes for CS patients.

Appendix

Appendix I - Python Script

PACKAGES IMPORT

```
import matplotlib.pyplot as plt
from datetime import datetime
import numpy as np
import math
import time
import pandas as pd
import os
from scipy.signal import butter,lfilter,freqz
from scipy.fft import fft
from scipy.signal import find_peaks
import statistics
import numpy as np
from scipy.integrate import simps
from numpy import trapz
%matplotlib inline
```

FUNCTION LIST

```
def pulse_minmax(pressure, start_index, end_index, title, dist, heig):
    data = pressure[start_index:end_index]
    invert_data = data * -1
    # Adjust bounds
    mins_idx, _ = find_peaks(invert_data, distance=dist, height=-heig)
    output_mins = np.concatenate((mins_idx), axis=None).tolist()
    output_mins = [x+start_index for x in output_mins]
    #Find local maximas
```

```python
    maxs_idx, _ = find_peaks(data, distance=dist, height=-heig)
    output_maxs = np.concatenate((maxs_idx), axis=None).tolist()
    output_maxs = [x+start_index for x in output_maxs]
    plt.figure(figsize=(15,5))
    plt.plot(data)
    plt.title(title)
    plt.grid()
    plt.ylabel('Pressure [mmHg]')
    plt.xlabel('Time [ms]')
    plt.plot(pressure[mins_idx+start_index],'go')
    plt.plot(pressure[maxs_idx+start_index],'ro')
    plt.show()
    return output_mins, output_maxs


def waveform_plot(signal, start, end, signal_label):
    plt.figure(figsize=(10,6))
    plt.plot(signal[start:end], label=signal_label)
    plt.legend(loc='upper right')
    plt.ylabel("Pressure [mmHg]")
    plt.xlabel("Time [ms]")
    plt.ylim(0,140)
    plt.show()
    return signal[start:end]


### Function without MAP, adding MAP
# def pulse_pressure(pressure, start_index, end_index, title, dist, heig):
#     output_mins, output_maxs = pulse_minmax(pressure, start_index, end_index, title, dist, heig)
#     idx_list_max = output_maxs
#     idx_list_min = output_mins
```

```python
#    if idx_list_max[0]>idx_list_min[0]:
#        idx_list_min.pop(0)
#    len_min = len(idx_list_min)
#    len_max = len(idx_list_max)
#    if len_min<=len_max:
#        calc_range = len_min
#    else:
#        calc_range = len_max
#    pp = []
#    print(calc_range)
#    for x in range(calc_range):
#        pp_calc = (pressure[idx_list_max[x]]-pressure[idx_list_min[x]]).tolist()
#        #print(pressure[idx_list_max[x]],pressure[idx_list_min[x]])
#        pp.append(pp_calc)
#    avg_pp = sum(pp)/len(pp)
#    res = statistics.pstdev(pp)
#    print("pp = ",avg_pp,"+/-", res)
#    return(avg_pp, res)


def pulse_pressure(pressure, start_index, end_index, title, dist, heig):
    output_mins, output_maxs = pulse_minmax(pressure, start_index, end_index, title, dist, heig)
    idx_list_max = output_maxs
    idx_list_min = output_mins
    if idx_list_max[0]>idx_list_min[0]:
        idx_list_min.pop(0)
    len_min = len(idx_list_min)
    len_max = len(idx_list_max)
    if len_min<=len_max:
        calc_range = len_min
```

```python
    else:
        calc_range = len_max
    print(calc_range)
    pp = []
    MAP = []
    peak_sys = max(pressure[idx_list_max])
    min_dias = min(pressure[idx_list_min])
    for x in range(calc_range):
        pp_calc = (pressure[idx_list_max[x]]-pressure[idx_list_min[x]]).tolist()
        pp.append(pp_calc)
        map_calc = (((pressure[idx_list_max[x]])*(1/3)) + ((pressure[idx_list_min[x]])*(2/3))).tolist()
        MAP.append(map_calc)
    avg_map = sum(MAP)/len(MAP)
    map_res = statistics.pstdev(MAP)
    avg_pp = sum(pp)/len(pp)
    res = statistics.pstdev(pp)
    print("PP = ",avg_pp,"+/-", res)
    print("MAP = ",avg_map,"+/-", map_res)
    print("Peak Sys = ",peak_sys)
    print("Min Dias = ",min_dias)
    return(avg_pp, res, avg_map, map_res, peak_sys,min_dias)


def meanarterial_pressure(pressure, start_index, end_index, title, dist, heig):
    output_mins, output_maxs = pulse_minmax(pressure, start_index, end_index, title, dist, heig)
    idx_list_max = output_maxs
    idx_list_min = output_mins
    if idx_list_max[0]>idx_list_min[0]:
        idx_list_min.pop(0)
    len_min = len(idx_list_min)
```

```python
    len_max = len(idx_list_max)
    if len_min<=len_max:
        calc_range = len_min
    else:
        calc_range = len_max
    MAP = []
    for x in range(calc_range):
        map_calc = (((pressure[idx_list_max[x]])*(1/3)) + ((pressure[idx_list_min[x]])*(2/3))).tolist()
        MAP.append(map_calc)
    avg_map = sum(MAP)/len(MAP)
    res = statistics.pstdev(MAP)
    print("MAP = ",avg_map,"+/-", res)
    return(avg_map, res)


def volume_minmax(volume, start_index, end_index, dist, heig, title):
    data = volume[start_index:end_index]
    invert_data = data * -1
    # Adjust bounds
    mins_idx, _ = find_peaks(invert_data, distance=dist, height=-heig)
    output_mins = np.concatenate((mins_idx), axis=None).tolist()
    output_mins = [x+start_index for x in output_mins]
    #Find local maximas
    maxs_idx, _ = find_peaks(data, distance=dist, height=-heig)
    output_maxs = np.concatenate((maxs_idx), axis=None).tolist()
    output_maxs = [x+start_index for x in output_maxs]
    plt.figure(figsize=(15,5))
    plt.plot(data)
    plt.title(title)
    plt.grid()
```

```python
    plt.ylabel('Volume [mmHg]')
    plt.xlabel('Time [ms]')
    plt.plot(volume[mins_idx+start_index],'go')
    plt.plot(volume[maxs_idx+start_index],'ro')
    plt.show()
    return output_mins, output_maxs


def stroke_volume(volume, start_index, end_index, dist, heig, title):
    output_mins, output_maxs = volume_minmax(volume, start_index, end_index, dist, heig, title)
    idx_list_max = output_maxs
    idx_list_min = output_mins
    if idx_list_max[o]>idx_list_min[o]:
        idx_list_min.pop(o)
    len_min = len(idx_list_min)
    len_max = len(idx_list_max)
    if len_min<=len_max:
        calc_range = len_min
    else:
        calc_range = len_max
    sv = []
#    print(calc_range)
    for x in range(calc_range):
        sv_calc = (volume[idx_list_max[x]]-volume[idx_list_min[x]]).tolist()
#        print(volume[idx_list_max[x]],volume[idx_list_min[x]])
        sv.append(sv_calc)
    avg_sv = (sum(sv)/len(sv))
    res_sv = statistics.pstdev(sv)
    print("SV =",avg_sv,"+/-",res_sv)
    return(avg_sv, res_sv)
```

```python
def end_diastole(LVV,LVP):
    return LVV.idxmax()


def end_systole(LVV,LVP):
    ratio = LVP/LVV
    return ratio.idxmax()


def Ea_line(x1,y1,x2,y2):
    x_values = [x1, x2]
    y_values = [y1, y2]
    plt.plot(x_values, y_values,'k--')



def ea_slope(x1,y1,x2,y2):
    slope = (y2-y1)/(x2-x1)
    if slope > 0:
        slope = -1*slope
    return slope


def Ees_line(LVV, LVP, vo):
    x_values = [vo, LVV]
    y_values = [0, LVP]
    es_slope = (LVP)/(LVV-vo)
    plt.plot(x_values, y_values,'k--')
    return es_slope



def envelope(LVV, LVP, vo):
```

```python
    pt1 = max(LVV)

    ratio_ees_idx = end_systole(LVV, LVP)

    Ea_line(pt1, 0, LVV[ratio_ees_idx], LVP[ratio_ees_idx])

    sv = pt1-(LVV[ratio_ees_idx])

    pp = LVP[ratio_ees_idx]-(min(LVP))

    ees_slope = Ees_line(LVV[ratio_ees_idx], LVP[ratio_ees_idx], vo)

    ea_slope_value = ea_slope(LVV[ratio_ees_idx], LVP[ratio_ees_idx], pt1, 0)

    potential_energy = (pp*LVV[ratio_ees_idx])/2

    sw = sv*pp

    pva = sw+potential_energy

    plt.plot(LVV[ratio_ees_idx], LVP[ratio_ees_idx],'ro')

    plt.plot(pt1,0,'ro')

    print("Ea =",ea_slope_value ,"Ees =",ees_slope,"SV = ",sv,"PP =",pp,"SW =",sw,"PE
=",potential_energy)

    return ea_slope_value, ees_slope, sv, pp, sw, potential_energy, pva
def envelope_plot(LVV, LVP, vo):

    pt1 = max(LVV)

    ratio_ees_idx = end_systole(LVV, LVP)

    Ea_line(pt1, 0, LVV[ratio_ees_idx], LVP[ratio_ees_idx])

    sv = pt1-(LVV[ratio_ees_idx])

    pp = LVP[ratio_ees_idx]-(min(LVP))

    ees_slope = Ees_line(LVV[ratio_ees_idx], LVP[ratio_ees_idx], vo)

    ea_slope_value = ea_slope(LVV[ratio_ees_idx], LVP[ratio_ees_idx], pt1, 0)

    potential_energy = (pp*LVV[ratio_ees_idx])/2

    sw = sv*pp

    pva = sw+potential_energy

    min_lvp = min(LVP)

    plt.plot(LVV,LVP)

    plt.plot(LVV[ratio_ees_idx], LVP[ratio_ees_idx],'ro')
```

```python
        plt.plot(pt1,0,'ro')

        edv = pt1

        print("Ea =",ea_slope_value,"Ees =",ees_slope,"SV = ",sv,"PP =",pp,"SW =",sw,"PE
=",potential_energy, "EDV = ",edv,"LVP_min = ",min_lvp)

        return ea_slope_value, ees_slope, sv, pp, sw, potential_energy, pva,edv



def find_hr(signal,start_idx,end_idx,time_inmin,distance):

        ecg = signal[start_idx:end_idx]*-1

        plt.figure(figsize=(20,8))

        plt.plot(ecg, label='ECG')

        peaks, _ = find_peaks(ecg, height=0, distance=distance)

        plt.plot(start_idx+peaks, ecg[start_idx+peaks], "x")

        plt.legend()

        plt.show()

        HR = len(peaks)/time_inmin

        peaks_idx = start_idx+peaks

        return HR, peaks_idx


def global_min(pressure, st_idx, end_idx): # Find end expiration (ventilated animals) and take
then one loop from there

        index_min = np.argmin(pressure[st_idx:end_idx])

        return index_min


def flow_calculation(flow_signal,start_idx,end_idx,label,samp_rate):

        plt.figure(figsize=(6,4))

        flow_calc_array=flow_signal[start_idx:end_idx]

        length_array = len(flow_calc_array)

        end_time = float(length_array/samp_rate)
```

```python
        time_array = np.linspace(0.0, end_time, length_array)
        plt.plot(time_array,flow_calc_array, label=label)
        plt.xlabel('Time [sec]')
        plt.ylabel('Carotid Flow [ml/min]')
        plt.legend()
        plt.show()
        avg_flow = sum(flow_calc_array)/len(flow_calc_array)
        std_flow = statistics.pstdev(flow_calc_array)
        peak_flow = max(flow_calc_array)
        min_flow = min(flow_calc_array)
        print(avg_flow,std_flow,peak_flow,min_flow)
        return avg_flow,std_flow,peak_flow,min_flow


def overlay_pressure_flow(lvp,aop,flow,start_idx,end_idx,title,samp_freq):
    fig, ax = plt.subplots(figsize=(10,6))
    fig.subplots_adjust(right=0.75)
    twin1 = ax.twinx()
    #twin2 = ax.twinx()
    lvp_signal=lvp[start_idx:end_idx]
    end_time = float(len(lvp_signal)/samp_freq)
    time_scale = np.linspace(0.0, end_time, len(lvp_signal))
    # Offset the right spine of twin2.  The ticks and label have already been
    # placed on the right by twinx above.
    #twin2.spines.right.set_position(("axes", 1.2))
    p1, = ax.plot(time_scale, lvp[start_idx:end_idx], "b-", label="LVP")
    p4, = ax.plot(time_scale, aop[start_idx:end_idx], "g-", label="AOP")
    p2, = twin1.plot(time_scale, flow[start_idx:end_idx], "r-", label="Carotid Flow")
    #p3, = twin2.plot([0, 1, 2], [50, 30, 15], "g-", label="Velocity")
    #ax.set_xlim(0, 2)
```

```python
    ax.set_ylim(0, 130)
    twin1.set_ylim(0, 700)
    #twin2.set_ylim(1, 65)
    ax.set_xlabel("Time [sec]")
    ax.set_ylabel("Pressure [mmHg]")
    ax.set_title(title)
    twin1.set_ylabel("Flow [ml/min]")
    #twin2.set_ylabel("Velocity")
    ax.yaxis.label.set_color(p1.get_color())
    twin1.yaxis.label.set_color(p2.get_color())
    #twin2.yaxis.label.set_color(p3.get_color())
    tkw = dict(size=4, width=1.5)
    ax.tick_params(axis='y', colors=p1.get_color(), **tkw)
    twin1.tick_params(axis='y', colors=p2.get_color(), **tkw)
    #twin2.tick_params(axis='y', colors=p3.get_color(), **tkw)
    ax.tick_params(axis='x', **tkw)
    ax.legend(handles=[p1, p4, p2])
    plt.show()
    return


def map_mean_calculation(aop,start_idx,end_idx,title):
    signal = aop[start_idx:end_idx]
    plt.figure(figsize=(10,4))
    plt.plot(signal)
    plt.title(title)
    plt.grid()
    plt.ylabel('Pressure [mmHg]')
    plt.xlabel('Time [ms]')
    plt.show()
```

```python
    mean_pressure = sum(signal)/len(signal)
    stdv_pressure = statistics.pstdev(signal)
    print(mean_pressure, stdv_pressure)
    return mean_pressure, stdv_pressure


def coronary_perfusion(lvp,aop,start_idx,end_idx):
    lvp_sig = lvp[start_idx:end_idx]
    aop_sig = aop[start_idx:end_idx]
    coronary_dp = np.subtract(aop_sig,lvp_sig)
    mean_cdp = (sum(coronary_dp))/(len(coronary_dp))
    stdv_cdp = statistics.pstdev(coronary_dp)
    print(mean_cdp, stdv_cdp)
    plt.plot(coronary_dp)
    return mean_cdp, stdv_cdp




def venous_p(aop, cvp, pap, start_idx, end_idx, title):
    aortic = aop[start_idx:end_idx]
    venous = cvp[start_idx:end_idx]
    pa = pap[start_idx:end_idx]
    perf_press = np.subtract(aortic,venous)
    mean_perf_press = sum(perf_press)/len(perf_press)
    mean_pa = sum(pa)/len(pa)
    pa_sys = max(pa)
    pa_dia = min(pa)
    mean_cvp = sum(venous)/len(venous)
    print(title)
    print("cvp=",mean_cvp, "sys_perf=", mean_perf_press, "PAP=", mean_pa, pa_sys, pa_dia)
    return mean_cvp, mean_perf_press, mean_pa, pa_sys, pa_dia
```

CREATE DATA FRAME, READ IN RAW DATA

```
time_pre = pd.read_csv("Time_table.txt")

aop_pre = pd.read_csv("LabChart_AOP_sections1to5_LPF45Hz.txt", sep=" ")

n = len(aop_pre)

print(n)

cvp_pre = pd.read_csv("LabChart_CVP_sections1to5_LPF45Hz.txt", sep=" ")

ext_ecg_pre = pd.read_csv("LabChart_Ext_ECG_sections1to5_LPF45Hz.txt", sep=" ")

fap_pre = pd.read_csv("LabChart_FAP_sections1to5_LPF45Hz.txt", sep=" ")

flow_pre = pd.read_csv("LabChart_Flow_sections1to5_LPF45Hz.txt", sep=" ")

int_ecg_pre = pd.read_csv("LabChart_Int_ECG_sections1to5_LPF45Hz.txt", sep=" ")

lvp_pre = pd.read_csv("LabChart_LVP_sections1to5_LPF45Hz.txt", sep=" ")

lvv_pre = pd.read_csv("LabChart_LVV_sections1to5_LPF45Hz.txt", sep=" ")

lv_s1_pre = pd.read_csv("LabChart_LV_S1_sections1to5_LPF45Hz.txt", sep=" ")

lv_s2_pre = pd.read_csv("LabChart_LV_S2_sections1to5_LPF45Hz.txt", sep=" ")

lv_s3_pre = pd.read_csv("LabChart_LV_S3_sections1to5_LPF45Hz.txt", sep=" ")

lv_s4_pre = pd.read_csv("LabChart_LV_S4_sections1to5_LPF45Hz.txt", sep=" ")

lv_s5_pre = pd.read_csv("LabChart_LV_S5_sections1to5_LPF45Hz.txt", sep=" ")

lv_s6_pre = pd.read_csv("LabChart_LV_S6_sections1to5_LPF45Hz.txt", sep=" ")

lv_s7_pre = pd.read_csv("LabChart_LV_S7_sections1to5_LPF45Hz.txt", sep=" ")

pap_pre = pd.read_csv("LabChart_PAP_sections1to5_LPF45Hz.txt", sep=" ")

rvp_pre = pd.read_csv("LabChart_RVP_sections1to5_LPF45Hz.txt", sep=" ")

rvv_pre = pd.read_csv("LabChart_RVV_sections1to5_LPF45Hz.txt", sep=" ")


df_pre =
pd.concat([time_pre,aop_pre,cvp_pre,ext_ecg_pre,fap_pre,flow_pre,int_ecg_pre,lvp_pre,lvv_pre,l
v_s1_pre,

          lv_s2_pre,lv_s3_pre,lv_s4_pre,lv_s5_pre,lv_s6_pre,lv_s7_pre,pap_pre,rvp_pre,rvv_pre],
axis=1)
```

```python
df_pre.columns = ['times','aop','cvp','ext_ecg','fap','flow','int_ecg','lvp','lvv','lv_s1',
                  'lv_s2','lv_s3','lv_s4','lv_s5','lv_s6','lv_s7','pap','rvp','rvv']

print(df_pre)

# READ ALL FILES INTO ONE DATA FRAME

# READING JUST THE DATA POST IMPELLA INSERTION


df =
pd.concat(map(pd.read_csv,['RTLog_20211208T113231_sync_all.csv','RTLog_20211208T115308_sync_
all.csv','RTLog_20211208T121110_sync_all.csv',


'RTLog_20211208T122912_sync_all.csv','RTLog_20211208T124714_sync_all.csv','RTLog_20211208T130
516_sync_all.csv',


'RTLog_20211208T132318_sync_all.csv','RTLog_20211208T134121_sync_all.csv','RTLog_20211208T1359
24_sync_all.csv',


'RTLog_20211208T141727_sync_all.csv','RTLog_20211208T143529_sync_all.csv','RTLog_20211208T145
331_sync_all.csv']), ignore_index=True)

print(df)


# DELETE unnecessary COLUMNS

columns = ['Pressure1', 'Pressure2', "MotorSpeed2", "MotorCurrent2","OptSensor2", "Pressure3",
"OptSensor3", "OptSensorRaw", "PurgePressure",

"PumpCurrent","PumpSpeed",'PumpPressure',"PurgeFlow","OptSnr1","OptCtr1","PurgeFlowTicks",
"PurgeAveragePress","PurgeVolume","Cpld1","Cpld2","DPressure","LvpSuggOffset","Lvedp","Lvedp
Average","OptSensorContrast","OptSensorLampLevel","OptSensorGain","x33","x34","x35","x36","x3
7","x38","x39","EventSet","EventClr","EventPumpPosDetect",

      "RVV", "RV_S1", "RV_S2", "RV_S3", "RV_S4", "RV_S5", "RV_S6", "RV_S7"]

df.drop(columns, inplace=True, axis=1)


# Volume calibration

#LVV calibration
```

```python
start_idx = 3750000

end_idx = 3760000


plt.figure(figsize=(20,8))

#plt.plot(df_pre.lvv[start_idx:end_idx], label='LVV')

plt.plot(df_pre.lv_s1[start_idx:end_idx], label='LV_S1')

plt.plot(df_pre.lv_s2[start_idx:end_idx], label='LV_S2')

plt.plot(df_pre.lv_s3[start_idx:end_idx], label='LV_S3')

plt.plot(df_pre.lv_s4[start_idx:end_idx], label='LV_S4')

plt.plot(df_pre.lv_s5[start_idx:end_idx], label='LV_S5')

#   Eliminate s6, s7 as they appear to be outside the ventricle

#plt.plot(df_pre.lv_s6[start_idx:end_idx], label='LV_S6')

#plt.plot(df_pre.lv_s7[start_idx:end_idx], label='LV_S7')

plt.legend()

plt.show()
```
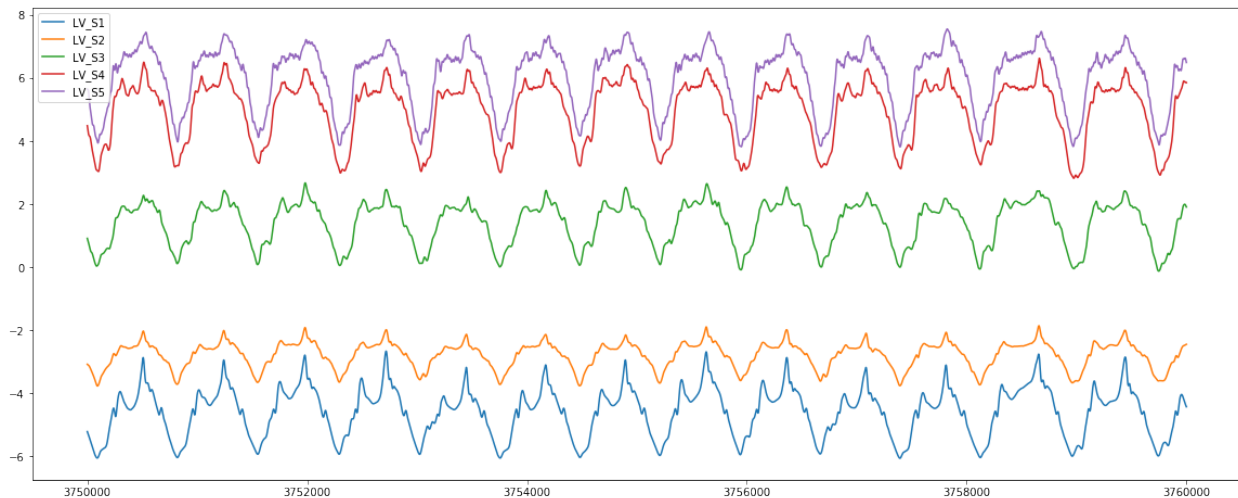


```python
# After picking the relevant channels, create the composite volume signal

comp_vol = df_pre.lv_s1[0:]+df_pre.lv_s2[0:]+df_pre.lv_s3[0:]+df_pre.lv_s4[0:]+df_pre.lv_s5[0:]

#comp_vol = df_pre.lv_s3[0:]+df_pre.lv_s4[0:]+df_pre.lv_s5[0:]

# Plot LVV raw vs. composite lvv, with LVP:

start_idx = 3750000
```

```
end_idx = 3752000

plt.figure(figsize=(20,8))

plt.plot(df_pre.lvv[start_idx:end_idx], label='LVV raw')

plt.plot(comp_vol[start_idx:end_idx], label='LVV_new_composite')

plt.plot(df_pre.lvp[start_idx:end_idx], label='LVP')

plt.xlabel('Time [ms]')

plt.ylabel('Pressure [mmHg]')

plt.legend()

plt.show()
```
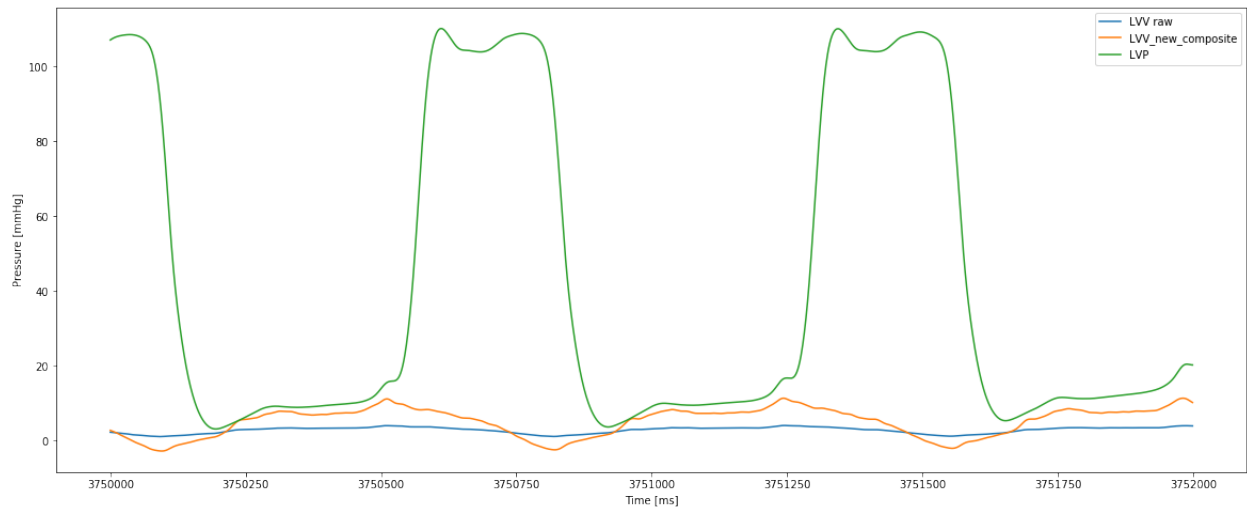

Add the new composite volume to the data frame df

```
df_pre['comp_lvv'] = comp_vol

# HR calc

HR1, peaks1 = find_hr(df_pre.int_ecg,3745100,3760100,0.25,400)

print(peaks1),len(peaks1)
```
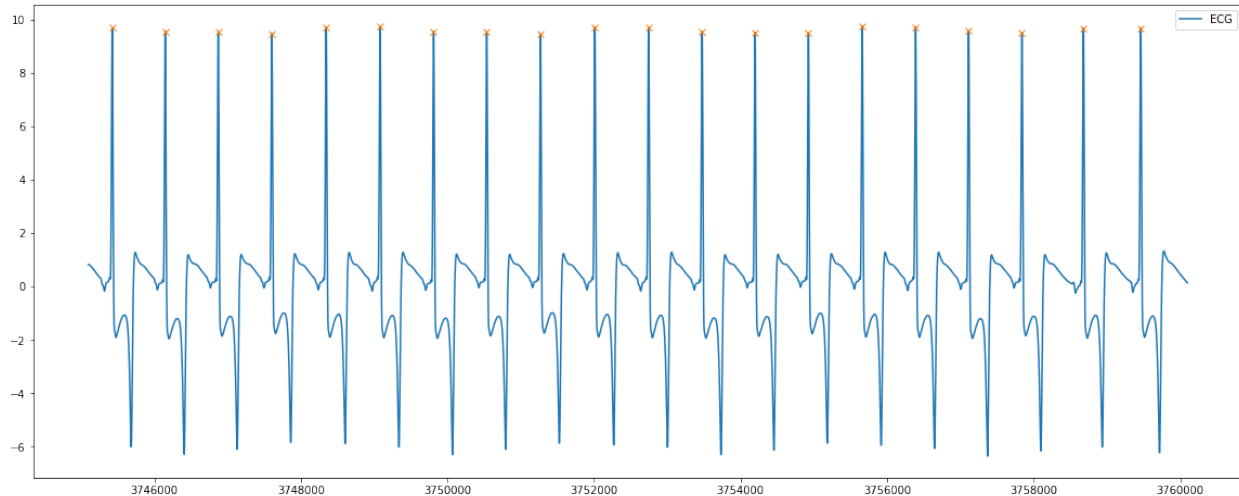
print(HR1)

CO = 6.3

sv_calibration = CO/(HR1)

calculated_SV = sv_calibration*1000

print(sv_calibration*1000,"ml")


```
# Find the scaling factor for the volume signal
def findmax_min(signal,start_idx,end_idx,distance):
    mins = signal[start_idx:end_idx]*-1
    plt.figure(figsize=(20,8))
    plt.plot(signal[start_idx:end_idx], label='raw_signal')
    mins_peaks, _ = find_peaks(mins, height=-10, distance=distance)
    max_peaks, _ = find_peaks(signal[start_idx:end_idx], height=8, distance=distance)
    plt.plot(start_idx+mins_peaks, signal[start_idx+mins_peaks], "x")
    plt.plot(start_idx+max_peaks, signal[start_idx+max_peaks], "gx")
    plt.legend()
    plt.show()
    max_values = signal[start_idx+max_peaks]
    min_values = signal[start_idx+mins_peaks]
```

144

```
    zip_object = zip(max_values, min_values)

    difference = []

    for max_values_i, min_values_i in zip_object:

        difference.append(max_values_i-min_values_i)

    average_diff = sum(difference) / len(difference)

    return average_diff
```

```
difference_voltage = findmax_min(df_pre.comp_lvv,3745000,3760000,600)

scaling_factor = calculated_SV/difference_voltage

print(scaling_factor)
```
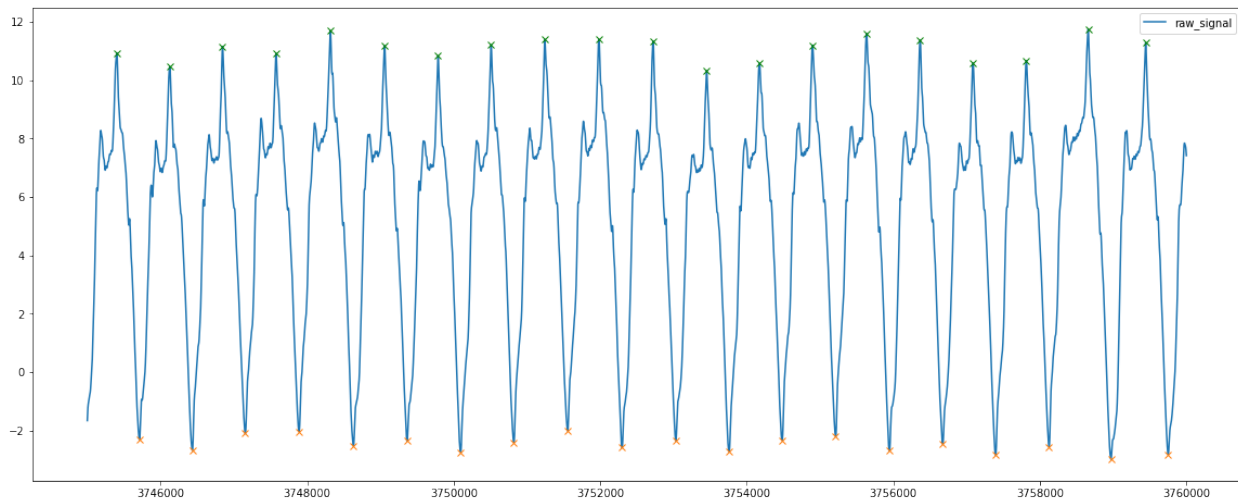


```
#Set 0 mL volume point as minimum voltage during baseline IVC occlusions

st_idx=3800000

end_idx=4000000

plt.plot(df_pre.lvp[st_idx:end_idx], label='LVP')

plt.plot(df_pre.comp_lvv[st_idx:end_idx], label='raw composite lvv')

plt.legend(loc='upper right')

plt.show()

min_lvv_voltage = abs(min(df_pre.comp_lvv[st_idx:end_idx]))

offset_volume = (df_pre.comp_lvv)+(min_lvv_voltage)
```

```
scaled_volume = (offset_volume)*(scaling_factor)

print(scaling_factor)
```
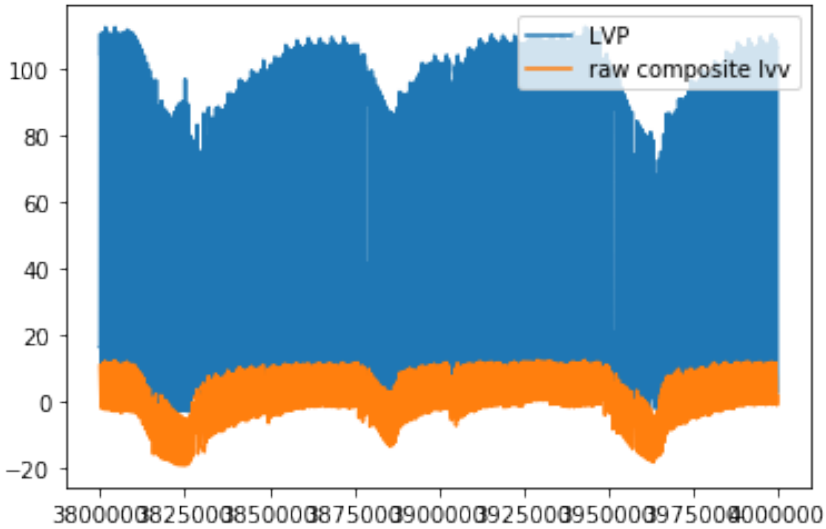


```
plt.plot(offset_volume[3800000:3900000])

plt.show()

plt.plot(scaled_volume[3800000:3900000])

plt.ylabel("LV Volume [ml]")

plt.xlabel("Time [ms]")

plt.show()

# Add the final LVV after offsetting and scaling to the dataframe

df_pre['scaled_lvv'] = scaled_volume
```
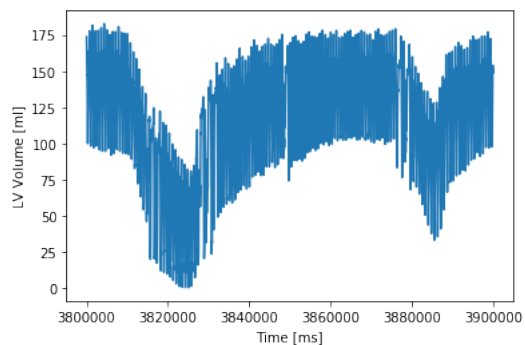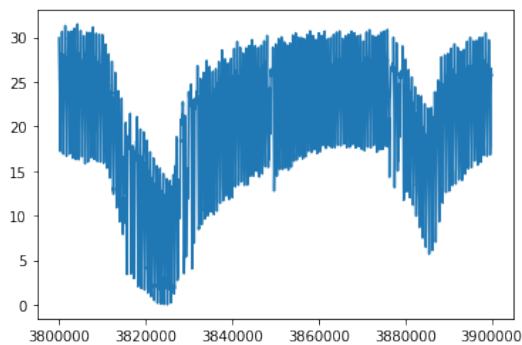
TIMEPOINTS – Library for stable beats, two resp cycles at peak intervention

all data until the Impella part is in df_pre:

bl_ivc = [3800000,3840000]

bl_5peep_8vt = [6160000,6169000]

shock_final = [7950000,7958000] # shock_td = 4.3

Beginning ECMO - 40ml/kg -> 2.8 lpm, 50ml/kg -> 3.5 lpm, 60ml/kg -> 4.2 lpm

ecmo_28ml = [11270000,11278000]

ecmo_35ml = [8529000,8538000]

ecmo_42ml = [11497000,11504000]

ecmo_35ml_end = [11807000,11815000]

Break -- DF dataframe - sample every 10 min

ecmo_35ml_p2_init = [188750,191000]

ecmo_35ml_p2_break1 = [341000,343500]

ecmo_35ml_p2_break2 = [490000,492500]

ecmo_35ml_p2_break3 = [643500,646000]

ecmo_35ml_p2_break4 = [794000,796000]

Unloading

ecmo_35ml_p2 = [974000,976500]

ecmo_35ml_p4 = [1370000,1372000]

ecmo_35ml_p6 = [1810500,1812900]

ecmo_28ml_p2 = [2120000,2122000]

ecmo_28ml_p4 = [2137000,2139000]

ecmo_28ml_p6 = [2170000,2172000]

ecmo_28ml_p8 = [2200100,2202600]

ecmo_42ml_p2 = [2248000,2250200]

ecmo_42ml_p4 = [2280080,2282080]

ecmo_42ml_p6 = [2333000,2335000]

ecmo_42ml_p8 = [2364500,2366500]

```
# Find End expiration and take one loop from there
# ecmo_35ml_p2_init = [188750,191000]
# ecmo_35ml_p2_break1 = [341000,343500]
# ecmo_35ml_p2_break2 = [490000,492500]
# ecmo_35ml_p2_break3 = [643500,646000]
# ecmo_35ml_p2_break4 = [794000,796000]
impella_start = global_min(df.LVP,ecmo_35ml_p2_init[0],ecmo_35ml_p2_init[1])
break1_offset = global_min(df.LVP,ecmo_35ml_p2_break1[0],ecmo_35ml_p2_break1[1])
break2_offset = global_min(df.LVP,ecmo_35ml_p2_break2[0],ecmo_35ml_p2_break2[1])
break3_offset = global_min(df.LVP,ecmo_35ml_p2_break3[0],ecmo_35ml_p2_break3[1])
break4_offset = global_min(df.LVP,ecmo_35ml_p2_break4[0],ecmo_35ml_p2_break4[1])


## END EXPIRATION POINT FOR ALL SELECTED BEATS
bl_5peep_8vt_exp = global_min(df_pre.lvp,bl_5peep_8vt[0],bl_5peep_8vt[1])
shock_final_exp = global_min(df_pre.lvp,shock_final[0],shock_final[1])
ecmo_28ml_exp = global_min(df_pre.lvp,ecmo_28ml[0],ecmo_28ml[1])
ecmo_35ml_exp = global_min(df_pre.lvp,ecmo_35ml[0],ecmo_35ml[1])
ecmo_42ml_exp = global_min(df_pre.lvp,ecmo_42ml[0],ecmo_42ml[1])
ecmo_35ml_end_exp = global_min(df_pre.lvp,ecmo_35ml_end[0],ecmo_35ml_end[1])
ecmo_35ml_p2_exp = global_min(df.LVP,ecmo_35ml_p2[0],ecmo_35ml_p2[1])
ecmo_35ml_p4_exp = global_min(df.LVP,ecmo_35ml_p4[0],ecmo_35ml_p4[1])
ecmo_35ml_p6_exp = global_min(df.LVP,ecmo_35ml_p6[0],ecmo_35ml_p6[1])
ecmo_28ml_p2_exp = global_min(df.LVP,ecmo_28ml_p2[0],ecmo_28ml_p2[1])
ecmo_28ml_p4_exp = global_min(df.LVP,ecmo_28ml_p4[0],ecmo_28ml_p4[1])
ecmo_28ml_p6_exp = global_min(df.LVP,ecmo_28ml_p6[0],ecmo_28ml_p6[1])
ecmo_28ml_p8_exp = global_min(df.LVP,ecmo_28ml_p8[0],ecmo_28ml_p8[1])
ecmo_42ml_p2_exp = global_min(df.LVP,ecmo_42ml_p2[0],ecmo_42ml_p2[1])
ecmo_42ml_p4_exp = global_min(df.LVP,ecmo_42ml_p4[0],ecmo_42ml_p4[1])
ecmo_42ml_p6_exp = global_min(df.LVP,ecmo_42ml_p6[0],ecmo_42ml_p6[1])
```

```python
## dpdt max - for 250hz should be 0.004, for 1000hz should be 0.001
# def dpdt(data, dt):
#     data["gradient"] = np.gradient(data.LVP_lpf, dt)
#     return data


def dpdt_max_min(data):
    print (max(data), data.idxmax(), min(data), data.idxmin())
    return max(data), data.idxmax(), min(data), data.idxmin()



# for data in total_data:
#     data = dpdt(data, 0.04)


df["dpdt"] = np.gradient(df.LVP,0.004)
df_pre["dpdt"] = np.gradient(df_pre.lvp,0.001)


# Find dpdtmax for each state
dpdt_bl = dpdt_max_min(df_pre.dpdt[bl_5peep_8vt[0]:bl_5peep_8vt[1]])
dpdt_shock = dpdt_max_min(df_pre.dpdt[shock_final[0]:shock_final[1]])
dpdt_ecmo28 = dpdt_max_min(df_pre.dpdt[ecmo_28ml[0]:ecmo_28ml[1]])
dpdt_ecmo35 = dpdt_max_min(df_pre.dpdt[ecmo_35ml[0]:ecmo_35ml[1]])
dpdt_ecmo42 = dpdt_max_min(df_pre.dpdt[ecmo_42ml[0]:ecmo_42ml[1]])
dpdt_ecmo35_end = dpdt_max_min(df_pre.dpdt[ecmo_35ml_end[0]:ecmo_35ml_end[1]])
print("------")
print("ECMO 2800")
dpdt_ecmo28_p2 = dpdt_max_min(df.dpdt[ecmo_28ml_p2[0]:ecmo_28ml_p2[1]])
dpdt_ecmo28_p4 = dpdt_max_min(df.dpdt[ecmo_28ml_p4[0]:ecmo_28ml_p4[1]])
dpdt_ecmo28_p6 = dpdt_max_min(df.dpdt[ecmo_28ml_p6[0]:ecmo_28ml_p6[1]])
dpdt_ecmo28_p8 = dpdt_max_min(df.dpdt[ecmo_28ml_p8[0]:ecmo_28ml_p8[1]])
```

```
print("------")
print("ECMO 3500")
dpdt_ecmo35_p2_pre = dpdt_max_min(df.dpdt[ecmo_35ml_p2_init[0]:ecmo_35ml_p2_init[1]])
dpdt_ecmo35_p2_post = dpdt_max_min(df.dpdt[ecmo_35ml_p2[0]:ecmo_35ml_p2[1]])
dpdt_ecmo35_p4 = dpdt_max_min(df.dpdt[ecmo_35ml_p4[0]:ecmo_35ml_p4[1]])
dpdt_ecmo35_p6 = dpdt_max_min(df.dpdt[ecmo_35ml_p6[0]:ecmo_35ml_p6[1]])
print("------")
print("ECMO 4200")
dpdt_ecmo42_p2 = dpdt_max_min(df.dpdt[ecmo_42ml_p2[0]:ecmo_42ml_p2[1]])
dpdt_ecmo42_p4 = dpdt_max_min(df.dpdt[ecmo_42ml_p4[0]:ecmo_42ml_p4[1]])
dpdt_ecmo42_p6 = dpdt_max_min(df.dpdt[ecmo_42ml_p6[0]:ecmo_42ml_p6[1]])
([[dpdt_ecmo42_p8 = dpdt_max_min(df.dpdt[ecmo_42ml_p8[0]:ecmo_42ml_p8[1
```

```
plt.plot(df_pre.dpdt[bl_5peep_8vt[0]:bl_5peep_8vt[1]], label='baseline')
plt.legend()
plt.ylabel("dP/dt [mmHg/sec]")
plt.show()
plt.plot(df_pre.dpdt[shock_final[0]:shock_final[1]], label='shock')
plt.legend()
plt.ylabel("dP/dt [mmHg/sec]")
()plt.show
```
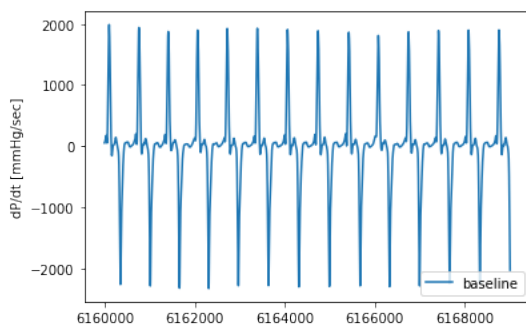

AOP

PP MAP SBP DBP

#UNLOADING

ecmo_28p8_aop_p = pulse_pressure(df.AOP, ecmo_28ml_p8[0], ecmo_28ml_p8[1], 'ECMO 2.8 lpm, P8', 130, 100)

ecmo_28p6_aop_p = pulse_pressure(df.AOP, ecmo_28ml_p6[0], ecmo_28ml_p6[1], 'ECMO 2.8 lpm, P6', 130, 100)

ecmo_28p4_aop_p = pulse_pressure(df.AOP, ecmo_28ml_p4[0]+100, ecmo_28ml_p4[1], 'ECMO 2.8 lpm, P4', 130, 100)

ecmo_28p2_aop_p = pulse_pressure(df.AOP, ecmo_28ml_p2[0], ecmo_28ml_p2[1], 'ECMO 2.8 lpm, P2', 180, 100)

ecmo_42p8_aop_p = pulse_pressure(df.AOP, ecmo_42ml_p8[0], ecmo_42ml_p8[1], 'ECMO 4.2 lpm, P8', 130, 100)

ecmo_42p6_aop_p = pulse_pressure(df.AOP, ecmo_42ml_p6[0], ecmo_42ml_p6[1], 'ECMO 4.2 lpm, P6', 130, 100)

ecmo_42p4_aop_p = pulse_pressure(df.AOP, ecmo_42ml_p4[0], ecmo_42ml_p4[1], 'ECMO 4.2 lpm, P4', 130, 100)

ecmo_42p2_aop_p = pulse_pressure(df.AOP, ecmo_42ml_p2[0]+50, ecmo_42ml_p2[1], 'ECMO 4.2 lpm, P2', 130, 100)

ecmo_35p6_aop_p = pulse_pressure(df.AOP, ecmo_35ml_p6[0]+50, ecmo_35ml_p6[1], 'ECMO 3.5 lpm, P6', 130, 100)

ecmo_35p4_aop_p = pulse_pressure(df.AOP, ecmo_35ml_p4[0], ecmo_35ml_p4[1], 'ECMO 3.5 lpm, P4', 150, 100)

ecmo_35p2_aop_p_post = pulse_pressure(df.AOP, ecmo_35ml_p2[0], ecmo_35ml_p2[1], 'ECMO 3.5 lpm, P2 after break', 150, 100)

ecmo_35p2_aop_p_before = pulse_pressure(df.AOP, ecmo_35ml_p2_init[0], ecmo_35ml_p2_init[1], 'ECMO 3.5 lpm, P2 before break', 150, 100)

#ECMO

ecmo_35_aop_p_end = pulse_pressure(df_pre.aop_offset, ecmo_35ml_end[0], ecmo_35ml_end[1], 'ECMO 3.5 lpm end', 500, 100)

ecmo_42_aop_p = pulse_pressure(df_pre.aop_offset, ecmo_42ml[0], ecmo_42ml[1], 'ECMO 4.2 lpm', 500, 100)

ecmo_35_aop_p = pulse_pressure(df_pre.aop_offset, ecmo_35ml[0], ecmo_35ml[1], 'ECMO 3.5 lpm', 500, 80)

ecmo_28_aop_p = pulse_pressure(df_pre.aop_offset, ecmo_28ml[0], ecmo_28ml[1], 'ECMO 2.8 lpm', 500, 75)

shock_aop_p = pulse_pressure(df_pre.aop_offset, shock_final[0], shock_final[1], 'Shock', 500, 103)

bl_aop_p = pulse_pressure(df_pre.aop_offset, bl_5peep_8vt[0], bl_5peep_8vt[1], 'Baseline', 300, 103)
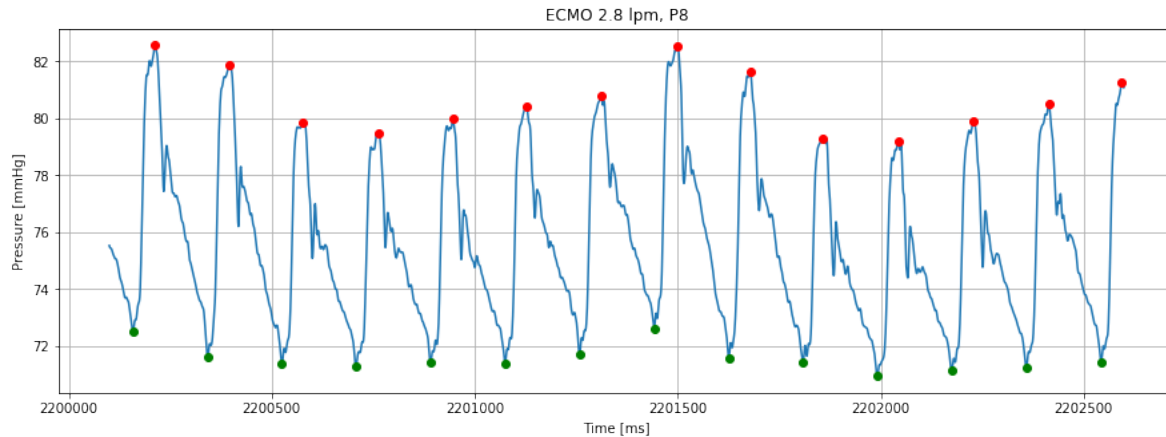

```
PP  =   9.153846153846152 +/- 1.056535546466253
MAP =  74.51905128205128 +/- 0.5256031105775393
Peak Sys =  82.566
Min Dias =  70.936
```

HEMODYNAMIC PLOTS

ecmo_35p6_aop_p = pulse_pressure(df.AOP, ecmo_35ml_p6[0]+50, ecmo_35ml_p6[1], 'ECMO 3.5 lpm, P6', 130, 100)

ecmo_35p4_aop_p = pulse_pressure(df.AOP, ecmo_35ml_p4[0], ecmo_35ml_p4[1], 'ECMO 3.5 lpm, P4', 150, 100)

ecmo_35p2_aop_p_post = pulse_pressure(df.AOP, ecmo_35ml_p2[0], ecmo_35ml_p2[1], 'ECMO 3.5 lpm, P2 after break', 150, 100)

ecmo_35p2_aop_p_before = pulse_pressure(df.AOP, ecmo_35ml_p2_init[0], ecmo_35ml_p2_init[1], 'ECMO 3.5 lpm, P2 before break', 150, 100)

#ECMO

ecmo_35_aop_p_end = pulse_pressure(df_pre.aop_offset, ecmo_35ml_end[0], ecmo_35ml_end[1], 'ECMO 3.5 lpm end', 500, 100)

ecmo_42_aop_p = pulse_pressure(df_pre.aop_offset, ecmo_42ml[0], ecmo_42ml[1], 'ECMO 4.2 lpm', 500, 100)

```python
# ecmo_35_aop_p = pulse_pressure(df_pre.aop_offset, ecmo_35ml[0], ecmo_35ml[1], 'ECMO 3.5 lpm', 500, 80)

# ecmo_28_aop_p = pulse_pressure(df_pre.aop_offset, ecmo_28ml[0], ecmo_28ml[1], 'ECMO 2.8 lpm', 500, 75)

# shock_aop_p = pulse_pressure(df_pre.aop_offset, shock_final[0], shock_final[1], 'Shock', 500, 103)

# bl_aop_p = pulse_pressure(df_pre.aop_offset, bl_5peep_8vt[0], bl_5peep_8vt[1], 'Baseline', 300, 103)


tim_arr = np.linspace(0,4,4000)

tim_arr_df = np.linspace(0,4,1000)

plt.figure(figsize=(15,7))

# plt.plot(tim_arr,df_pre.aop[bl_5peep_8vt[0]:bl_5peep_8vt[0]+4000], label='BL',linewidth=3)

# plt.plot(tim_arr,df_pre.aop[shock_final[0]+170:shock_final[0]+170+4000], label='Shock',linewidth=3)

plt.plot(tim_arr,df_pre.aop[ecmo_35ml[0]:ecmo_35ml[0]+4000], label='ECMO 50',linewidth=3)

plt.plot(tim_arr_df,df.AOP[ecmo_35ml_p6[0]+90:ecmo_35ml_p6[0]+90+1000], label='ECMO 50 + P6',linewidth=3)


plt.ylabel("Aortic Pressure [mmHg]")

plt.xlabel("Time [sec]")

plt.title("Representative Hemodynamics - ECMO + pVAD")

plt.legend()

plt.ylim([50,110])

plt.show()
# plt.ylabel("Aortic Pressure [mmHg]")

# plt.xlabel("Time [sec]")
```

Representative Hemodynamics - ECMO + pVAD
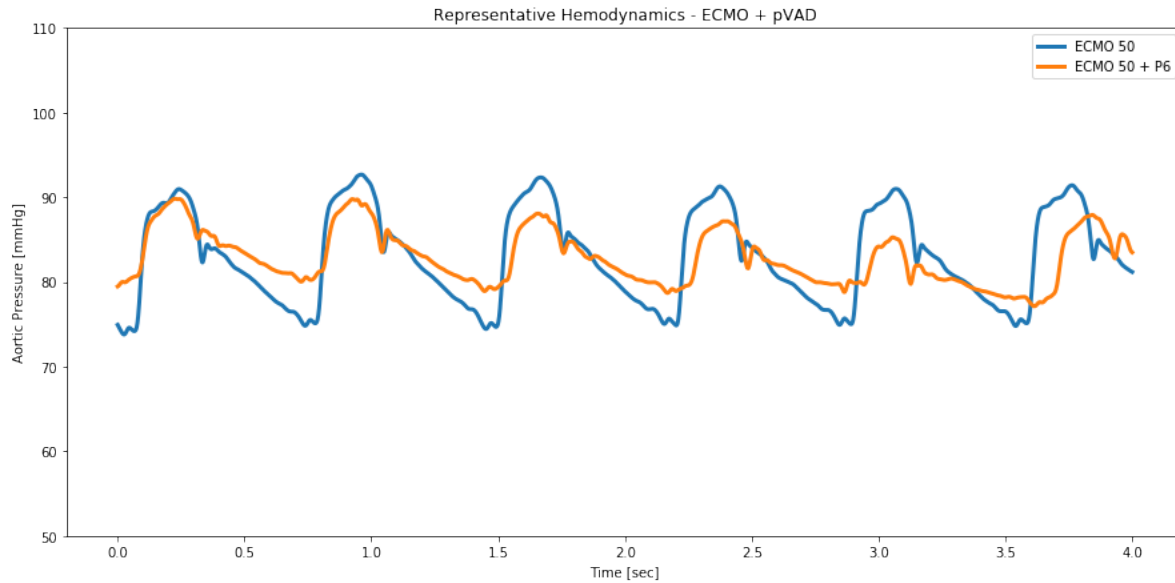
Average flow - carotid

flow_baseline = flow_calculation(df_pre.flow,bl_5peep_8vt[0],bl_5peep_8vt[1],'Baseline',1000)

flow_shock = flow_calculation(df_pre.flow,shock_final[0],shock_final[1],'Shock',1000)

flow_ecmo28 = flow_calculation(df_pre.flow,ecmo_28ml[0],ecmo_28ml[1],'ECMO 40 ml/kg',1000)

flow_ecmo35 = flow_calculation(df_pre.flow,ecmo_35ml[0],ecmo_35ml[1],'ECMO 50 ml/kg',1000)

flow_ecmo42 = flow_calculation(df_pre.flow,ecmo_42ml[0],ecmo_42ml[1],'ECMO 60 ml/kg',1000)

flow_ecmo35 = flow_calculation(df_pre.flow,ecmo_35ml_end[0],ecmo_35ml_end[1],'ECMO 50 ml/kg - End part 1',1000)

numpy dot product (.dot) between diff and samples to get the

sum over i Δt_i * value_i for all I such bthat t_0 to t_i is one minute
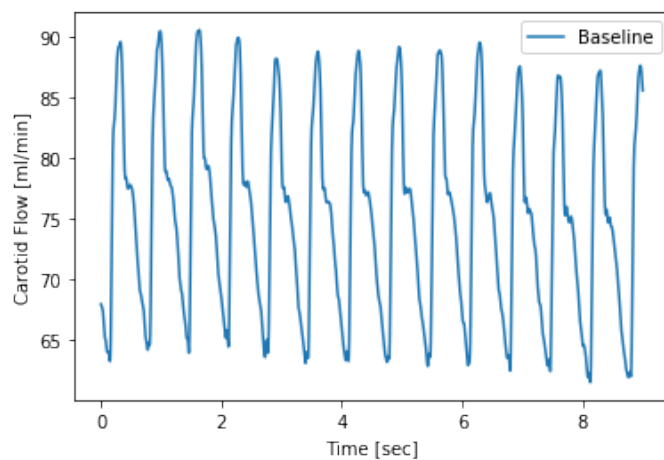
```
flow_ecmo35_p2 = flow_calculation(df.Flow,ecmo_35ml_p2_init[0],ecmo_35ml_p2_init[1],'ECMO
50 ml/kg - P2',250)
```


AVG MAP

```
map_mean_calculation(df_pre.aop,bl_5peep_8vt[0],bl_5peep_8vt[1],'Baseline')

map_mean_calculation(df_pre.aop,shock_final[0],shock_final[1],'Shock')

map_mean_calculation(df_pre.aop,ecmo_28ml[0],ecmo_28ml[1],'ECMO 40 ml/kg')

map_mean_calculation(df_pre.aop,ecmo_35ml[0],ecmo_35ml[1],'ECMO 50 ml/kg')

map_mean_calculation(df_pre.aop,ecmo_42ml[0],ecmo_42ml[1],'ECMO 60 ml/kg')

map_mean_calculation(df_pre.aop,ecmo_35ml_end[0],ecmo_35ml_end[1],'ECMO 50 ml/kg - End
part 1')

print('------')

map_mean_calculation(df.AOP,ecmo_35ml_p2_init[0],ecmo_35ml_p2_init[1],'ECMO 50 ml/kg -
P2')

map_mean_calculation(df.AOP,ecmo_35ml_p2[0],ecmo_35ml_p2[1],'ECMO 50 ml/kg - P2 post')

map_mean_calculation(df.AOP,ecmo_35ml_p4[0],ecmo_35ml_p4[1],'ECMO 50 ml/kg - P4')

map_mean_calculation(df.AOP,ecmo_35ml_p6[0],ecmo_35ml_p6[1],'ECMO 50 ml/kg - P6')

map_mean_calculation(df.AOP,ecmo_42ml_p2[0],ecmo_42ml_p2[1],'ECMO 60 ml/kg - P2')

map_mean_calculation(df.AOP,ecmo_42ml_p4[0],ecmo_42ml_p4[1],'ECMO 60 ml/kg - P4')

map_mean_calculation(df.AOP,ecmo_42ml_p6[0],ecmo_42ml_p6[1],'ECMO 60 ml/kg - P6')

map_mean_calculation(df.AOP,ecmo_42ml_p8[0],ecmo_42ml_p8[1],'ECMO 60 ml/kg - P8')

map_mean_calculation(df.AOP,ecmo_28ml_p2[0],ecmo_28ml_p2[1],'ECMO 40 ml/kg - P2')

map_mean_calculation(df.AOP,ecmo_28ml_p4[0],ecmo_28ml_p4[1],'ECMO 40 ml/kg - P4')

map_mean_calculation(df.AOP,ecmo_28ml_p6[0],ecmo_28ml_p6[1],'ECMO 40 ml/kg - P6')

map_mean_calculation(df.AOP,ecmo_28ml_p8[0],ecmo_28ml_p8[1],'ECMO 40 ml/kg - P8')
```


SYSTEMIC

```
venous_p(df_pre.aop, df_pre.cvp, df_pre.pap, bl_5peep_8vt[0],bl_5peep_8vt[1],'Baseline')

venous_p(df_pre.aop, df_pre.cvp, df_pre.pap,shock_final[0],shock_final[1],'Shock')

venous_p(df_pre.aop, df_pre.cvp, df_pre.pap,ecmo_28ml[0],ecmo_28ml[1],'ECMO 40 ml/kg')
```

```
venous_p(df_pre.aop, df_pre.cvp, df_pre.pap,ecmo_35ml[0],ecmo_35ml[1],'ECMO 50 ml/kg')

venous_p(df_pre.aop, df_pre.cvp, df_pre.pap,ecmo_42ml[0],ecmo_42ml[1],'ECMO 60 ml/kg')

venous_p(df_pre.aop, df_pre.cvp, df_pre.pap,ecmo_35ml_end[0],ecmo_35ml_end[1],'ECMO 50
ml/kg - End part 1')

print('------')

venous_p(df.AOP, df.CVP, df.PAP, ecmo_35ml_p2_init[0],ecmo_35ml_p2_init[1],'ECMO 50 ml/kg
- P2')

venous_p(df.AOP, df.CVP, df.PAP, ecmo_35ml_p2[0],ecmo_35ml_p2[1],'ECMO 50 ml/kg - P2
post')

venous_p(df.AOP, df.CVP, df.PAP, ecmo_35ml_p4[0],ecmo_35ml_p4[1],'ECMO 50 ml/kg - P4')

venous_p(df.AOP, df.CVP, df.PAP, ecmo_35ml_p6[0],ecmo_35ml_p6[1],'ECMO 50 ml/kg - P6')

venous_p(df.AOP, df.CVP, df.PAP, ecmo_42ml_p2[0],ecmo_42ml_p2[1],'ECMO 60 ml/kg - P2')

venous_p(df.AOP, df.CVP, df.PAP, ecmo_42ml_p4[0],ecmo_42ml_p4[1],'ECMO 60 ml/kg - P4')

venous_p(df.AOP, df.CVP, df.PAP, ecmo_42ml_p6[0],ecmo_42ml_p6[1],'ECMO 60 ml/kg - P6')

venous_p(df.AOP, df.CVP, df.PAP, ecmo_42ml_p8[0],ecmo_42ml_p8[1],'ECMO 60 ml/kg - P8')

venous_p(df.AOP, df.CVP, df.PAP, ecmo_28ml_p2[0],ecmo_28ml_p2[1],'ECMO 40 ml/kg - P2')

venous_p(df.AOP, df.CVP, df.PAP, ecmo_28ml_p4[0],ecmo_28ml_p4[1],'ECMO 40 ml/kg - P4')

venous_p(df.AOP, df.CVP, df.PAP, ecmo_28ml_p6[0],ecmo_28ml_p6[1],'ECMO 40 ml/kg - P6')

venous_p(df.AOP, df.CVP, df.PAP, ecmo_28ml_p8[0],ecmo_28ml_p8[1],'ECMO 40 ml/kg - P8')


### CREATE PLOTS – PV LOOPS with Ea, Ees all @ end expiration

envelope_plot(df.scaled_lvv[ecmo_42ml_p2[0]+ecmo_42ml_p2_exp:ecmo_42ml_p2[0]+ecmo_42
ml_p2_exp+250],

df.LVP[ecmo_42ml_p2[0]+ecmo_42ml_p2_exp:ecmo_42ml_p2[0]+ecmo_42ml_p2_exp+250],0)

plt.show()

envelope_plot(df.scaled_lvv[ecmo_42ml_p4[0]+ecmo_42ml_p4_exp:ecmo_42ml_p4[0]+ecmo_42
ml_p4_exp+250],

df.LVP[ecmo_42ml_p4[0]+ecmo_42ml_p4_exp:ecmo_42ml_p4[0]+ecmo_42ml_p4_exp+250],0)

plt.show()
```

```python
envelope_plot(df.scaled_lvv[ecmo_42ml_p6[0]+ecmo_42ml_p6_exp:ecmo_42ml_p6[0]+ecmo_42ml_p6_exp+250],

df.LVP[ecmo_42ml_p6[0]+ecmo_42ml_p6_exp:ecmo_42ml_p6[0]+ecmo_42ml_p6_exp+250],0)

plt.show()

envelope_plot(df.scaled_lvv[ecmo_42ml_p8[0]+ecmo_42ml_p8_exp:ecmo_42ml_p8[0]+ecmo_42ml_p8_exp+250],

df.LVP[ecmo_42ml_p8[0]+ecmo_42ml_p8_exp:ecmo_42ml_p8[0]+ecmo_42ml_p8_exp+250],0)

plt.show()


print('-------')

envelope_plot(df.scaled_lvv[ecmo_35ml_p2_init[0]+ecmo_35ml_p2init_exp:ecmo_35ml_p2_init[0]+ecmo_35ml_p2init_exp+250],

df.LVP[ecmo_35ml_p2_init[0]+ecmo_35ml_p2init_exp:ecmo_35ml_p2_init[0]+ecmo_35ml_p2init_exp+250],0)

plt.show()


envelope_plot(df.scaled_lvv[ecmo_35ml_p2[0]+ecmo_35ml_p2_exp:ecmo_35ml_p2[0]+ecmo_35ml_p2_exp+250],

df.LVP[ecmo_35ml_p2[0]+ecmo_35ml_p2_exp:ecmo_35ml_p2[0]+ecmo_35ml_p2_exp+250],0)

plt.show()


envelope_plot(df.scaled_lvv[ecmo_35ml_p4[0]+ecmo_35ml_p4_exp:ecmo_35ml_p4[0]+ecmo_35ml_p4_exp+250],

df.LVP[ecmo_35ml_p4[0]+ecmo_35ml_p4_exp:ecmo_35ml_p4[0]+ecmo_35ml_p4_exp+250],0)

plt.show()


envelope_plot(df.scaled_lvv[ecmo_35ml_p6[0]+ecmo_35ml_p6_exp:ecmo_35ml_p6[0]+ecmo_35ml_p6_exp+250],
```

```python
df.LVP[ecmo_35ml_p6[0]+ecmo_35ml_p6_exp:ecmo_35ml_p6[0]+ecmo_35ml_p6_exp+250],0)

plt.show()



print('-------')



envelope_plot(df.scaled_lvv[ecmo_28ml_p2[0]+ecmo_28ml_p2_exp:ecmo_28ml_p2[0]+ecmo_28ml_p2_exp+250],

df.LVP[ecmo_28ml_p2[0]+ecmo_28ml_p2_exp:ecmo_28ml_p2[0]+ecmo_28ml_p2_exp+250],0)

plt.show()

envelope_plot(df.scaled_lvv[ecmo_28ml_p4[0]+ecmo_28ml_p4_exp:ecmo_28ml_p4[0]+ecmo_28ml_p4_exp+250],

df.LVP[ecmo_28ml_p4[0]+ecmo_28ml_p4_exp:ecmo_28ml_p4[0]+ecmo_28ml_p4_exp+250],0)

plt.show()

envelope_plot(df.scaled_lvv[ecmo_28ml_p6[0]+ecmo_28ml_p6_exp:ecmo_28ml_p6[0]+ecmo_28ml_p6_exp+250],

df.LVP[ecmo_28ml_p6[0]+ecmo_28ml_p6_exp:ecmo_28ml_p6[0]+ecmo_28ml_p6_exp+250],0)

plt.show()

envelope_plot(df.scaled_lvv[ecmo_28ml_p8[0]+ecmo_28ml_p8_exp:ecmo_28ml_p8[0]+ecmo_28ml_p8_exp+250],

df.LVP[ecmo_28ml_p8[0]+ecmo_28ml_p8_exp:ecmo_28ml_p8[0]+ecmo_28ml_p8_exp+250],0)

plt.show()



print('-------')
```

envelope_plot(df_pre.scaled_lvv[ecmo_35ml_end[0]+ecmo_35ml_end_exp:ecmo_35ml_end[0]+ecmo_35ml_end_exp+650],

df_pre.lvp[ecmo_35ml_end[0]+ecmo_35ml_end_exp:ecmo_35ml_end[0]+ecmo_35ml_end_exp+650],0)

plt.show()

envelope_plot(df_pre.scaled_lvv[ecmo_42ml[0]+ecmo_42ml_exp:ecmo_42ml[0]+ecmo_42ml_exp+650],

        df_pre.lvp[ecmo_42ml[0]+ecmo_42ml_exp:ecmo_42ml[0]+ecmo_42ml_exp+650],0)

plt.show()

envelope_plot(df_pre.scaled_lvv[ecmo_35ml[0]+ecmo_35ml_exp:ecmo_35ml[0]+ecmo_35ml_exp+650],

        df_pre.lvp[ecmo_35ml[0]+ecmo_35ml_exp:ecmo_35ml[0]+ecmo_35ml_exp+650],0)

plt.show()

envelope_plot(df_pre.scaled_lvv[ecmo_28ml[0]+ecmo_28ml_exp:ecmo_28ml[0]+ecmo_28ml_exp+650],

        df_pre.lvp[ecmo_28ml[0]+ecmo_28ml_exp:ecmo_28ml[0]+ecmo_28ml_exp+650],0)

plt.show()

```python
#coronary_perfusion(lvp,aop,start_idx,end_idx)
```
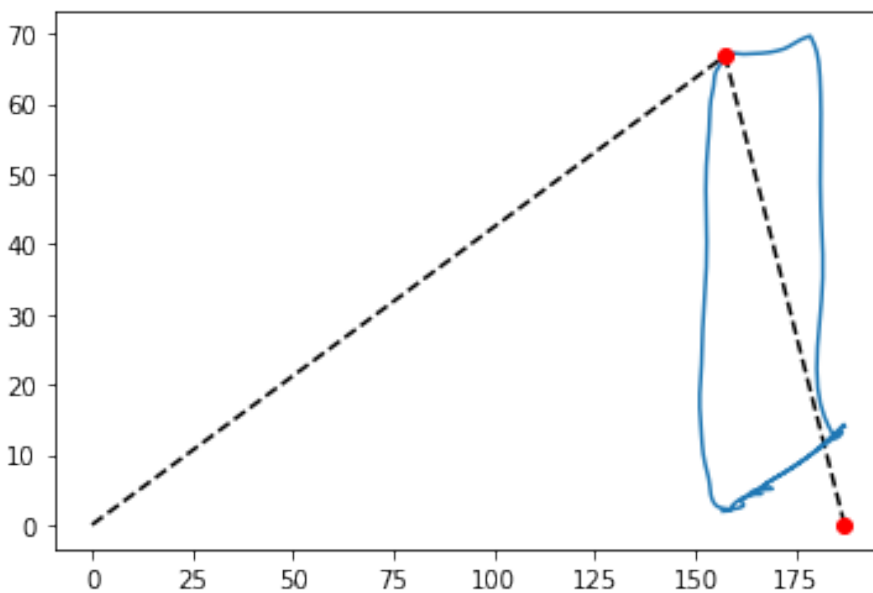
```python
coronary_perfusion(df.LVP, df.AOP,ecmo_42ml_p2[0]+ecmo_42ml_p2_exp,
ecmo_42ml_p2[0]+ecmo_42ml_p2_exp+250)

coronary_perfusion(df.LVP,
df.AOP,ecmo_42ml_p4[0]+ecmo_42ml_p4_exp,ecmo_42ml_p4[0]+ecmo_42ml_p4_exp+250)

coronary_perfusion(df.LVP,
df.AOP,ecmo_42ml_p6[0]+ecmo_42ml_p6_exp,ecmo_42ml_p6[0]+ecmo_42ml_p6_exp+250)

coronary_perfusion(df.LVP,
df.AOP,ecmo_42ml_p8[0]+ecmo_42ml_p8_exp,ecmo_42ml_p8[0]+ecmo_42ml_p8_exp+250)

plt.plot(df_pre.scaled_lvv[bl_5peep_8vt[0]+bl_5peep_8vt_exp:bl_5peep_8vt[0]+bl_5peep_8vt_exp
+700],

df_pre.lvp[bl_5peep_8vt[0]+bl_5peep_8vt_exp:bl_5peep_8vt[0]+bl_5peep_8vt_exp+700],label='BL'
)

plt.plot(df_pre.scaled_lvv[shock_final[0]+shock_final_exp:shock_final[0]+shock_final_exp+700],

df_pre.lvp[shock_final[0]+shock_final_exp:shock_final[0]+shock_final_exp+700],label='Shock')

plt.ylabel("Pressure [mmHg]")

plt.xlabel("Volume [ml]")

plt.legend()

plt.ylim(0,140)

plt.xlim(0,200)
```
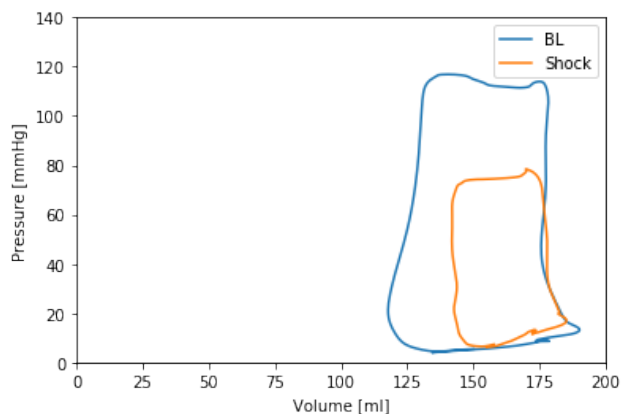
```
#
plt.plot(df_pre.scaled_lvv[bl_5peep_8vt[0]+bl_5peep_8vt_exp:bl_5peep_8vt[0]+bl_5peep_8vt_exp
+700],

#
df_pre.lvp[bl_5peep_8vt[0]+bl_5peep_8vt_exp:bl_5peep_8vt[0]+bl_5peep_8vt_exp+700],label='BL'
,color='green',linewidth=3.0)

#
envelope(df_pre.scaled_lvv[bl_5peep_8vt[0]+bl_5peep_8vt_exp:bl_5peep_8vt[0]+bl_5peep_8vt_ex
p+700],

#
df_pre.lvp[bl_5peep_8vt[0]+bl_5peep_8vt_exp:bl_5peep_8vt[0]+bl_5peep_8vt_exp+700],0)


plt.plot(df_pre.scaled_lvv[shock_final[0]+shock_final_exp:shock_final[0]+shock_final_exp+700],


df_pre.lvp[shock_final[0]+shock_final_exp:shock_final[0]+shock_final_exp+700],label='Shock',col
or='black',linewidth=3.0)

envelope(df_pre.scaled_lvv[shock_final[0]+shock_final_exp:shock_final[0]+shock_final_exp+700],

        df_pre.lvp[shock_final[0]+shock_final_exp:shock_final[0]+shock_final_exp+700],0)


plt.plot(df_pre.scaled_lvv[ecmo_35ml_end[0]+ecmo_35ml_exp:ecmo_35ml_end[0]+ecmo_35ml_e
xp+800],

df_pre.lvp[ecmo_35ml_end[0]+ecmo_35ml_exp:ecmo_35ml_end[0]+ecmo_35ml_exp+800],label='
ECMO 50',color='royalblue',linewidth=3.0)

envelope(df_pre.scaled_lvv[ecmo_35ml_end[0]+ecmo_35ml_exp:ecmo_35ml_end[0]+ecmo_35ml_
exp+800],

df_pre.lvp[ecmo_35ml_end[0]+ecmo_35ml_exp:ecmo_35ml_end[0]+ecmo_35ml_exp+800],0)


#
plt.plot(df.scaled_lvv[ecmo_35ml_p6[0]+ecmo_35ml_p6_exp:ecmo_35ml_p6[0]+ecmo_35ml_p6_e
xp+250],

#
df.LVP[ecmo_35ml_p6[0]+ecmo_35ml_p6_exp:ecmo_35ml_p6[0]+ecmo_35ml_p6_exp+250],label=
'ECMO 50 - P6',color='maroon')
```

```
#
envelope(df.scaled_lvv[ecmo_35ml_p6[0]+ecmo_35ml_p6_exp:ecmo_35ml_p6[0]+ecmo_35ml_p6
_exp+250],
```

```
#
df.LVP[ecmo_35ml_p6[0]+ecmo_35ml_p6_exp:ecmo_35ml_p6[0]+ecmo_35ml_p6_exp+250],0)
```

plt.ylabel("Pressure [mmHg]")

plt.xlabel("Volume [ml]")

plt.title("Animal #2 - Impella")

plt.legend()

plt.ylim(0,100)

plt.xlim(0,200)

```
Ea = -1.9092763657651337 Ees = 0.5020910849838793 SV =  38.56330142676538
PP = 67.362 SW = 2597.701110709769 PE = 4939.073292009599
Ea = -2.59363450949066 Ees = 0.5961134945489198 SV =  33.91341365876315 PP
= 78.923 SW = 2676.5483461905637 PE = 5822.7067668154505
```


plt.plot(df_pre.scaled_lvv[shock_final[0]+shock_final_exp:shock_final[0]+shock_final_exp+700],

df_pre.lvp[shock_final[0]+shock_final_exp:shock_final[0]+shock_final_exp+700],label='Shock',col
or='black',linewidth=3.0)

```python
envelope(df_pre.scaled_lvv[shock_final[0]+shock_final_exp:shock_final[0]+shock_final_exp+700],
        df_pre.lvp[shock_final[0]+shock_final_exp:shock_final[0]+shock_final_exp+700],0)


plt.plot(df_pre.scaled_lvv[ecmo_28ml[0]+ecmo_28ml_exp:ecmo_28ml[0]+ecmo_28ml_exp+650],

df_pre.lvp[ecmo_28ml[0]+ecmo_28ml_exp:ecmo_28ml[0]+ecmo_28ml_exp+650],label='ECMO
40',color='plum',linewidth=3.0)
envelope(df_pre.scaled_lvv[ecmo_28ml[0]+ecmo_28ml_exp:ecmo_28ml[0]+ecmo_28ml_exp+650]
,
        df_pre.lvp[ecmo_28ml[0]+ecmo_28ml_exp:ecmo_28ml[0]+ecmo_28ml_exp+650],0)


plt.plot(df_pre.scaled_lvv[ecmo_35ml_end[0]+ecmo_35ml_exp:ecmo_35ml_end[0]+ecmo_35ml_e
xp+800],

df_pre.lvp[ecmo_35ml_end[0]+ecmo_35ml_exp:ecmo_35ml_end[0]+ecmo_35ml_exp+800],label='
ECMO 50',color='royalblue',linewidth=3.0)
envelope(df_pre.scaled_lvv[ecmo_35ml_end[0]+ecmo_35ml_exp:ecmo_35ml_end[0]+ecmo_35ml_
exp+800],

df_pre.lvp[ecmo_35ml_end[0]+ecmo_35ml_exp:ecmo_35ml_end[0]+ecmo_35ml_exp+800],0)


plt.plot(df_pre.scaled_lvv[ecmo_42ml[0]+ecmo_42ml_exp:ecmo_42ml[0]+ecmo_42ml_exp+800],

df_pre.lvp[ecmo_42ml[0]+ecmo_42ml_exp:ecmo_42ml[0]+ecmo_42ml_exp+800],label='ECMO
60',color='turquoise',linewidth=3.0)
envelope(df_pre.scaled_lvv[ecmo_42ml[0]+ecmo_42ml_exp:ecmo_42ml[0]+ecmo_42ml_exp+800]
,
        df_pre.lvp[ecmo_42ml[0]+ecmo_42ml_exp:ecmo_42ml[0]+ecmo_42ml_exp+800],0)


plt.ylabel("Pressure [mmHg]")
plt.xlabel("Volume [ml]")
plt.title("Animal #2 - Impella")
plt.legend()
```
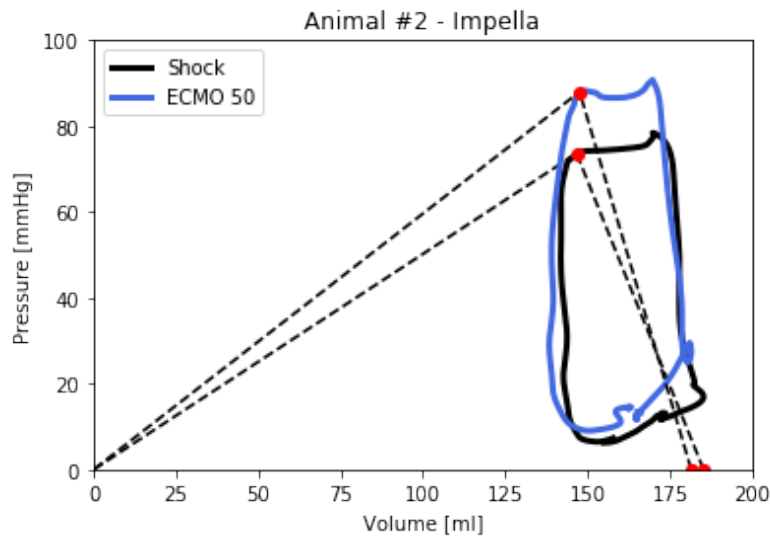
plt.ylim(0,100)

plt.xlim(70,200) Ea = -1.9092763657651337 Ees = 0.5020910849838793 SV = 38
.56330142676538 PP = 67.362 SW = 2597.701110709769 PE = 4939.073292009599
Ea = -2.6588163291702003 Ees = 0.5632121817675891 SV = 31.916458112954444
PP = 80.029 SW = 2554.2422263216313 PE = 6029.043014203153
Ea = -2.59363450949066 Ees = 0.5961134945489198 SV = 33.91341365876315 PP
= 78.923 SW = 2676.5483461905637 PE = 5822.7067668154505
Ea = -2.862370157199663 Ees = 0.5852357075398179 SV = 31.30692226321628 P
P = 84.00200000000001 SW = 2629.8440839546943 PE = 6431.2439646275725

164
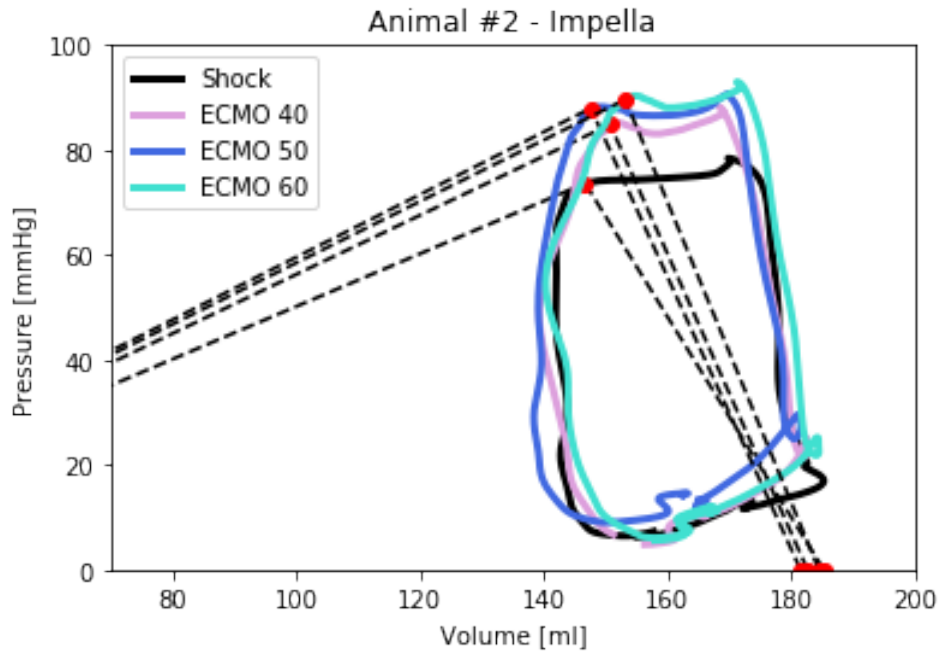
Appendix II - Doppler Blood Mimicking Fluid

In each liter:

419 mL PBS, 419 mL water

100.6 g (80 mL) glycerin

20 g particles

9 g synperonic F108

Dextran:

      2 liters have 33.6 g 150 kD

      1 liter has 17.85 g 150 kD + 15.75 g 40 kD

      2 liters have 33.6 g 40 kD

      3 liters have no dextran

Total weight of all 8 liters = 7908.8 g

Percentages by weight:

      42.4% PBS

      42.4% Water

      10.2 % Glycerin

      2.0% polyamide particles (5 um)

      0.9 % Synperonic F108 surfactant (as wetting agent)

      Averaging molec. weights of dextran: 2.1% Dextran of average molecular weight 95700 kD

      Or keeping weights separate: 1.1% 150 kD   1.0% 40 kD (edited)

References

1.   Virani SS, Alonso A, Benjamin EJ, Bittencourt MS, Callaway CW, Carson AP, et al. Heart disease and stroke statistics—2020 update: A report from the American Heart Association. Circulation. 2020. 139–596 p.

2.   Acharya D, Loyaga-Rendon RY, Pamboukian S V., Tallaj JA, Holman WL, Cantor RS, et al. Ventricular Assist Device in Acute Myocardial Infarction. J Am Coll Cardiol. 2016;67(16):1871–80.

3.   Buerke M, Lemm H, Dietz S, Werdan K. Pathophysiology, diagnosis, and treatment of infarction-related cardiogenic shock. Herz. 2011;36(2):73–83.

4.   Werdan K, Gielen S, Ebelt H, Hochman JS. Mechanical circulatory support in cardiogenic shock. Eur Heart J. 2014;35(3):156–67.

5.   Iakobishvili Z, Hasdai D. Cardiogenic Shock: Treatment. Med Clin North Am. 2007;91(4):713–27.

6.   Thiele H, Ohman EM, Desch S, Eitel I, De Waha S. Management of cardiogenic shock. European Heart Journal. 2015.

7.   Abraham J, BLUMER V, BURKHOFF DAN, PAHUJA M, SINHA SS, ROSNER C, et al. Heart Failure-Related Cardiogenic Shock: Pathophysiology, Evaluation and Management Considerations: Review of Heart Failure-Related Cardiogenic Shock. J Card Fail [Internet]. 2021;27(10):1126–40. Available from: https://doi.org/10.1016/j.cardfail.2021.08.010

8.   Van Diepen S, Katz JN, Albert NM, Henry TD, Jacobs AK, Kapur NK, et al. Contemporary Management of Cardiogenic Shock: A Scientific Statement from the American Heart Association. Vol. 136, Circulation. 2017. 232–268 p.

9.   Stretch R, Sauer CM, Yuh DD, Bonde P. National Trends in the Utilization of Short-Term Mechanical Circulatory Support Incidence, Outcomes, and Cost Analysis.

10.   Cme JJ. Hemodynamics of Mechanical Circulatory Support. 2015;66(23).

11.   Basir MB, Schreiber TL, Grines CL, Dixon SR, Moses JW, Maini BS, et al. Effect of Early Initiation of Mechanical Circulatory Support on Survival in Cardiogenic Shock. Am J Cardiol. 2017;

12.   Thiele H, Zeymer U, Thelemann N, Neumann FJ, Hausleiter J, Abdel-Wahab M, et al. Intraaortic Balloon Pump in Cardiogenic Shock Complicating Acute Myocardial Infarction: Long-Term 6-Year Outcome of the Randomized IABP-SHOCK II Trial. Circulation. 2019;139(3):395–403.

13.   Kadakia S, Moore R, Ambur V, Toyoda Y. Current status of the implantable LVAD. Gen Thorac Cardiovasc Surg. 2016;64(9):501–8.

14.   Miller LW, Pagani FD, Russell SD, John R, Boyle AJ, Aaronson KD, et al. Use of a continuous-flow device in patients awaiting heart transplantation. N Engl J Med. 2007;357(9):885–96.

15.   Slaughter MS, Rogers JG, Milano CA, Russell SD, Conte J V., Feldman D, et al. Advanced

heart failure treated with continuous-flow left ventricular assist device. N Engl J Med. 2009;361(23):2241–51.

16. Mebazaa A, Tolppanen H, Mueller C, Lassus J, DiSomma S, Baksyte G, et al. Acute heart failure and cardiogenic shock: a multidisciplinary practical guidance. Intensive Care Med. 2016;42(2):147–63.

17. Wernly B, Seelmaier C, Leistner D, Stähli BE, Pretsch I, Lichtenauer M, et al. Mechanical circulatory support with Impella versus intra-aortic balloon pump or medical treatment in cardiogenic shock—a critical appraisal of current data. Clin Res Cardiol [Internet]. 2019;108(11):1249–57. Available from: http://dx.doi.org/10.1007/s00392-019-01458-2

18. Glazier JJ, Kaki A. The Impella Device: Historical Background, Clinical Applications and Future Directions. Int J Angiol. 2019;28(2):118–23.

19. Strom JB, Zhao Y, Shen C, Chung M, Pinto DS, Popma JJ, et al. National Trends, Predictors of Use, and In-Hospital Outcomes in the Mechanical Circulatory Support for Cardiogenic Shock. EuroIntervention [Internet]. 2018; Available from: http://www.ncbi.nlm.nih.gov/pubmed/29400657

20. Keller SP. Management of Peripheral Venoarterial Extracorporeal Membrane Oxygenation in Cardiogenic Shock. Crit Care Med. 2019;47(9):1235–42.

21. Sun T, Guy A, Sidhu A, Finlayson G, Grunau B, Ding L, et al. Veno-arterial extracorporeal membrane oxygenation (VA-ECMO) for emergency cardiac support. J Crit Care [Internet]. 2018;44:31–8. Available from: https://doi.org/10.1016/j.jcrc.2017.10.011

22. Makdisi G, Wang IW. Extra Corporeal Membrane Oxygenation (ECMO) review of a lifesaving technology. J Thorac Dis. 2015;7(7):E166–76.

23. Brown JL, Estep JD. Temporary Percutaneous Mechanical Circulatory Support in Advanced Heart Failure. Vol. 12, Heart Failure Clinics. 2016. p. 385–98.

24. Meani P, Lorusso R, Pappalardo F. ECPella: Concept, Physiology and Clinical Applications. J Cardiothorac Vasc Anesth. 2021;li.

25. Kar B, Basra SS, Shah NR, Loyalka P. Percutaneous circulatory support in cardiogenic shock interventional bridge to recovery. Circulation. 2012;125(14):1809–17.

26. Levy B, Clere-Jehl R, Legras A, Morichau-Beauchant T, Leone M, Frederique G, et al. Epinephrine Versus Norepinephrine for Cardiogenic Shock After Acute Myocardial Infarction. J Am Coll Cardiol. 2018 Jul 10;72(2):173–82.

27. Baskurt OK, Meiselman HJ. Blood Rheology and Hemodynamics. Semin Thromb Hemost. 2003;29(5):435–50.

28. Gimbrone MA, García-Cardeña G. Vascular endothelium, hemodynamics, and the pathobiology of atherosclerosis. Cardiovasc Pathol [Internet]. 2013;22(1):9–15. Available from: http://dx.doi.org/10.1016/j.carpath.2012.06.006

29. Ostadal P, Mlcek M, Strunina S, Hrachovina M, Kruger A, Vondrakova D, et al. Synchronized Pulsatile Extracorporeal Life Support Preserves Left Ventricular Functions in Comparison With Continuous Extracorporeal Flow in Porcine Model of Cardiogenic Shock.

Circulation. 2015;132(Suppl 3):A19380 LP-A19380.

30. Chirinos JA, Segers P. Noninvasive evaluation of left ventricular afterload: Part 2: Arterial pressure-flow and pressure-volume relations in humans. Hypertension. 2010;56(4):563–70.

31. Chirinos JA, Segers P. Noninvasive evaluation of left ventricular afterload: Part 1: Pressure and flow measurements and basic principles of wave conduction and reflection. Hypertension. 2010;56(4):555–62.

32. Sunagawa K, Maughan WL, Burkhoff D, Sagawa K. Left ventricular interaction with arterial load studied in isolated canine ventricle.

33. Gaasch WH, Levine HJ, Quinones MA, Alexander JK. Left ventricular compliance: Mechanisms and clinical implications. Am J Cardiol. 1976;38(5):645–53.

34. O' MF, And R, Avolio AP. Pulsatile Flow and Pressure in Human Systemic Arteries Studies in Man and in a Multibranched Model of the Human Systemic Arterial Tree [Internet]. Vol. 46, Circ Res. 1980. Available from: http://ahajournals.org

35. Flow B, Flow B. Contours of pressure and flow waves in arteries. McDonald's Blood Flow Arter 6th Ed Theor Exp Clin Princ. 2011;225–53.

36. Alastruey J, Passerini T, Formaggia L, Peiró J. Physical determining factors of the arterial pulse waveform: Theoretical analysis and calculation using the 1-D formulation. J Eng Math. 2012;77(1):19–37.

37. Safar ME. Systolic blood pressure, pulse pressure and arterial stiffness as cardiovascular risk factors. Curr Opin Nephrol Hypertens. 2001;10(2):257–61.

38. Blacher J, Fournier V, Asmar R, Guerin AP, Pannier B, Safar ME, et al. Aortic pulse wave velocity as a marker of atherosclerosis in hypertension. Cardiovasc Rev Reports. 2001;22(7):420-425+431.

39. Guarracino F, Baldassarri R, Pinsky MR. Ventriculo-arterial decoupling in acutely altered hemodynamic states. Critical Care. 2013.

40. Richter Y, Edelman ER. Cardiology is flow. Circulation. 2006;113(23):2679–82.

41. Boutsianis E, Frauenfelder T, Wildermuth S, Poulikakos D, Ventikos Y. Anatomically Accurate Haemodynamic Simulations of Abdominal Aortic Aneurysms [Internet]. 2003. p. 61–2. Available from: https://doi.org/10.1115/IMECE2003-42766

42. Bluestein D. Utilizing Computational Fluid Dynamics in Cardiovascular Engineering and Medicine—What You Need to Know. Its Translation to the Clinic/Bedside. Artif Organs. 2017;41(2):117–21.

43. Balakrishnan B, Tzafriri AR, Seifert P, Groothuis A, Rogers C, Edelman BR. Strut position, blood flow, and drug deposition: Implications for single and overlapping drug-eluting stents. Circulation. 2005;111(22):2958–65.

44. Katritsis DG, Theodorakakos A, Pantos I, Gavaises M, Karcanias N, Efstathopoulos EP. Flow patterns at stented coronary bifurcations: Computational fluid dynamics analysis. Circ Cardiovasc Interv. 2012;5(4):530–9.

45. Tsukiya T, Toda K, Sumikura H, Takewa Y, Watanabe F, Taenaka Y, et al. Computational fluid dynamic analysis of the flow field in the newly developed inflow cannula for a bridge-to-decision mechanical circulatory support. J Artif Organs. 2011;14(4):381–4.

46. Khodaee F, Nezami FR, Zampell BA, Galper E, Edelman ER, Keller SP. Effect of anatomical variation on extracorporeal membrane oxygenation circulatory support: A computational study. Comput Biol Med [Internet]. 2022;141(December 2021):105178. Available from: https://doi.org/10.1016/j.compbiomed.2021.105178

47. Nezami FR, Ramezanpour M, Khodaee F, Goffer E, Edelman ER, Keller SP. Simulation of Fluid-Structure Interaction in Extracorporeal Membrane Oxygenation Circulatory Support Systems. J Cardiovasc Transl Res. 2022;15(2):249–57.

48. Karmonik C, Partovi S, Rengier F, Meredig H, Farag MB, Müller-Eschner M, et al. Hemodynamic assessment of partial mechanical circulatory support: data derived from computed tomography angiographic images and computational fluid dynamics. Cardiovasc Diagn Ther. 2015;5(2):160–5.

49. Biglino G, Cosentino D, Steeden JA, De Nova L, Castelli M, Ntsinjana H, et al. Using 4D Cardiovascular Magnetic Resonance Imaging to Validate Computational Fluid Dynamics: A Case Study. Front Pediatr. 2015;

50. McCormick M, Nordsletten D, Lamata P, Smith NP. Computational analysis of the importance of flow synchrony for cardiac ventricular assist devices. Comput Biol Med. 2014 Jun 1;49(1):83–94.

51. Alastruey J, Xiao N, Fok H, Schaeffter T, Figueroa CA. On the impact of modelling assumptions in multi-scale, subject-specific models of aortic haemodynamics. J R Soc Interface. 2016;13(119).

52. Schampaert S, Pennings KAMA, Van De Molengraft MJG, Pijls NHJ, Van De Vosse FN, Rutten MCM. A mock circulation model for cardiovascular device evaluation. Physiol Meas. 2014;35(4):687–702.

53. KALKHORAN, Sara; BENOWITZ, Neal L .; RIGOTTI NA. 乳鼠心肌提取 HHS Public Access. Rev del Col Am Cardiol. 2018;72(23):2964–79.

54. Groves EM, Falahatpisheh A, Su JL, Kheradvar A. The effects of positioning of transcatheter aortic valves on fluid dynamics of the aortic root. ASAIO J. 2014;60(5):545–52.

55. Pasta S, Scardulla F, Rinaudo A, Raffa GM, D'Ancona G, Pilato M, et al. An in vitro phantom study on the role of the bird-beak configuration in endograft infolding in the aortic arch. J Endovasc Ther. 2016;23(1):172–81.

56. Falahatpisheh A, Kheradvar A. High-speed particle image velocimetry to assess cardiac fluid dynamics in vitro: From performance to validation. Eur J Mech B/Fluids [Internet]. 2012;35:2–8. Available from: http://dx.doi.org/10.1016/j.euromechflu.2012.01.019

57. Ostadal P, Mlcek M, Strunina S, Hrachovina M, Kruger A, Vondrakova D, et al. Novel porcine model of acute severe cardiogenic shock developed by upper-body hypoxia. Physiol Res. 2016;65(4):711–5.

58. Krombach GA, Kinzel S, Mahnken AH, Günther RW, Buecker A. Minimally invasive close-

chest method for creating reperfused or occlusive myocardial infarction in swine. Invest Radiol. 2005;40(1):14–8.

59. Shirakawa T, Kuratani T, Yoshitatsu M, Shimamura K, Fukui S, Kurata A, et al. Towards a Clinical Implementation of Measuring the Elastic Modulus of the Aorta from Cardiac Computed Tomography Images. IEEE Trans Biomed Eng. 2021;68(12):3543–53.

60. Gao F, Guo Z, Sakamoto M, Matsuzawa T. Fluid-structure interaction within a layered aortic arch model. J Biol Phys. 2006;32(5):435–54.

61. Bude RO, Adler RS. An easily made, low-cost, tissue-like ultrasound phantom material. J Clin Ultrasound. 1995;23(4):271–3.

62. Rosalia L, Ozturk C, Fan Y, Jaume Coll-Font, Chen S, Eder RA, et al. A soft robotic sleeve mimicking the hemodynamics and biomechanics of left ventricular pressure overload and aortic stenosis. Nature biomedical engineering. 2021;1134.

63. O'Rourke MF, Yaginuma T, Avolio AP. Physiological and pathophysiological implications of ventricular/vascular coupling. Ann Biomed Eng [Internet]. 1984;12(2):119–34. Available from: http://link.springer.com/10.1007/BF02584226

64. Nichols WW, O'Rourke MF, Avolio AP, Yaginuma T, Murgo JP, Pepine CJ, et al. Effects of age on ventricular-vascular coupling. Am J Cardiol. 1985;55(9):1179–84.

65. Nozawa T, Yasumura Y, Futaki S, Tanaka N, Uenishi M, Suga H. Efficiency of energy transfer from pressure-volume area to external mechanical work increases with contractile state and decreases with afterload in the left ventricle of the anesthetized closed-chest dog. Circulation. 1988;77(5):1116–24.

66. Kass DA. Ventricular arterial stiffening: Integrating the pathophysiology. In: Hypertension. 2005.

67. Starling MR. Left ventricular-arterial coupling relations in the normal human heart. Am Heart J. 1993;

68. Chantler PD, Lakatta EG, Najjar SS. Arterial-ventricular coupling: mechanistic insights into cardiovascular performance at rest and during exercise. J Appl Physiol [Internet]. 2008;105(4):1342–51. Available from: http://jap.physiology.org/cgi/doi/10.1152/japplphysiol.90600.2008

69. Chang BY, Keller SP, Bhavsar SS, Josephy N, Edelman ER. Mechanical circulatory support device-heart hysteretic interaction can predict left ventricular end diastolic pressure. Sci Transl Med. 2018;10(430).

70. Keller SP, Chang BY, Tan Q, Zhang Z, El Katerji A, Edelman ER. Dynamic Modulation of Device-Arterial Coupling to Determine Cardiac Output and Vascular Resistance. Ann Biomed Eng. 2020;48(9):2333–42.

71. Vahdatpour C, Collins D, Goldberg S. Cardiogenic Shock. J Am Heart Assoc. 2019;8(8):1–12.

72. Kim Y, Shapero K, Ahn SS, Goldsweig AM, Desai N, Altin SE. Outcomes of mechanical circulatory support for acute myocardial infarction complicated by cardiogenic shock. Catheter Cardiovasc Interv. 2021;(June):1–6.

73.   Kolte D, Khera S, Aronow WS, Mujib M, Palaniswamy C, Sule S, et al. Trends in incidence, management, and outcomes of cardiogenic shock complicating ST-elevation myocardial infarction in the United States. J Am Heart Assoc. 2014;3(1):1–17.

74.   Khorsandi M, Dougherty S, Bouamra O, Pai V, Curry P, Tsui S, et al. Extra-corporeal membrane oxygenation for refractory cardiogenic shock after adult cardiac surgery: A systematic review and meta-analysis. J Cardiothorac Surg. 2017;12(1).

75.   Chang C-H, Chen H-C, Caffrey JL, Hsu J, Lin J-W, Lai M-S, et al. Survival Analysis After Extracorporeal Membrane Oxygenation in Critically Ill Adults: A Nationwide Cohort Study. Circulation [Internet]. 2016;133(24):2423–33. Available from: http://www.ncbi.nlm.nih.gov/pubmed/27199466

76.   Distelmaier K, Wiedemann D, Lampichler K, Toth D, Galli L, Haberl T, et al. Interdependence of VA-ECMO output, pulmonary congestion and outcome after cardiac surgery. Eur J Intern Med [Internet]. 2020;81(April):67–70. Available from: https://doi.org/10.1016/j.ejim.2020.07.014

77.   Chang BY, Keller SP, Edelman ER. Leveraging Device-Arterial Coupling to Determine Cardiac and Vascular State. IEEE Trans Biomed Eng. 2019;66(10):2800–8.

78.   Chang BY, Moyer C, El Katerji A, Keller SP, Edelman ER. A scalable approach to determine intracardiac pressure from mechanical circulatory support device signals. IEEE Trans Biomed Eng. 2020;9294(c):1–1.

79.   Chang BY, Zhang Z, Feng K, Josephy N, Keller SP, Edelman ER. Hysteretic device characteristics indicate cardiac contractile state for guiding mechanical circulatory support device use. Intensive Care Med Exp [Internet]. 2021;9(1). Available from: https://doi.org/10.1186/s40635-021-00426-3

80.   Khan MH, Corbett BJ, Hollenberg SM. Mechanical circulatory support in acute cardiogenic shock. F1000Prime Rep. 2014 Jan 1;6(3):91.

81.   Fiorelli F, Panoulas V. Impella as unloading strategy during VA-ECMO: systematic review and meta-analysis. Rev Cardiovasc Med. 2021;22(4):1503–11.

82.   Russo JJ, Aleksova N, Pitcher I, Couture E, Parlow S, Faraz M, et al. Left Ventricular Unloading During Extracorporeal Membrane Oxygenation in Patients With Cardiogenic Shock. J Am Coll Cardiol. 2019;73(6).

83.   Donker DW, Brodie D, Henriques JPS, Broomé M. Left ventricular unloading during veno-arterial ECMO: a review of percutaneous and surgical unloading interventions. Vol. 34, Perfusion (United Kingdom). SAGE Publications Ltd; 2019. p. 98–105.

84.   Donker DW, Brodie D, Henriques JPS, Broomé M. Left ventricular unloading during veno-arterial ECMO: A simulation study. ASAIO J. 2019 Jan 1;65(1):11–20.

85.   Donker DW, Burkhoff D, Mack MJ. ECMO: We Need to Vent About the Need to Vent! J Am Coll Cardiol. 2022;79(13):1251–3.

86.   Parissis H, Graham V, Lampridis S, Lau M, Hooks G, Mhandu PC. IABP: History-evolution-pathophysiology-indications: What we need to know. J Cardiothorac Surg [Internet]. 2016;11(1):1–13. Available from: http://dx.doi.org/10.1186/s13019-016-0513-0